

RESEARCH TRIANGLE INSTITUTE

N 70 21528

CR-66894
NASA CR 66894

PHASE II REPORT

INVESTIGATION OF THE PERFORMANCE CHARACTERISTICS OF A
DOPPLER RADAR TECHNIQUE FOR AIRCRAFT COLLISION HAZARD WARNING

**CASE FILE
COPY**

Distribution of this report is provided in the interest of
information exchange. Responsibility for the contents
resides in the author or organization that prepared it.

Prepared under Contract No. NAS1-7537 by
Research Triangle Institute
Research Triangle Park
North Carolina 27709

for

NATIONAL AERONAUTICS AND SPACE ADMINISTRATION

November 18, 1969

ACKNOWLEDGMENT

This report was prepared by the Research Triangle Institute, Durham, North Carolina, under Contract NAS1-7537. The work is being administered by the Communications Research Section, Telecommunications Research Branch, Flight Instrumentation Division, Langley Research Center. Mr. Richard H. Couch is the Langley technical representative for the contract.

This report presents the results of Phase II of a two-phase program which began on July 6, 1967. Additional Phase II results were presented in an interim report dated July 15, 1969. RTI staff members participating in the study were as follows: C. L. Britt, Project Leader; E. L. Sheppard, Systems Engineer; R. C. Haws, Systems Analyst; E. H. Young, Programmer; and Mrs. C. M. Davis, Programmer.

TABLE OF CONTENTS

	<u>Page No.</u>
ACKNOWLEDGMENT	i
I. SUMMARY	1
II. INTRODUCTION	1
III. SIMULATION TECHNIQUES	3
A. SYSTEM DESCRIPTION	3
B. SYSTEM SIMULATIONS	8
C. ANALYTICAL MODELS	9
IV. SATURATION AND INTERFERENCE STUDIES	13
A. GENERAL	13
B. TRANSPONDER CHARACTERISTICS	14
C. RECEIVER	18
D. RECEIVED SIGNAL AND INTERFERENCE LEVELS VS TIME	25
E. DISTRIBUTION OF POWER LEVELS FOR IDEALIZED SYSTEMS	30
V. FLIGHT TEST EVALUATION OF RANGE MEASUREMENT ERROR	41
A. GENERAL DESCRIPTION	41
B. FLIGHT TEST SIMULATIONS	41
C. FLIGHT TEST RESULTS	46
VI. MISCELLANEOUS STUDIES	63
A. GENERAL	63
B. DEFINITION OF WARNING TIMES	63
C. ALARM SUPPRESSION DUE TO RELATIVE RANGE ACCELERATION THRESHOLDS	67
D. WARNING TIMES OF VARIOUS SYSTEMS WITH EQUAL ALARM PROBABILITY	76
E. WARNING TIMES REQUIRED FOR ESCAPE MANEUVERS	77
F. SUMMARY	80
VII. CONCLUSIONS	83
VIII. LIST OF REFERENCES	85
IX. APPENDICES	87
APPENDIX A - EXTENSIONS OF THE "MODIFIED TAU" WARNING CRITERIA	89
APPENDIX B - THE D.C. OUTPUT OF A PRODUCT DETECTOR- LIMITER CIRCUIT WITH MULTIPLE INPUT SIGNALS	101

TABLE OF CONTENTS (Continued)

	<u>Page No.</u>
APPENDIX C - PHASE PLANE PLOT OF A SET OF COLLISION TRAJECTORIES UNDER AN ACCELERATION CONSTRAINT	113
APPENDIX D - RECEIVER DATA PROCESSING	115
APPENDIX E - SYSTEM PARAMETERS	121
APPENDIX F - FLIGHT TEST DATA	123
APPENDIX G - ANTENNA PATTERN MODELS	139
APPENDIX H - ANTENNA GAIN VARIATION WITH RELATIVE ELEVATION ANGLE	151

LIST OF TABLES

<u>Table No.</u>		<u>Page</u>
1	Examples of signal levels and frequencies while in an alarm status. (S_1 , S_2 etc are the signal levels in dbm, f_1 , f_2 , etc. are the corresponding doppler frequencies in cps)	26
2	Flight test parameters.	42
3	Warning times t_n and t_m as defined in VI-B for various system types. The maximum closing velocity assumed is V_m , the maximum relative acceleration is U and the maximum relative rate of descent or ascent is \dot{h}_m .	66
4	Detection range and warning times for system with equal (1%) fraction of flying time in an alarm status (from hour 11 data). Warning times are defined in Section VI-B.	78

LIST OF FIGURES

<u>Figure No.</u>		<u>Page No.</u>
1	Functional system diagram.	5
2	Receiver (one-channel).	5
3	Modulation spectra at various points in the system.	6
4	Technique for generation of alarm based on $R^2\tau$ criteria.	7
5	Simulation flow diagram.	10
6	Average percent of time that the transponder saturation factor is greater than S_k for hour 11 data.	16
7	Average percent of time that the power output of the transponder is greater than P_k for various outputs.	17
8	Average percentage of time that the power level at the IF Amp. input is greater than P_k . (hour 11 data)	19
9	Average percentage of time that the received power (differentiated signals) is greater than R_k (hour 11 data).	21
10	Average percentage of time that the received power (differentiated signals) is greater than R_k (hour 11 data).	23
11	Average percentage of time that the receiver signal to noise and interference power ratio is greater than SNR_k for alarm situations only.	24
12	Signals and noise power received at receiver on aircraft of track 98 (hour 11). Time base is the time from the start of the track.	27
13	Flight path of track 98 (hour 11) indicating alarms received. Numbers in parentheses are times in minutes from the start of the track.	29

LIST OF FIGURES (Continued)

<u>Figure No.</u>		<u>Page No.</u>
14	Distribution of relative range to closest aircraft.	31
15	Distribution of relative range to second closest aircraft	33
16	Relative range distributions plotted on lognormal scale to indicate fit of data to the lognormal distribution function.	34
17	Approximate probability that the power level from the kth closest aircraft exceeds the stated level. 0 db is the power level received from a target at 1 n. mi. range.	40
18	Example of computer printout for flight test data were obtained at five second intervals during each flight test.	44
19 - 33	(Flight test plots for tests 7A-10E.)	48-62
	a. Ground tracks for flight tests.	
	b. Ground radar, experimental and calculated values of relative range vs. time.	
	c. Percent error between calculated and experimental range measurements plotted vs ground radar (geometrical) range.	
34	Phase plane sketch for the tau-range-normal velocity system indicating possible alarm suppression due to the $\sqrt{R \dot{R} } < V_{nk}$ threshold (i.e. the <u>magnitude</u> of \dot{R} is used). See text for definition of the nomenclature and assumed constraints.	69
35	Phase plane plot for the tau-range-normal velocity system indicating possible alarm suppression due to a $\sqrt{R\dot{R}} < V_{nk}$ threshold when only positive \dot{R} is used (decreasing closing velocity). For the sketch, $\tau_k = 30$ secs. and $V_{nk} = 240$ kts.	73

LIST OF FIGURES (Continued)

<u>Figure No.</u>		<u>Page No.</u>
36	Phase plane plot for the $R^2\tau$ -range-normal velocity system indicating possible alarm suppression due to a $R/R < \gamma_k$ threshold. For the sketch, $\gamma_k = .004 \text{ sec}^{-1}$, and $R^2\tau = 1000 \text{ nm}^2\text{-sec}$ are used.	75
A-1	Coordinate system.	92
A-2	Plot of the extended modified tau criteria (assumes acceleration components normal to the velocity vectors).	92
A-3	Curves of constant τ_{em} and τ_m compared in the R, \dot{R} plane.	98
B-1	Detection block diagram.	101
B-2	Definition of β .	107
B-3	Normalized gain of limiter for fundamental component of input signal (P) for various levels of signals P and Q.	111
B-4	Normalized gain of limiter for fundamental component of input signal (P) for various levels of signals P and Q for third signal (R) of unity level.	112
C-1	Phase plane plot indicating slope isoclines for trajectories with acceleration not exceeding $\pm 1/2 \text{ g}$. A set of allowable trajectories is also sketched.	114
D-1	Receiver detector and doppler filter characteristics.	117
D-2	Power at IF Amp. input (DBM).	118
F-1 thru F-15	Computer printout of flight test simulation for Flight 7A - 10E	124 - 138
G-1	Transmitter Az. pattern (4.252 GHz).	142
G-2	Transmitter El. pattern (4.252 GHz).	143

LIST OF FIGURES (Continued)

<u>Figure No.</u>		<u>Page No.</u>
G-3	Transponder receiver, El.(4.252 GHz).	144
G-4	Transponder receiver, El.(2.702 GHz).	145
G-5	Transponder transmitter, El.(1.5 GHz).	146
G-6	Receiver El.(1.5 GHz).	147
G-7	Receiver Az.(1.5 GHz).	148
G-8	Example of Fourier fit.	149
H-1	Measured range/actual range based on $R \sim (Pwr)^{-1/6}$	152

INVESTIGATION OF THE PERFORMANCE CHARACTERISTICS OF A
DOPPLER RADAR TECHNIQUE FOR AIRCRAFT COLLISION HAZARD WARNING

I. SUMMARY

This report presents the results of a computer simulation study of a cooperative doppler radar system for aircraft collision-hazard warning under development by NASA-Langley Research Center personnel. The system performance under multiple aircraft conditions, with particular emphasis on the problems of saturation and interference, is evaluated by simulation of the system using a data base consisting of twelve one-hour samples of aircraft position data obtained from the ground radar at the Atlanta, Georgia airport. In addition, the system error sources are determined by comparison of simulated data with flight test data, and other miscellaneous system problems are considered. Statistical studies of the data base have been previously documented in the Phase I final report [1] and Phase II interim report [2] of this contract.

II. INTRODUCTION

In phase I of this contract, the feasibility of a dynamic computer simulation of the aircraft collision hazard warning system developed by NASA-Langley personnel was investigated. The simulation was found to be feasible and well within the capabilities of the available digital computers.

One of the major objectives of the phase I effort was to collect data defining aircraft motions in a typical airport terminal area. With FAA cooperation, twelve one-hour samples of digitized radar data, controller-aircraft voice communications tapes, and controller log sheets were collected at the Atlanta, Ga. terminal. These data were taken during morning, afternoon, and evening peak traffic periods over a five day interval during the month of August 1967. The data were edited by FAA personnel at National Aviation Facilities Experimental Center (NAFEC) and made available to RTI in the form of digital magnetic tape. The edited data contain, for

the majority of the aircraft within a 35 mile radius of the Atlanta Airport, (1) position data in xyz coordinates for all aircraft under track at four second intervals (approximately 700 aircraft tracks with a total flight time of approximately 119 hours), (2) coordinate rates at four second intervals for all aircraft under track and, (3) supplementary data such as identification of aircraft and time of day. The data base is described in detail in the Phase II Interim Report on this contract [2].

The objectives of the Phase II efforts have been to: (1) development of mathematical models of the collision avoidance system and development of computer simulation programs to evaluate the performance of the system; (2) to use the data describing a typical terminal area to conduct a detailed statistical analysis of the effectiveness of various parameters (i.e., normalized doppler rate, time to closest approach, or projected miss distance) in reducing the probability of false alarms; and, (3) to provide assistance in the planning and evaluation of flight test data by use of the simulation model.

The effort described under (2) above has been reported upon separately in the Phase II Interim Report. Hence, this report presents the studies having the objectives (1) and (3) described above.

Two experimental collision warning systems have been constructed by LRC personnel and have undergone flight test evaluation. This evaluation provided a good indication of the system performance when only two aircraft are involved. The computer simulations described in this report evaluate the system performance under multiple aircraft conditions and provide quantitative results on the severity of the problem of saturation due to multiple aircraft interrogations.

In the following, the simulation techniques used are described in detail and the analytical models documented. The results of the experimental flight tests are compared to simulated results and the sources of system error are determined. The severity of the problem of system saturation and interference in a multiple aircraft environment is investigated in detail, and conclusions and recommendations are given for future work.

III. SIMULATION TECHNIQUES

A. SYSTEM DESCRIPTION

Figure 1 indicates the basic operation of the system. The protected aircraft is equipped with a radar unit consisting of two transmitters, a receiver, and a display console, and all cooperating aircraft have a transponder. The protected aircraft transmits a pair of signals at different frequencies. These signals are received at the intruding aircraft and multiplied to obtain a difference frequency. The difference signal is then re-transmitted to the protected aircraft where its frequency is compared with the difference of the transmitted frequencies to obtain the Doppler frequency as a measure of closing velocity. Since the transponder output power is proportional to the product of the power of the two interrogating input signals, the signal power returned to the receiver varies inversely with range to the sixth power. This relatively sharp fall-off of received power with range permits a relatively accurate measure of range to be obtained from measurement of returned signal power.

To provide for multiple access to the transponder, pseudo-random transmitting coding is used. Both of the transmitted signals are randomly frequency modulated; a single frequency is derived at the transponder by multiplication and filtering, and the random modulated return signal is decoded at the receiver. The signals due to multiple aircraft interrogations appear at the ownship receiver to have a noise-like characteristic, while the ownship returned signals are essentially stationary in frequency.

Because of the range limitation of the radar and the use of random transmitter coding, all radars may operate on the same frequencies, eliminating the need for separate channel assignments for each aircraft. Also, because of the C.W. mode of operation, the peak transmitter powers are relatively low, allowing the use of solid-state equipment, and there is no specific requirement for a high degree of accuracy in any of the frequencies involved.

This system is primarily a cooperative, C.W. Doppler radar which provides a precise measure of the closing velocity of an intruding aircraft,

and a somewhat less precise measure of the relative range between aircraft. The relative range divided by the closing velocity is computed, and gives a measure of the "time to collision." An indication to the pilot of the direction to a hazardous target is provided by a multiple lobe receiving antenna and associated signal processing to provide nine separate indicators of relative target bearing (e.g. up-right, up-center, ahead-right, down-left, etc.).

Figure 2 shows a more detailed block diagram of the system. Not shown on this diagram are provisions for filtering the ownship transmitter signal from the ownship transponder and the ownship transponder return from the ownship receiver. The operation of the system under multiple interrogations may be understood by inspecting the spectral densities in Fig. 3. The transmitter outputs are composed of the sum and difference of the two frequency modulated oscillators. The transponder receives a pair of input signals from every radar interrogating it, and will generate an output signal for every cross product that exists. For instance, if two radars are interrogating the transponder, four cross products will be generated. Only two of these products are desirable, and to suppress the undesired products, the transmitted signals are randomly frequency modulated such that their power is evenly distributed over the transmitter bandwidth. This modulation is applied such that it is coherent between signals in a pair and not coherent between signals not in a pair. Thus, the noncoherent products are spread over a band roughly two times that of the transmitter bandwidth, whereas the desired returns from the transponder are spread over a band determined by the deviation of FM oscillator no. 2. A filter in the transponder passes only the desired signals and the noncoherent power contained within the desired signal bandwidth.

At the receiver, the incoming signals are mixed with the signal from FM oscillator no. 2 to derive the desired returns. The desired returns are thus stationary in frequency at the Doppler filter output (except for the Doppler shift). Signals entering the receiver which are returns to other receivers in the area are noncoherent with the mixer signal and are

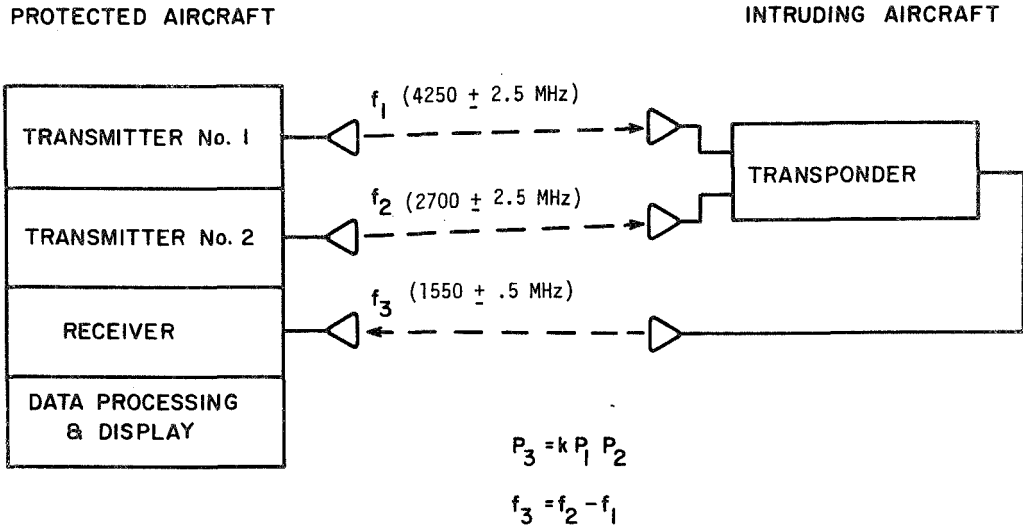


Figure 1. Functional system diagram.

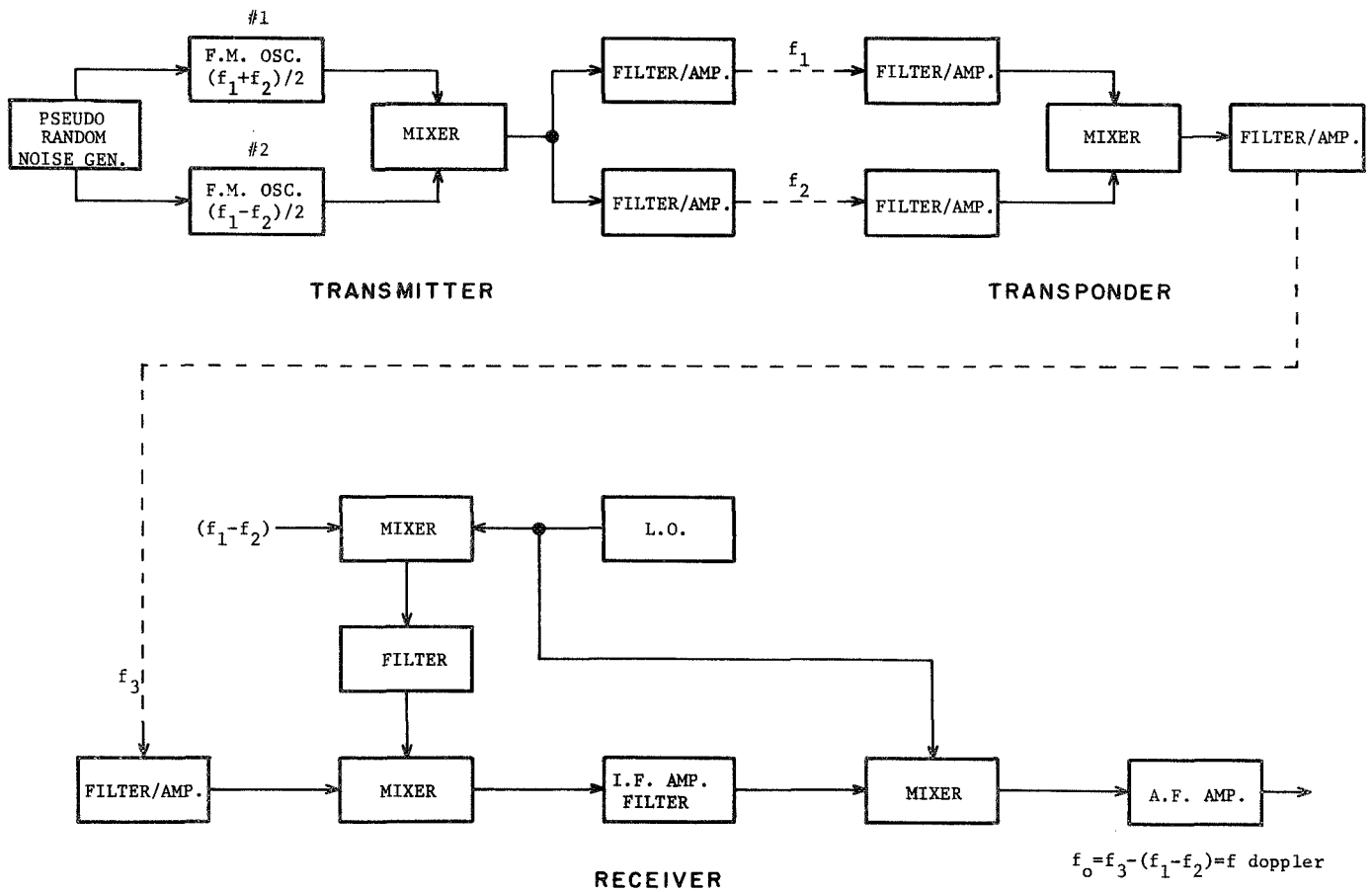


Figure 2. Simplified block diagram of transmitter, transponder and receiver.

APPROXIMATE SPECTRAL DENSITIES

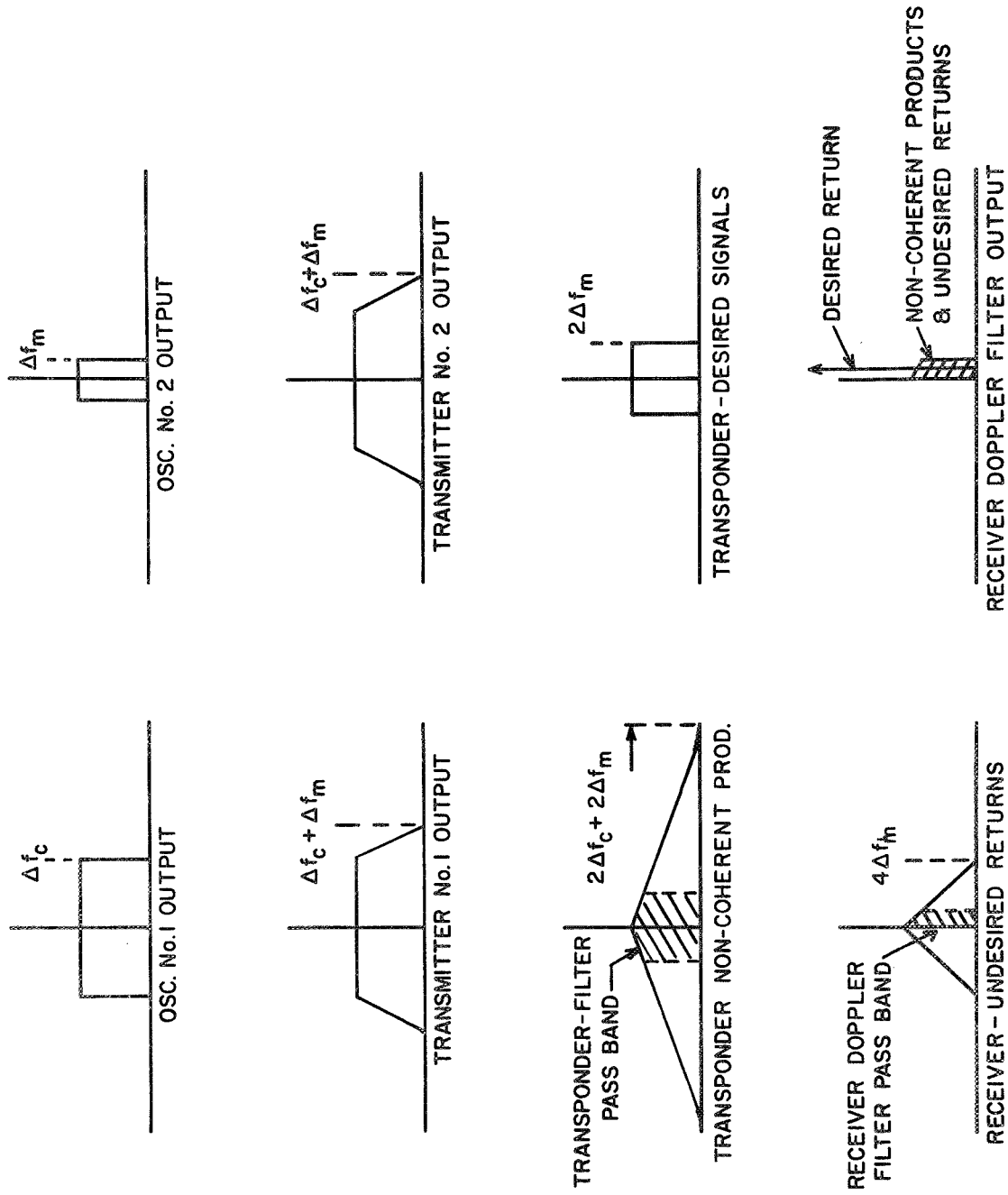
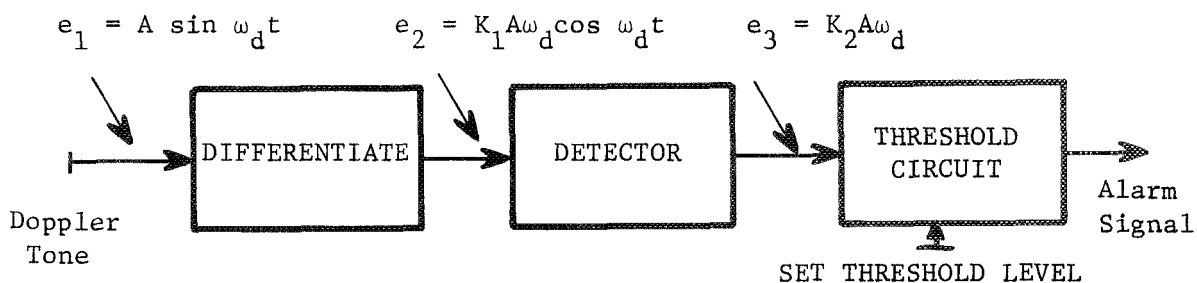


Figure 3. Modulation spectra at various points in the system.

spread over a bandwidth roughly twice that of the transponder output. These noncoherent products thus appear as noise within the Doppler filter bandwidth.

One technique for generating the warning alarm is shown in Fig. 4, utilizing a warning parameter designated as $(R^2\tau)$. In this technique, the Doppler signal is differentiated and detected to provide a voltage related to "time to collision." A threshold circuit is then used to give an alarm when this voltage exceeds a certain level.



A is proportional to R^{-3}
 ω_d is proportional to closing velocity (V_c),
 hence voltage e_3 is proportional to $(R^2\tau)^{-1}$

Fig. 4. Technique for generation of alarm based on $R^2\tau$ criteria.

Two of the systems have been constructed and installed in DC-4 aircraft for flight test evaluation.

In the systems subjected to flight tests, signal processing techniques were used that permitted derivation of voltages proportional to range, closing velocity, and rate of change of closing velocity, as well as combinations of these parameters. Both analog and digital data processing techniques have been evaluated during the flight test experiments.

Additional details of the system operation are given in reference [1] and [3], and in the following sections of this report.

B. SYSTEM SIMULATIONS

Several simulation programs have been developed, each somewhat similar, but differing in input data, output, and in certain internal details. A general description of each of these programs follows:

1. Linear path simulation:

inputs: positions and velocities of up to 15 aircraft, system parameters, and time intervals.

outputs: geometrical parameters and warning criteria, transponder and receiver power levels, frequencies, alarm status, signal-to-noise ratios, saturation condition, interference levels and output voltages vs time. (For all transponders and one selected receiver).

2. Atlanta data simulation:

inputs: Atlanta radar data, system parameters, track selected for analysis, and time intervals.

outputs: same as in (1)

3. Flight test simulation:

inputs: Radar data from Wallops FPQ-6 and FPS-16 radars, system parameters, and experimental flight test data.

outputs: Geometrical parameters and warning criteria, system outputs vs time as in (1), receiver voltages corresponding to geometrical parameters and warning criteria, breakdown of system errors, and comparison of geometrical (ground radar) calculated (simulated warning system) and experimental (flight test data) measurements.

4. Saturation evaluation:

inputs: Atlanta radar data and system parameters

outputs: Statistical data on system power levels, alarm condition, and saturation condition, assuming full simulated warning systems on all aircraft in the data base.

A general flow chart for the system simulation program is shown in Fig. 5. This chart indicates the basic program which is used, with slight modifications, in the programs described above.

C. ANALYTICAL MODELS

In the phase I report [1] analytical models are documented that provides for calculations of signal, noise, and interference levels at various points in the transponders and receivers. Additional analytical and empirical models have been developed in phase II of the study to provide a more realistic representation of the behavior of the systems as presently constructed.

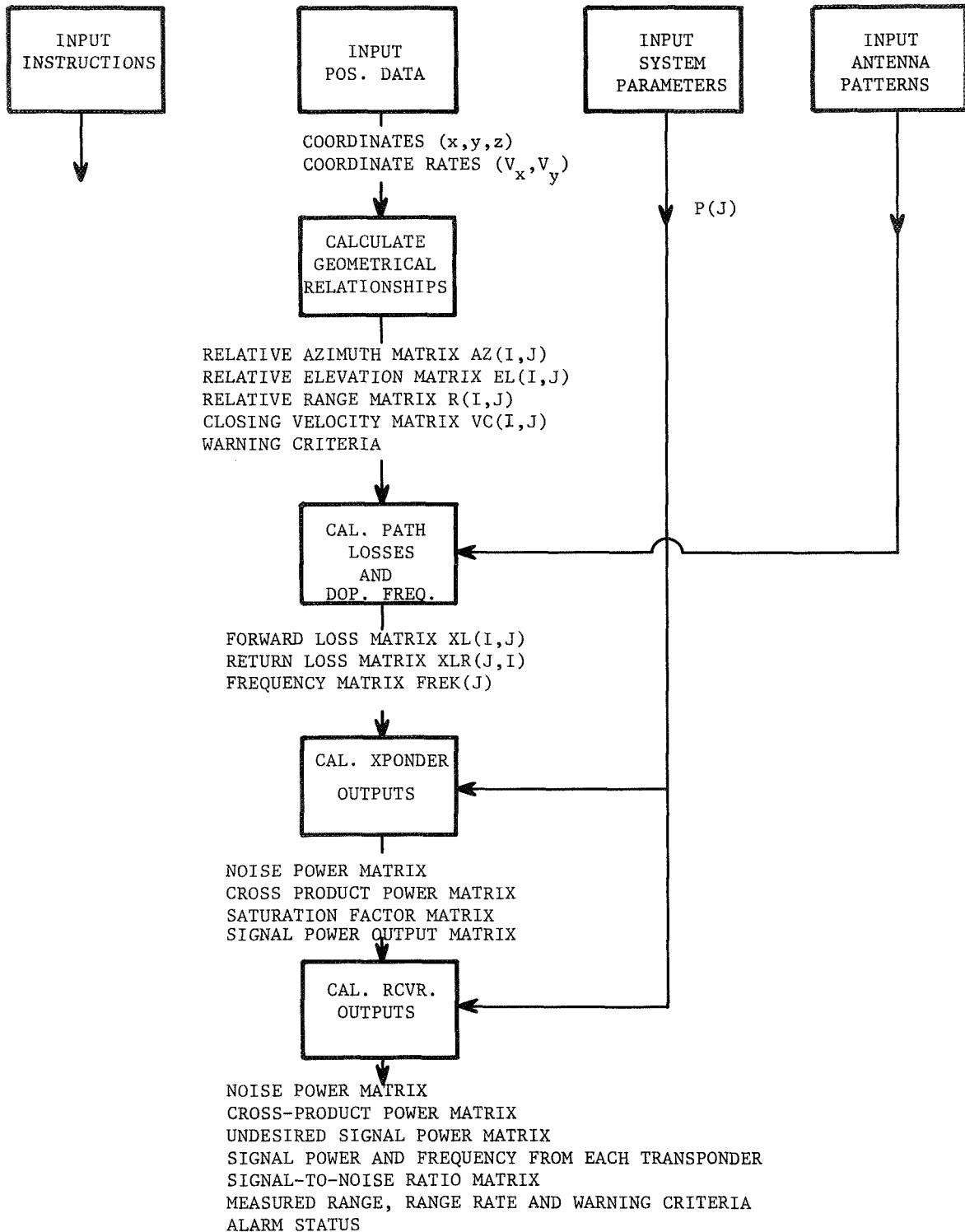


Figure 5. Simulation flow diagram.

The major refinements incorporated in the phase II simulations are summarized as:

1. More accurate representation of the system antenna patterns using a Fourier analysis of the experimental patterns.
2. Representation of the receiver amplitude-frequency response by empirical functions fitted to experimental calibration data taken at LRC.
3. Development of a mathematical model of the output of a limiter-product detector circuit with several input signals
4. Consideration of each transmitted signal separately instead of assuming equal path losses and antenna characteristics for both transmitted frequencies.
5. Incorporation of time response in the receiver calculations in accordance with time constants used in the actual systems.
6. Provision for the simulation of the analog data processing accomplished in the receiver based on experimental calibration data.
7. Incorporation of an error breakdown giving calculated measurement errors as referenced to an ideal receiver and to experimental flight test data.

Details of the above refinements are given in Appendix D (Receiver Data Processing), Appendix B (The Output of a Product-Detector Limiter Circuit) and Appendix G (Representation of Antenna Patterns).

IV. SATURATION AND INTERFERENCE STUDIES

A. GENERAL

The radar traffic data from the Atlanta terminal, as mentioned in the introduction and analyzed in detail in reference [2], permit studies of particular aspects of the system performance by computer simulation. A detailed warning system can be simulated on each aircraft in the data base, and statistics determined on performance measures of interest.

In the study of the saturation problem, the system parameters of interest include the signal, interference, and noise levels at various points in the transponder and receiver. A good measure of the severity of the saturation problem is given by a statistic such as "the average percentage of flying time in the terminal area that a certain power level exceeded a specified level." This statistic also provides an unbiased estimate of the probability that a randomly selected system will have a power level exceeding the specific level at any particular instant of time.

Another statistic of interest is "the average percentage of flying time in the terminal area that a certain power level exceeded a specified level while the system was in an alarm status." This statistic indicates the severity of both the multiple hazard and interference problems. For example, if the second largest signal power level at a given receiver exceeded the alarm threshold of the receiver for a large percentage of the time, a multiple target problem would exist. As another example, if the signal-to-interference ratio for the largest signal at a given receiver (while in an alarm status) is small for a large percentage of the time, an interference problem exists.

Thus, in the following, results are presented indicating the above mentioned statistics on various power levels for hour 11 of the Atlanta data base. During this hour, 68 aircraft were present with a total flying time of 13.6 hours [2].

B. TRANSPONDER CHARACTERISTICS

1. Mixer Saturation

The linear turn-around transponder deviates from linearity due to two major effects. One effect is that of exceeding the dynamic range of the balanced mixer circuit that effectively multiplies the two incoming signals and derives the low-level output signal (see figure 2). The other effect is the deviation from linearity of the output linear amplifier chain. Experimental data indicate that with one set of input signals, the balanced mixer is the component that tends to saturate first as the input power levels are increased.

A theoretical study of mixer saturation (see reference [1]) indicated that the mixer saturation was a function of the total power input to the mixer, and that the effect of transponder saturation could be represented satisfactorily by a model,

$$P_{s_{ij}} = \frac{F_x P_{a_{ij}} P_{b_{ij}}}{1 + K \sum_{i=1}^N (P_{a_{ij}} + P_{b_{ij}})} \quad (1)$$

where

$P_{s_{ij}}$ = power output of transponder j due to transmitter in aircraft i

$P_{a_{ij}}$ = power input from aircraft i at transponder j at frequency a

$P_{b_{ij}}$ = power input from aircraft i at transponder j at frequency b

F_x = overall gain constant for transponder

K = experimentally determined constant approximately equal to the gain of the transponder from the input to the mixer, divided by the mixer bias power (units of MW^{-1})

The denominator of eq. (1) has been designated as the "saturation factor" for the transponder. Notice that this term is also the nominal gain divided by the actual gain for a given signal, or

$$\text{Sat. factor } (S_K) = \frac{\text{nominal gain}}{\text{actual gain}} \quad (2)$$

Figure 6 shows the results of the simulation study indicating the average percentage of time that an aircraft transponder "saturation factor" exceeded a level specified along the horizontal axis. For example, a value of 1.3 was exceeded only .6% of the time; this corresponds to a gain reduction of only 1.1 db.

Inspection of the curve indicates that the median gain reduction factor is 1.05 and that there is a low ($\approx .01$) probability of exceeding 1.4. These levels are acceptable, hence transponder mixer saturation does not appear to be a problem under hour 11 (congested) flight conditions, and with the system parameters (gains, bandwidths, etc.) used in the construction and simulation of the system.

2. Signal and Interference Levels

Another factor of importance in judging the transponder performance is the level of the cross modulation products in the transponder resulting from multiple interrogations. If n aircraft are interrogating the transponder a total of $n(n-1)$ cross products are generated. Because of the random modulation of the transmitted signals, the cross products are spread over a bandwidth determined by the frequency deviation of the two oscillators in the transmitter (see spectral density in Fig. 3).

Curves indicating the average percent of time that the cross product power and the noise plus the cross product power exceeded a level greater than a specified value are shown in Fig. 7. The power levels are referred to the transponder output (30 dbm maximum output). As may be seen from the plots, the noise plus cross product power level referred to the output

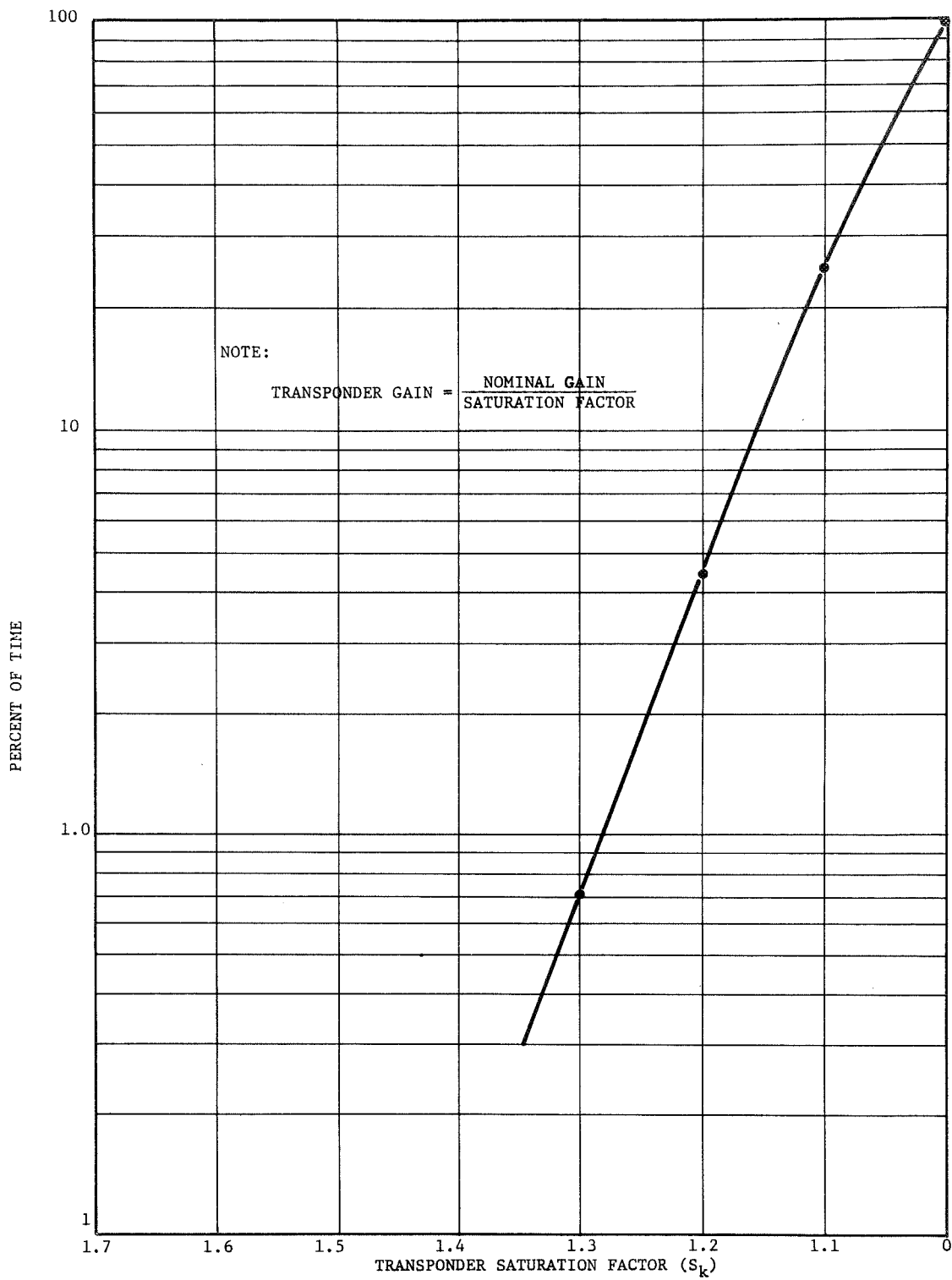


Figure 6. Average percent of time that the transponder saturation factor is greater than S_k for hour 11 data.

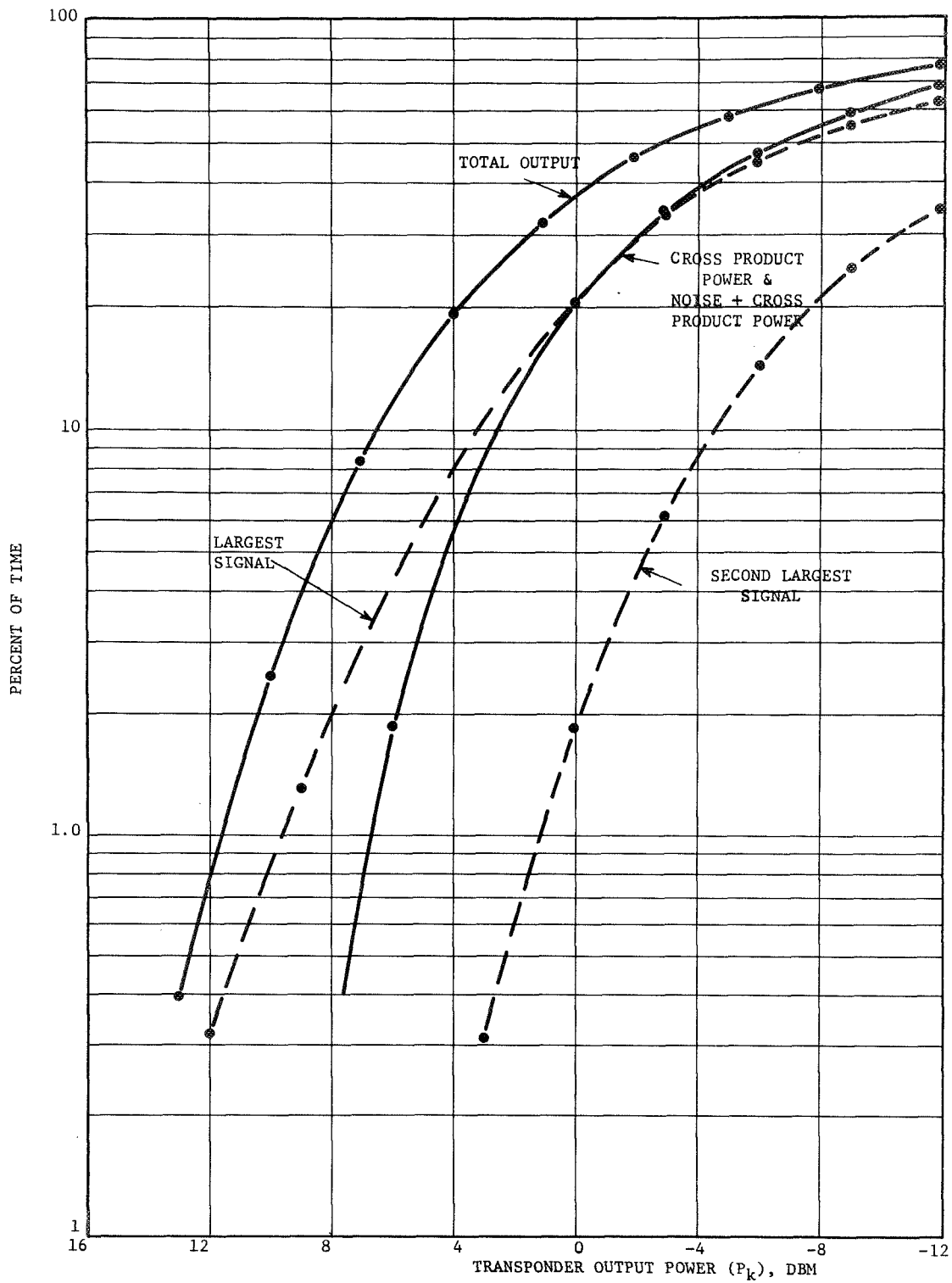


Figure 7. Average percent of time that the power output of the transponder is greater than P_k for various outputs.

rarely exceeds 9 dbm. The median value of noise plus cross product power is approximately -6 dbm.

Figure 7 also plots curves indicating the average percent of time that the total output, the largest signal output, and the second largest signal output exceeded the value specified on the horizontal axis. Note that the total output power is well below the 30 dbm maximum value for all cases.

From the curves of Fig. 7, we conclude that the transponder is operating well within its design values under hour 11 conditions. For conditions existing during this hour the cross product power is not an excessive percentage of the total output power, and the probability of exceeding the design maximum output of the transponder is very low.

C. RECEIVER

1. Signals in Receiver 60 MHz IF Amplifier

Figure 8 plots the largest, second largest, etc. up to the fifth largest signal in the receiver IF amplifier. Again these curves represent the percent of time that the power level exceeded the value along the horizontal axis, for hour 11 data. These power levels are referred to the input of the IF amplifier (-85 dbm corresponds to a target at a range of 5 miles).

The statistical analyses of the same hour of data reported in the Phase II Interim Report [2] indicated that 60 percent of the time there would be at least one aircraft within 5 miles of a randomly selected aircraft. The data in Fig. 8 indicate that the signal level from the closest aircraft exceeds the power level corresponding to 5 nautical miles only 30 percent of the time. The difference between these percentage values is evidently due to the filtering by the system antenna characteristics.

The receiver noise level is approximately -104 dbm, hence the signal-to-noise ratios are high for a large percentage of the time. The largest signal exceeds the noise level 75 percent of the time. The largest of the curves indicate that a dynamic range in the receiver IF of 45 db should be adequate to prevent saturation, with high probability.

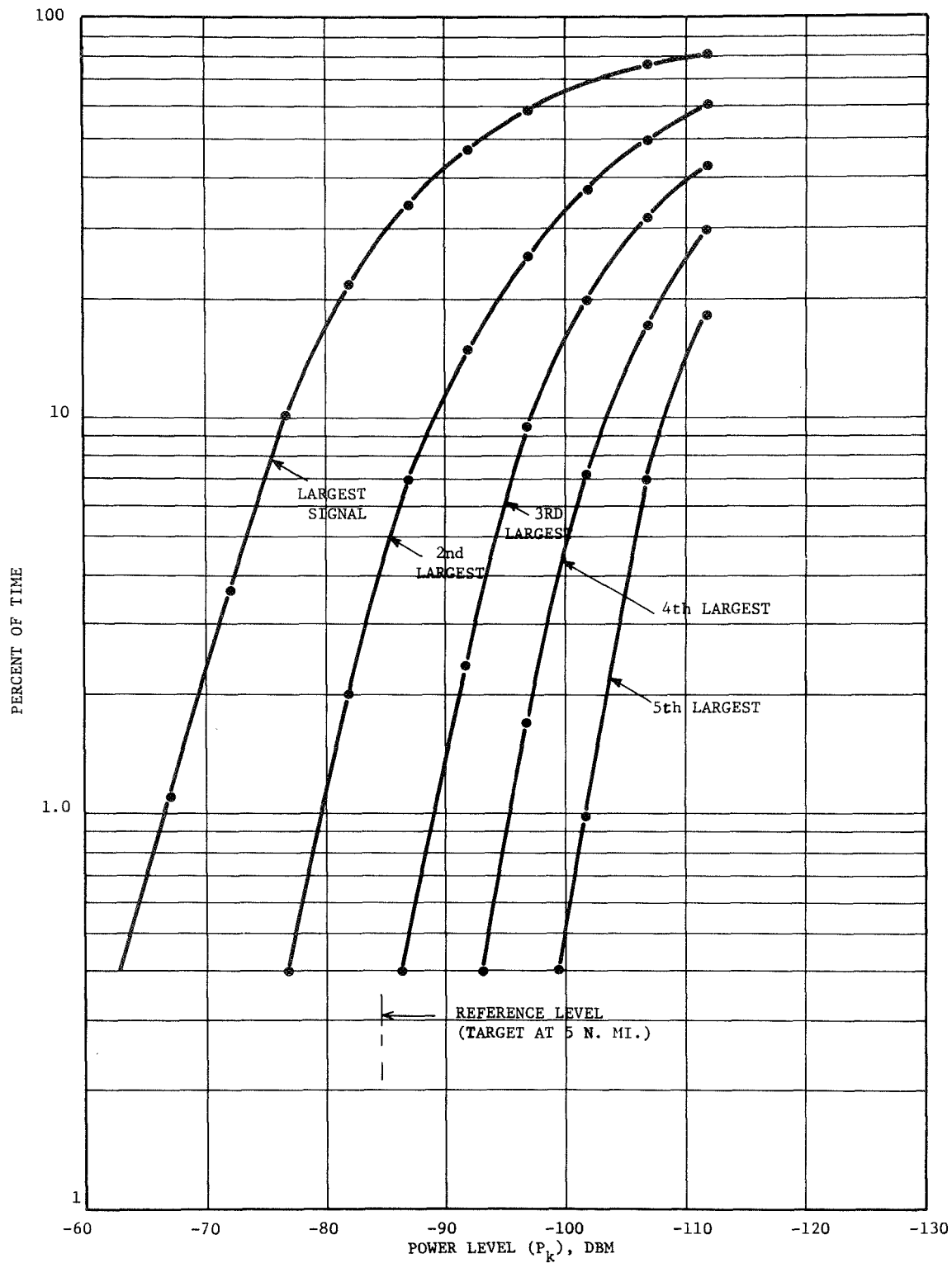


Figure 8. Average percentage of time that the power level at the IF amp. input is greater than P_k . (hour 11 data)

2. Receiver Doppler Filter Output

The Doppler filter in the receiver is assumed to have a 3 KHz bandwidth and an ideal frequency response from 100 to 3,000 Hz.

Figure 9 plots the percent of time that various power levels at the receiver Doppler filter exceeded the level plotted along the horizontal axis. The power levels are referenced to a level of -76.4 dbm, corresponding to a target at 4 nautical miles and closing at a velocity of 240 knots. This reference level was selected so that a 1,000 cycle Doppler signal from a target at 5 miles would provide a -85 dbm power level that was used in the preceding plot (Figure 8). Even though the signals are referenced to a level corresponding to the IF amplifier input, it should be noted that the signals have been passed through a differentiating amplifier, hence the power levels are a function of the Doppler frequency.

Figure 9 also plots "average percent of time" curves for the cross product power levels generated in the transponder and the "undesired signal power". This latter power represents signals that arise from transponder signals that are returns to other receivers in the population of aircraft. The cross product power and undesired signal power both represent noise like signals spread across the doppler bandwidth. These power levels have been combined with the noise power level in a composite curve designated as the noise plus interference power in Fig. 9.

We note from the curves that there is a low probability that the noise plus the interference power will exceed the threshold level of the detector. Thus, alarms caused by interfering signals should be negligible under the conditions represented during this hour of the data base. The cross product power term is the most significant interference source. By extrapolation of the noise plus interference power level curve, we can estimate the probability of a false alarm due to interference as 4×10^{-5} .

3. Receiver Signal Levels Under Alarm Conditions

The preceding curves on the receiver power levels have considered the overall receiver operation during flights in the terminal area. A major interest, however, is the signal level during an actual alarm

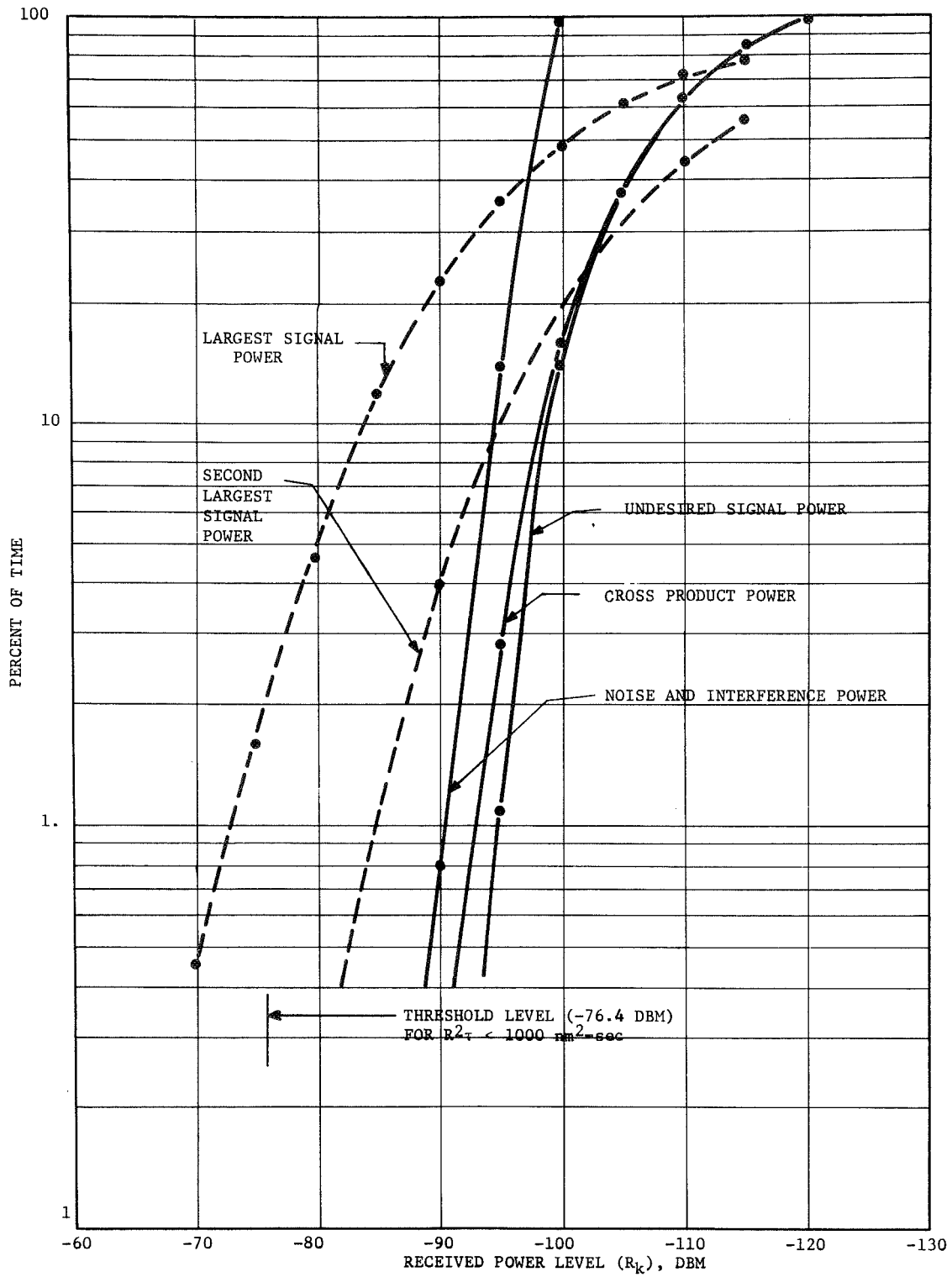


Figure 9. Average percentage of time that the received power (differentiated signals) is greater than R_k (hour 11 data).

condition. That is, we are interested in the noise and interfering signal levels while the system is in an alarm status.

Figure 10 plots the percent of time that the received signal exceeded a level R_k for the receiver in an alarm status. For these curves, a hazardous situation (alarm condition) is defined by

$$R^2 \tau < 1000 \text{ nm}^2\text{-sec} \quad (3)$$

where R is the relative range and τ is the approximate time to closest approach. The received power level corresponding to the above geometrical definition is -76.4 dbm. In terms of received power levels and doppler frequency, the expression for the differentiated power is given by equation (4)

$$P_d = -79 + 20 \log \left\{ \frac{f_d}{1000} \right\} \text{ dbm} \quad (4)$$

where P_d is the differentiated power and f_d is the doppler frequency in Hz.

As may be seen in Figure 10, the second largest signal and third largest signal while in an alarm status are less than the signal causing the alarm with high probability. The system under hour 11 conditions indicated an alarm 2.4 percent of the time while the second largest signal exceeded the threshold level approximately .04 percent of the time.

Figure 11 indicates the percent of time that the receiver signal to noise plus interference power ratio is greater than the level plotted along the horizontal axis for threat situations only. As may be seen from the curve, the probability that the largest signal to noise ratio exceeds 20 db is on the order of .9, given that the receiver is in an alarm status. No cases were observed in which the signal to noise ratio was less than 10 db for the signal causing the alarm.

From Figs. 10 and 11 we can conclude that, when in an alarm status with the threshold condition defined by eqs. 3 and 4, the interfering signals and

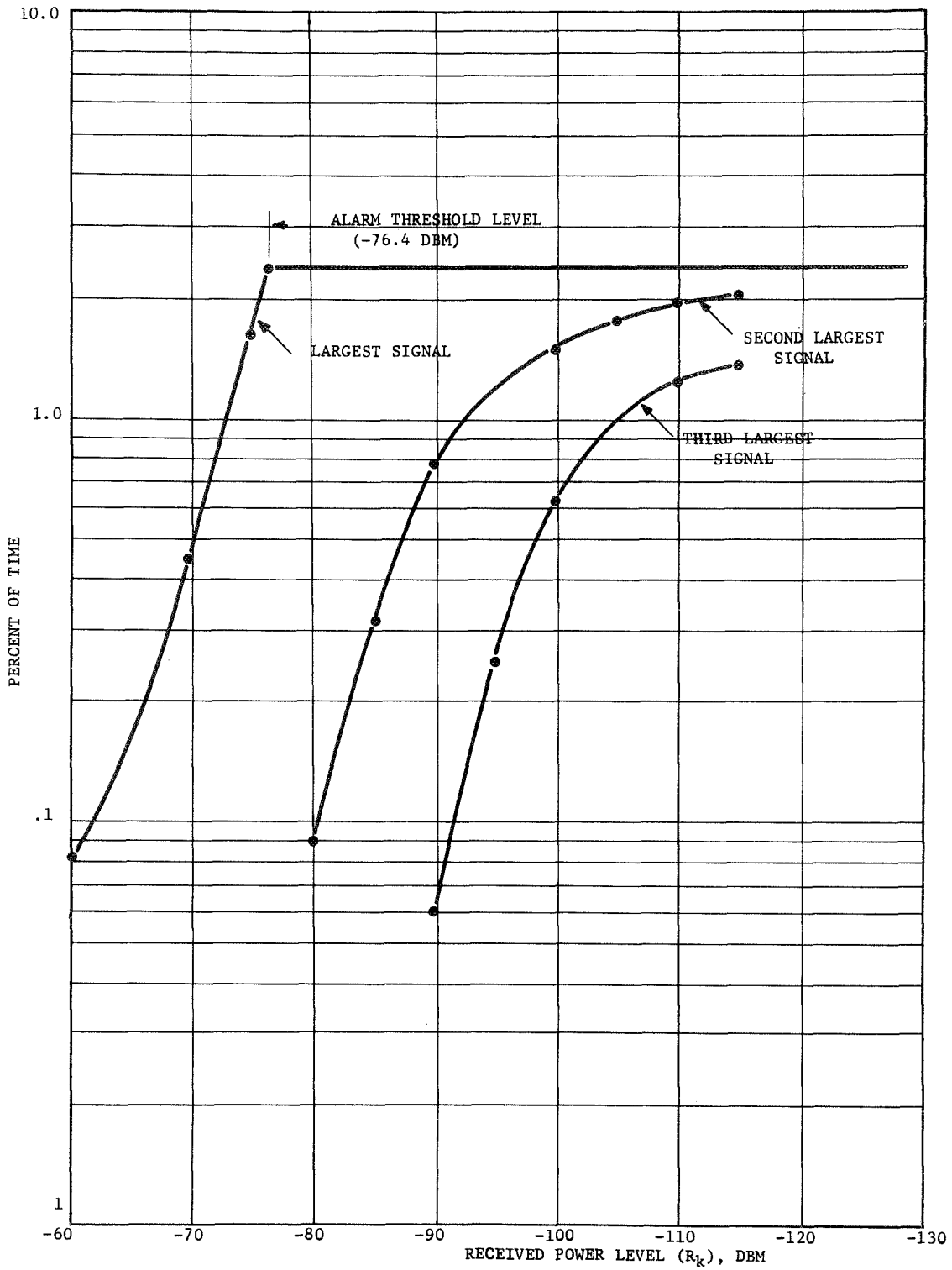


Figure 10. Average percentage of time that the received power level is greater than R_k for alarm situations only.

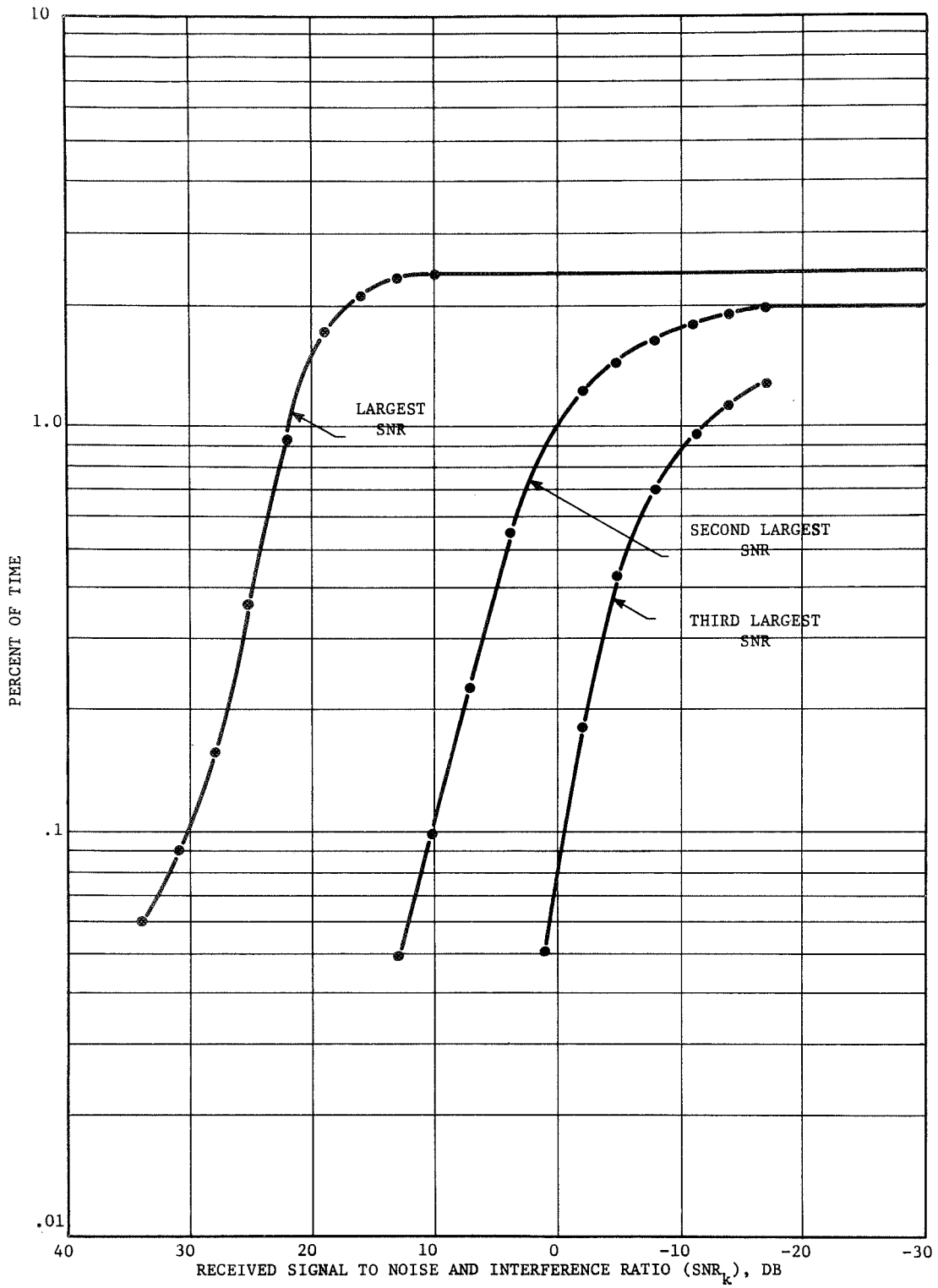


Figure 11. Average percentage of time that the receiver signal to noise and interference power ratio is greater than SNR_k for alarm situations only.

noise will not be at a level such that they interfere with the proper operation of the warning system. The signal to noise plus interference ratios during an alarm are sufficiently high such that additional information, such as range acceleration, can be derived with the signal processing equipment.

4. Typical Signal Spectra in While in Alarm Status

It is informative to note in detail the power levels and frequencies of the five largest signals (with closing doppler) from which the statistics of Fig. 10 and 11 are obtained. Table 1 shows a partial list of these five largest signals during alarm conditions. The Table indicates the power levels, signal to noise plus interference ratios, and doppler frequencies as shown in the Table heading. The specific cases shown in Table 1 were selected at random from the total of 131 alarm cases observed in the hour 11 data base.

It should be noted that in most cases the fifth largest signal is considerably below the receiver noise level hence, the data indicate approximately the situation that would be observed on a audio signal analyzer looking at the differentiated signal from the doppler filter in the receiver. (i.e. usually less than 5 signals are observable)

D. RECEIVED SIGNAL AND INTERFERENCE LEVELS VS TIME

While the operation of the system is adequately explained by the statistical curves given in the preceding sections, it is interesting to examine the time history of specific receiver operation. For this reason, a particular receiver was selected from the "threat selection tables" given in reference 1. This track was selected because a situation occurred in which an alarm should have been noted on the receiver. The track selected was track 98 in the hour 11 data base, which had a total flight time of approximately 11 minutes and was arriving at the terminal.

Figure 12 plots the received power levels versus time for the largest signal received, the largest differentiated signal, and the noise plus interference power level versus time. For this particular simulation run,

Table 1. Examples of signal levels and frequencies while in an alarm status.
 (S_1, S_2 etc are the signal levels in dbm, f_1, f_2 , etc. are the
 corresponding doppler frequencies in cps)

Receiver Noise and Interference Level (dbm)	S_1	S_2	S_3	S_4	S_5	f_1	f_2	f_3	f_4	f_5
-98	-76	-122	-245	-275	-303	1182	1142	517	451	543
-97	-75	-122	-245	-275	-303	1082	1102	516	445	543
-97	-74	-122	-245	-274	-305	951	1063	516	438	407
-96	-74	-122	-244	-277	-304	807	1024	516	323	407
-95	-72	-120	-238	-259	-269	797	1194	688	541	463
-95	-74	-120	-238	-261	-271	587	1132	687	406	339
-96	-76	-129	-136	-263	-269	1457	1257	1750	221	297
-95	-75	-95	-98	-98	-113	1457	968	1702	177	1385
-96	-73	-117	-129	-136	-265	1523	1236	1226	1923	218
-94	-72	-94	-95	-110	-118	1523	988	2061	1651	865
-95	-74	-114	-121	-132	-138	1264	33	897	1001	1511
-93	-71	-94	-95	-109	-129	1264	926	1934	1651	2127
-96	-75	-121	-132	-138	-199	985	842	973	1481	186
-92	-73	-94	-94	-108	-113	985	1786	893	1700	1099
-93	-75	-91	-95	-106	-111	757	2054	818	1851	1256
-90	-77	-90	-91	-101	-120	1585	1641	1312	1253	192
-92	-74	-83	-98	-106	-113	1721	1435	1626	1933	1894
-89	-71	-87	-90	-102	-113	1721	1820	1334	1173	385
-93	-72	-82	-97	-106	-113	1689	1356	1617	1720	1890
-90	-71	-85	-89	-101	-109	1689	1887	1334	1161	574
-93	-69	-82	-96	-105	-112	1645	1262	1606	1706	1885
-89	-69	-83	-89	-101	-106	1645	1888	1333	1150	764
-92	-68	-82	-95	-104	-112	1421	951	1596	1692	1792
-88	-68	-81	-92	-103	-103	1421	1818	952	945	963

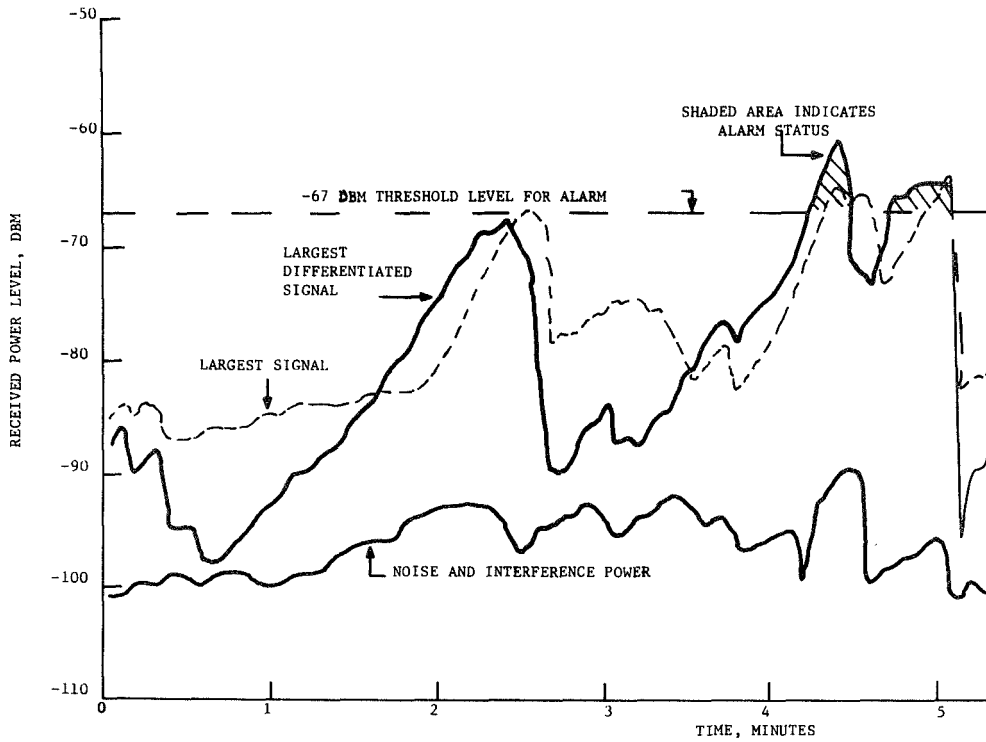


Figure 12. Signals and noise power received at receiver on aircraft of track 98 (hour 11). Time base is the time from the start of the track.

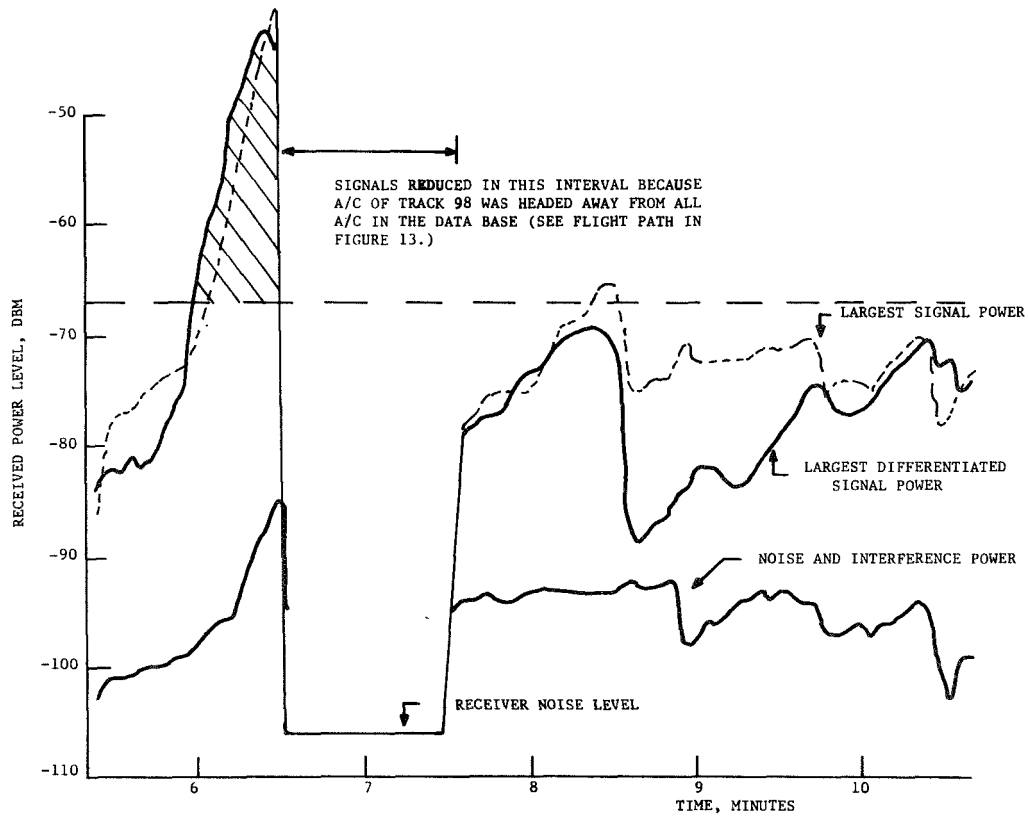


Figure 12. (Continued).

a minus 67 dbm power level represented a threshold corresponding to $R^2_{\tau} = 1,000 \text{ nm}^2\text{-sec}$ (note that the threshold level is different from that used on the statistical curves, however the geometrical warning criteria is the same as given in eq. 3). Note that the noise plus interference power level is well down from the signal levels throughout the whole track. Three separate alarm periods are indicated by the shaded area where the largest differentiated signal exceeds the threshold level.

At 6 1/2 minutes after the start of the track the signals appear to drop out and all power levels reduced to the receiver noise level. The reason for this dropout was examined in detail and determined to be due to the fact that the aircraft of track 98 was heading away from all other aircraft in the data base during the time interval of the dropout. Figure 13 plots the flight path of track 98 so that the position on the track can be correlated with the signals received. At the time of the signal dropouts the aircraft track 98 was headed away from the airport at a range of approximately 12 miles.

Also indicated on Fig. 13 are the tracks of aircraft that caused the receiver of track 97 to indicate an alarm. The first two alarms were received just after 4 minutes in the track when the aircraft observed other aircraft on the final approach to the runway (track 87). The third alarm occurred due to a crossover of track 97 just after 6 minutes into the track. At the time the alarm was received on track 98, the approximate time to closest approach was 33 seconds and the projected miss distance was .75 n. mi. Track 98 was at 2700 ft altitude and descending, while track 97 was at 1700 ft. and flying level. At the point of maximum signal, the slant range was .81 n. mi. and the approximate time to closest approach was 24 seconds. The altitude separation at the point of closest approach was somewhat less than 250 ft.

From examination of this specific case, which can probably be considered typical, we see again that the interference levels are not severe and that the differentiated signal does give a good indication of a potentially

hazardous situation. The first two alarms received at the receiver occurred during a turning maneuver by the tracked aircraft and hence did not represent a hazardous situation. The last alarm, however, would certainly be an encounter of the type that would be considered potentially hazardous.

E. DISTRIBUTION OF POWER LEVELS FOR IDEALIZED SYSTEMS

For system design, it is important to be able to estimate the range of signal levels to be received from the desired target as well as that from other targets which may cause interference. While this has been accomplished by direct simulation of the specific LRC system using the data base, certain general results from the statistical analyses of reference [2] prove useful for estimation of dynamic ranges and interference levels for other systems under consideration.

A histogram of the distribution of the range to the closest aircraft from hour 11 data is shown in Fig. 14. This histogram represents an approximation to the probability density function of the probability of observing, from a randomly selected aircraft, another aircraft within a range increment ΔR . The histogram data, when plotted on lognormal probability paper, indicates that the range distribution over the region 0-10 n. mi. can be approximated by a lognormal density function with mean (μ_1) and variance (σ_1^2) of:

$$\begin{aligned}\mu_1 &= \ln 4.0 \\ \sigma_1^2 &= .25\end{aligned}\tag{5}$$

where the basic units are nautical miles.

A plot of the lognormal distribution corresponding to these parameters is shown on Fig. 14 for comparison with the histogram data. Thus, we have,

$$f_1(R) \approx \frac{1}{\sqrt{2\pi} \sigma_1 R} \text{Exp} \left\{ -\frac{1}{2\sigma_1^2} (\ln R - \mu_1)^2 \right\}\tag{6}$$

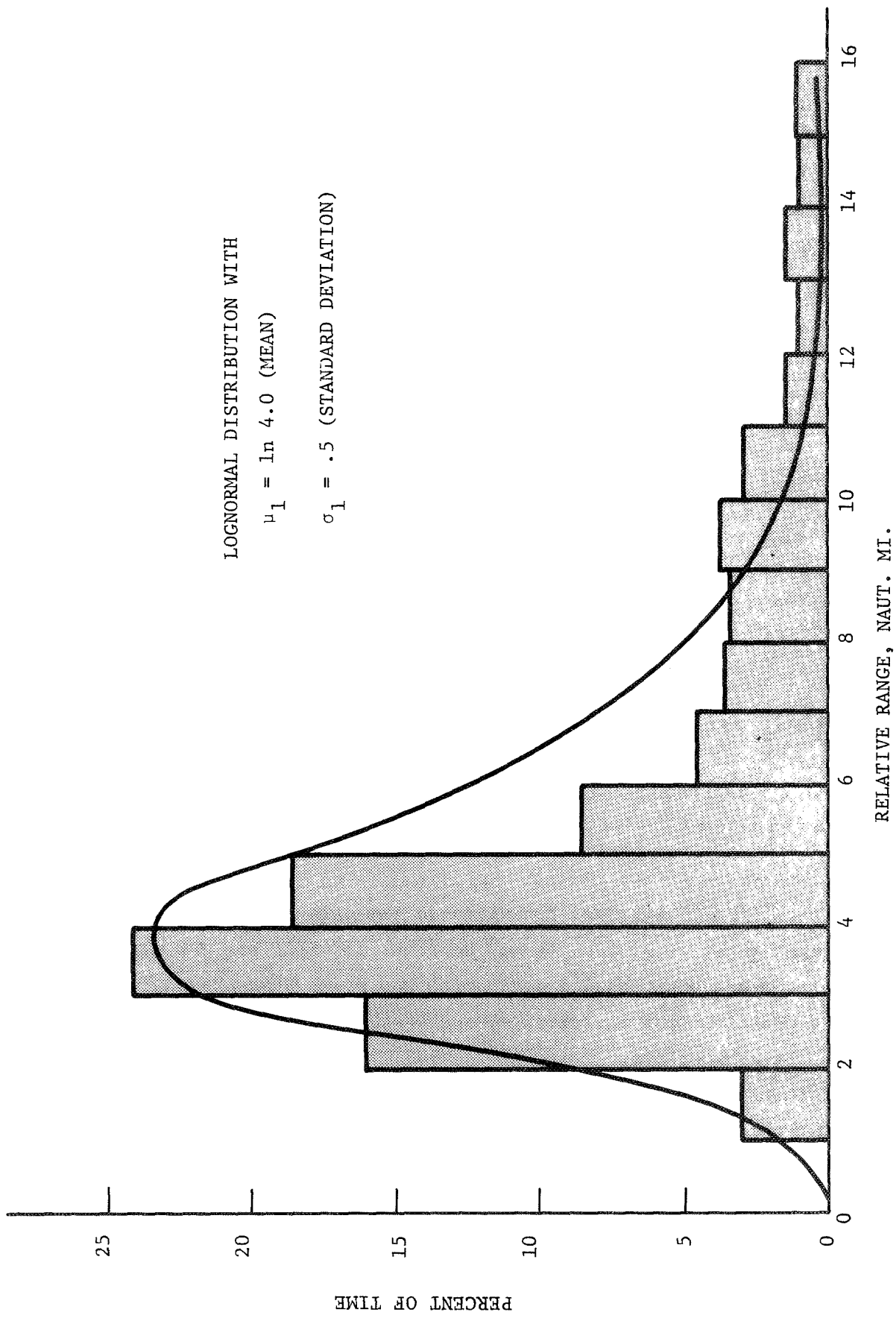


Figure 14. Distribution of relative range to closest aircraft.

where $f_k(R)$ is the probability density function of the range to the k th closest aircraft from a randomly selected aircraft under hour 11 conditions.

Similarly, for the second closest aircraft to a randomly selected aircraft, we have the distribution shown in Fig. 15. The mean and standard deviation for these data are

$$\begin{aligned}\mu_2 &= \ln 6.0 \\ \sigma_2^2 &= .44\end{aligned}\tag{7}$$

and $f_2(R) \approx \Lambda(\ln 6.0, .44)$, where $\Lambda(\mu, \sigma^2)$ designates the lognormal distribution with mean μ and variance σ^2 .

For the third, fourth, and fifth closest aircraft, we have from the data,

$$f_3(R) \approx \Lambda(\ln 8.0, .38),\tag{8}$$

$$f_4(R) \approx \Lambda(\ln 9.6, .25),\tag{9}$$

and $f_5(R) \approx \Lambda(\ln 11.4, .22).$ \tag{10}

The fits of the lognormal functions to the data are shown in the plot on lognormal paper, Fig. 16. As may be seen, the fits are not perfect, however, no other analytical distribution was found that provided a better fit. The distributions investigated included the Rayleigh, Rice, Poisson, and normal distributions.

Some theoretical justification can be given for the lognormal distribution in that it arises under conditions when a change in a variate is a random proportion of the previous value of the variate [5].

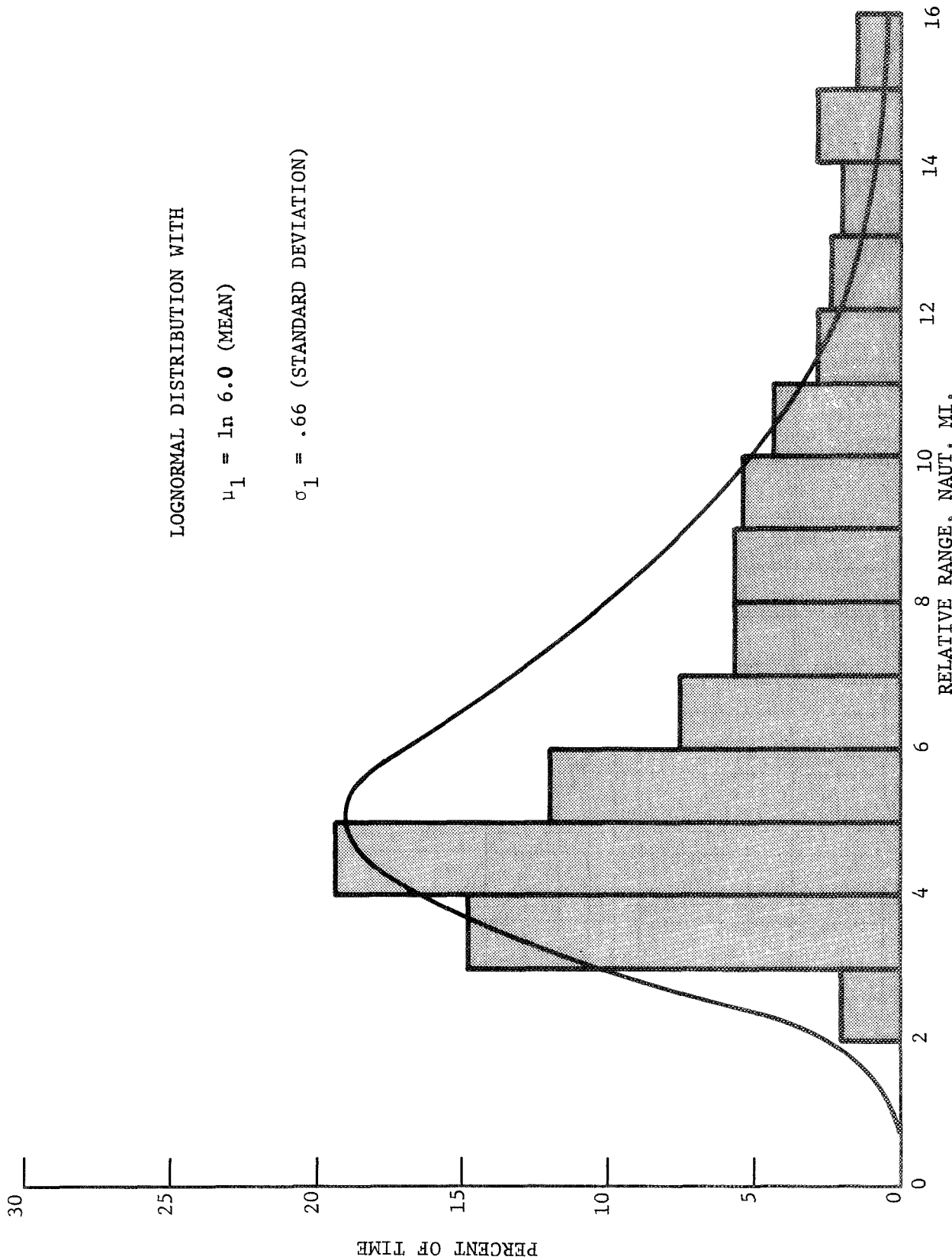


Figure 15. Distribution of relative range to second closest aircraft.

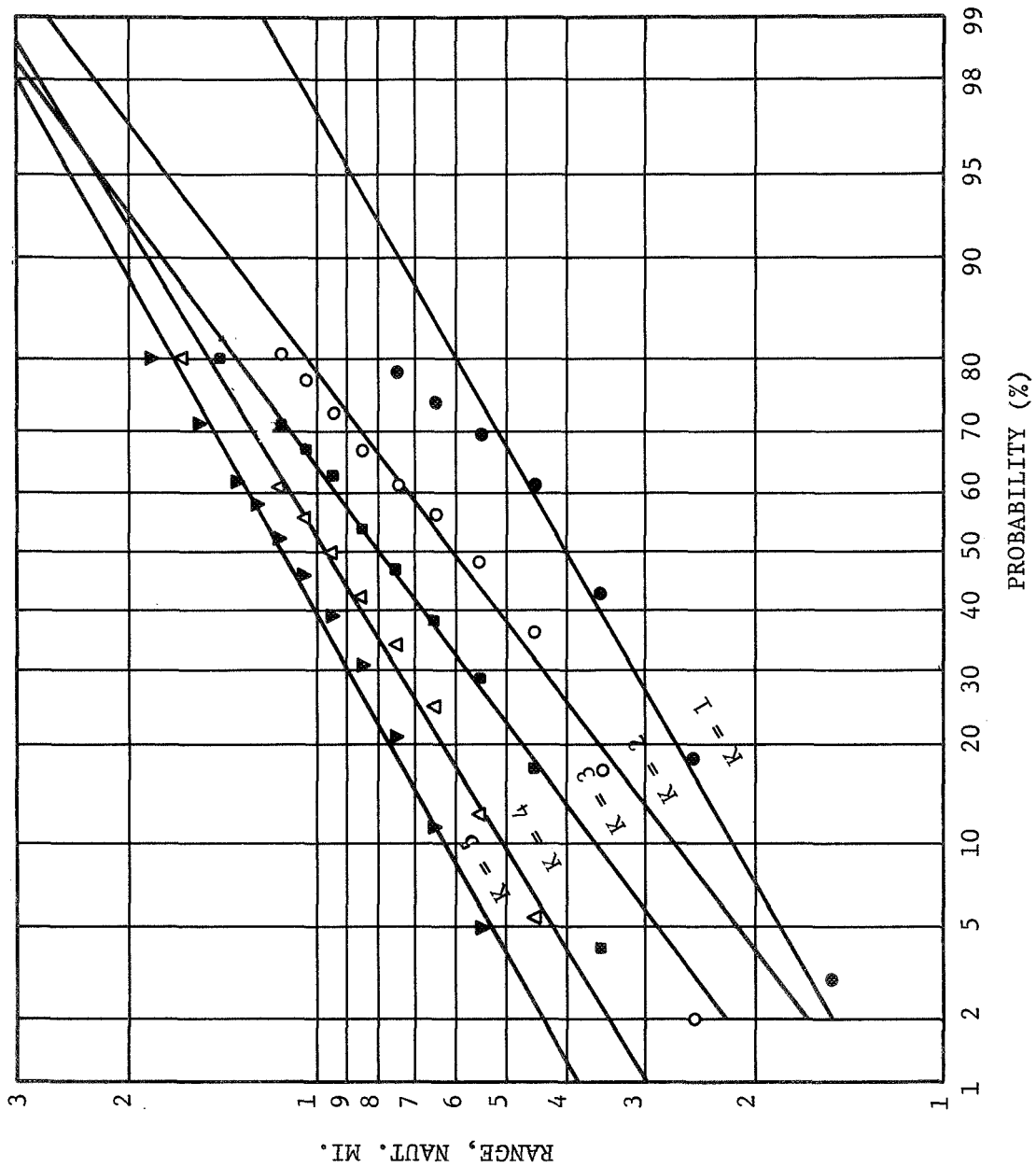


Figure 16. Relative range distributions plotted on lognormal scale to indicate fit of data to the lognormal distribution function.

Thus, if we assume that pilots fly such that the relative closing velocity is proportional to the relative range, with a random proportionality constant ϵ_j ; we have

$$\frac{\Delta R_j}{\Delta t} \approx \epsilon_j R_j \quad (11)$$

where the j subscript indicates the j th time instant and Δt is the time increment. Rearranging Equation (11) and summing over j gives

$$\sum_{j=1}^n \frac{\Delta R_j}{\Delta t R_j} = \sum_{j=1}^n \epsilon_j \quad (12)$$

If each increment is small, and taking $\Delta t = 1$ without loss of generality,

$$\frac{1}{\Delta t} \sum_{j=1}^n \frac{\Delta R_j}{R_j} \approx \int_{R_0}^{R_n} \frac{dR}{R} = \ln R_n - \ln R_0 \quad (13)$$

where R_0 is the initial range and R_n is the range at $j = n$. Thus,

$$\ln R_n = \ln R_0 + \epsilon_1 + \epsilon_2 + \dots + \epsilon_n \quad (14)$$

By the central limit theorem, $\ln R_n$ will be asymptotically normal (since it is the sum of a large number of small random effects), hence R_n will be distributed lognormally. Note that the same result is obtained if we assume that the change in relative range is randomly proportional to the existing range.

The lognormal distribution has transformation properties that are extremely useful. These properties are summarized in a theorem from Aitchison and Brown [5]:

If X is $\Lambda(\mu, \sigma^2)$ and b and c are constants ($c = e^a$),
then c_X^b is $\Lambda(a + b\mu, b^2\sigma^2)$."

Using this theorem, we can determine the probability density of the power received at a randomly selected aircraft i . To relate power received to the relative range, we assume isotropic antennas for both transmitting and receiving, and use the radar range equations:

$$R^{-6} \text{ case: } P_j = \frac{P_j \lambda^2}{(4\pi)^2 R^2 L_s} = K_j^b / R^6 \quad (15)$$

$$R^{-4} \text{ case: } P_j = \frac{P_i^t \lambda^2 \sigma_j}{(4\pi)^3 R^4 L_s} = K_j^r / R^4 \quad (16)$$

where P_j = power received at aircraft i from aircraft j
 P_j^t = power transmitted at aircraft j
 λ = transmitted wavelength
 L_s = system losses
 σ_j = radar cross section of target j
 P_i^t = power transmitted at i
 r, b = superscripts indicating R^{-6} and R^{-4} cases.

Thus, if $f_k^b(P)$ denotes the probability density function of the power received at i from the k th closest aircraft to aircraft i , we can write, using the theorem above and the previously found distributions;

R-6 case:

$$f_1^b(P) = \Lambda(\ln K_1^b - 6 \ln 4.0, 9) \quad (17)$$

$$f_2^b(P) = \Lambda(\ln K_2^b - 6 \ln 6.0, 15.8) \quad (18)$$

$$f_3^b(P) = \Lambda(\ln K_3^b - 6 \ln 8.0, 13.7) \quad (19)$$

$$f_4^b(P) = \Lambda(\ln K_4^b - 6 \ln 9.6, 9) \quad (20)$$

$$f_5^b(P) = \Lambda(\ln K_5^b - 6 \ln 11.4, 7.9) \quad (21)$$

Similar results are easily found for the R^{-4} (two-way path) case if desired.

Care should be taken in using these density functions since the $f_k^b(P)$ for $K > 1$ are conditional density functions, with the condition being that there are $K-1$ aircraft closer to aircraft i . For isotropic antennas, and if all K_k^b are equal, this is equivalent to saying that $K-1$ aircraft provide a larger power level at aircraft i .

A further useful property of the lognormal distribution is that:

$$\Lambda(x) = N(\ln x) \quad (22)$$

where N indicates a normal distribution. Using this property and the previously mentioned transformation theorem, we can write

$$10 \log x = 4.34 \ln x$$

$$\text{therefore,} \quad \Lambda(P^{4.34}) = N(\ln P^{4.34}) = N(10 \log P) \quad (23)$$

Hence, the power in db or dbm is normally distributed. We apply the transformation $P^{4.34}$ to the $f_k^b(P)$ functions using the transformation theorem as follows:

$$\text{if} \quad f_k^b(P) = \Lambda(\mu_k, \sigma_k^2)$$

$$\text{then} \quad f_k^b(P^{4.34}) = \Lambda(4.34\mu_k, 18.8\sigma_k^2)$$

$$\text{and} \quad f_k^b(P_{db}) = N(4.34\mu_k, 18.8\sigma_k^2) \quad (24)$$

where $P_{db} = 10 \log P$. Note that if the R^{-4} (two way path) range equation is used, the power in db or dbm is still distributed normally.

In order to illustrate the results, we assume all K_k^b are equal, and note that K_k^b represents the power received at aircraft i from another aircraft at a range of one nautical mile. $10 \log K_k^b$ is this power in db or dbm depending on the reference power units. If we designate this power level as S_{db}^b , the expressions for the density functions become:

$$\frac{R^{-6}}{f_1^b(P_{db})} = N(S_{db}^b - 36.0, 169) \quad (25)$$

$$f_2^b(P_{db}) = N(S_{db}^b - 46.8, 298) \quad (26)$$

$$f_3^b(P_{db}) = N(S_{db}^b - 54.3, 257) \quad (27)$$

$$f_4^b(P_{db}) = N(S_{db}^b - 58.8, 169) \quad (28)$$

$$f_5^b(P_{db}) = N(S_{db}^b - 68.7, 148) \quad (29)$$

The probability that the power received from the k th closest aircraft will exceed a level ξ is determined from

$$\text{Prob. } (P_{db}^k > \xi) = 1 - \int_{-\infty}^{\xi} f_k(P_{db}) dP_{db}. \quad (30)$$

Curves indicating this probability for $K = 1, \dots, 5$ are shown in Fig. 17.

The distributions for the R^{-4} case are, for equal K_j^r ;

R^{-4} case

$$f_1^r(P_{db}) = N(S_{db}^r - 24, 75.2) \quad (31)$$

$$f_2^r(P_{db}) = N(S_{db}^r - 31.2, 132.4) \quad (32)$$

$$f_3^r(P_{db}) = N(S_{db}^r - 36.2, 114.4) \quad (33)$$

$$f_4^r(P_{db}) = N(S_{db}^r - 39.2, 75.2) \quad (34)$$

$$f_5^r(P_{db}) = N(S_{db}^r - 45.8, 66.0) \quad (35)$$

where S_{db}^r is the reference power level (i.e. power received from target at one n. mi.).

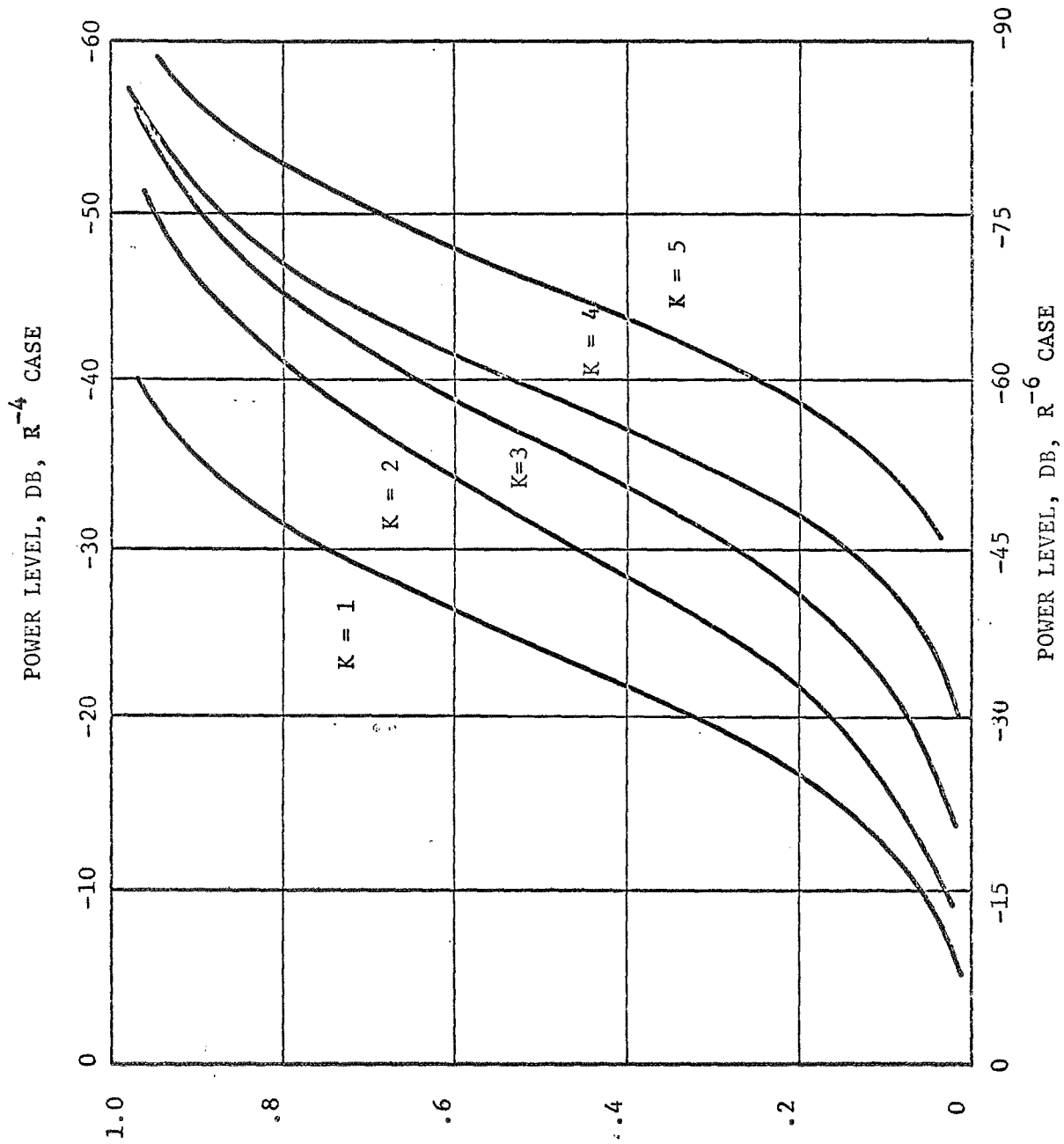


Figure 17. Approximate probability that the power level from the kth closest aircraft exceeds the stated level. 0 db is the power level received from a target at 1 n. mi. range.

V. FLIGHT TEST EVALUATION OF RANGE MEASUREMENT ERROR

A. GENERAL DESCRIPTION

Two of the warning systems constructed by LRC personnel were installed in a pair of DC-4 aircraft and subjected to flight tests. The major objectives of the flight test series were to evaluate measurement errors, to determine the sources and magnitudes of errors, and to determine the system performance under actual flight conditions.

During the flight test operations at Wallops Island, Virginia, the positions of the two aircraft were measured by the Wallops FPQ-6 and FPS-16 radar systems. The radar data obtained during the flight test was then processed by Wallops personnel to derive relative data between the pair of aircraft. This data was furnished to RTI on digital magnetic tape to provide an input to the flight test simulations and to permit comparison of simulated, experimental, and geometrical measurements.

The flight paths flown were a series of converging pairs with various predetermined miss distances, both horizontally and in altitude. In all cases, the aircraft were separated in altitude to prevent any danger to the aircraft. Table 2 summarizes the flight test designations, the altitude separation, the attempted and actual miss distances, and the magnetic headings of the aircrafts as provided by the pilots. The aircraft air speeds were on the order of 140-160 knots for all flights, and in all cases straight line flight paths were attempted by the pilots.

Two computer programs were developed to process the flight test data. One program designated as GE01 processed the Wallops radar data and generated the aircraft flight paths along with geometrical parameters and values of warning criteria calculated from the geometry. The second program was the modification of the simulation program as described in Section III. This latter program is discussed in detail in the following section.

B. FLIGHT TEST SIMULATIONS

During flight test operations, the relative azimuth angle, relative elevation angle and relative range between the two aircraft are measured with the ground radar system. Calculations made using the ground radar

Table 2. Flight test parameters.

Date	Flight No.	Run No.	Alt. Separation (ft)	Attempt Miss Dist. (nm)	Actual Miss (nm)	Heading (deg.)		Remarks
						Aircraft #432	Aircraft #438	
3/18/69	7a	10	1,000	0	1/8	348	263	Intended True Courses 270°; 348°
	7b	11	1,000	1	1 1/2	358	260	
	7c	11	1,000	1	1 1/4	335	278	
	7d	14	1,000	3	2 1/2 - 3	350	287	
3/25/69	8b	17	1,000	0	1/8	96	276	
	8c	18	1,000	1	1	297	117	
	9a	20	1,000	2	-	095	275	
3/27/69	9b	20	1,000	2	≈ 2	273	104	Head on Timer Failed
	9c	21	1,000	3	≈ 3	095	283	Head On
	9d	23	1,000	4	≈ 4	275	110	Head On
	9e	16	2,000	0	≈ 0	095	282	Head On
	10a	26	1,000	0	1/8	312	280	Intended True Courses 270°; 310°
3/28/69	10b	27	1,000	1	1 1/4	310	282	
	10c	28	1,000	2	2 1/4	313	286	
	10d	25	2,000	0	1/4	311	285	
	10e	24	3,000	0	1/8	311	290	

measurements are designated as geometrical values. Also, during flight test operations the received signal voltages are recorded to give the values of parameters as measured with the warning system. Calculations made using these latter measurements are designated as experimental values. Parameter values calculated using the simulation program are designated as calculated values.

Figure 18 shows an example of the computer printouts obtained at 5 second intervals throughout each of the flight test. The first line on the printout provides the flight identification, the elapsed time since the start of the flight, and the time of day (gmt). The next section on the printout indicates geometrical parameters calculated directly from the ground radar data. These parameters include:

- (1) xyz coordinates for both aircraft
- (2) the relative range between aircraft
- (3) closing velocity in knots (V_c)
- (4) the rate of change of closing velocity (V_{cd})
- (5) the normalized range acceleration, \dot{R}/R (v_{cn})
- (6) the normal velocity component (V_n)
- (7) the time to closest approach (T)
- (8) the approximate time to closest approach (τ)
- (9) the approximate miss distance (D)
- (10) the exact miss distance (R_o)
- (11) geometrical value of $R^2\tau$ (β)
- (12) the value of modified tau (τ_m)
- (13) the relative azimuth and elevation angles for both aircraft

The next section on the printout sheet gives the transponder outputs for system 1 and system 2. Following this list the gain variations of each of the system antennas are listed. The gain variations are referenced to a 0 db level (head-on conditions).

GEOMETRICAL PARAMETERS

AIRCRAFT 1 AIRCRAFT 2
 X Y Z X Y Z R VC VCD VCN VN T TAU D RO RFTA TM AZ EU
 (NM) (NM) (NM) (NM) (NM) (NM) (NM) (KTS) (FT/52)(1/4)(KTS)(SEC) (SEC) (NM) (NM) (NM) (NM) (NM) (DEG) (DEG)
 -5.86 -1.57 .82 -7.48 -2.98 .68 2.1 209. 0.0 0.00 0. 36. 37. 0.0 .4 171. 24. 334. 69. -4.

TRANSPONDER OUTPUTS

NOISE POWER (DRM) SYSTEM 1 SYSTEM 2
 SIGNAL POWER (DRM) -23. -23.
 SATURATION FACTOR 8. 9.
 1.14 1.17

ANTENNA GAIN VARIATIONS (DB)

SYSTEM 1 SYSTEM 2
 4.25 TRANSMITTER -1.9 -2.9
 4.25 TRANSPONDER -2.2 -1.1
 2.70 TRANSMITTER -1.9 -1.7
 2.70 TRANSPONDER -2.2 -1.1
 1.95 TRANSPONDER -1.2 -1.1
 1.55 RECEIVER -1.1 -1.2
 TOTAL -3.2 -5.2

RECEIVER OUTPUTS

SYSTEM 1 SYSTEM 2
 SIGNAL LEVEL AT I.F. AMP (DRM) -59.8 -71.6
 SNR AT DOPLER FILTER OUTPUT (DB) -37.1 -35.3
 AGC VOLTAGE (VOLTS) -1.7 -1.6
 VOLTAGE AT L.F. FILTER OUTPUT (VOLTS) -3.3 -3.6
 DOPLER FREQUENCY (CPS) 1112. 1112.
 ALARM STATUS ON ON

MEASURED PARAMETERS

RANGE (NM) 2.1 3.1 3.3 3.95 4.2 5.5
 RANGE RATE (KTS) 209. 209. 209. 209. 209. 209.
 RANGE ACCEL (FT/AS2) 0.0 0.0 0.0 0.0 0.0 0.0
 NORMAL VEL (KTS) 0. 0. 0. 0. 0. 0.
 TAU (SEC) 37. 53. 58. 58. 58. 58.
 RFTA (NM2SEC) 171. 513. 648. 1.99 109.2 1701.4
 MISS DISTANCE (NM) 0.0 0.0 0.0 0.0 0.0 0.0
 MODIFIED TAU (SEC) 24. 30. 30. 30. 30. 30.

CALCULATED % ERROR BREAKDOWN

EXP. SFD DOPLER FIL SLOPE DETECTOR EL TOTAL GAIN RESIDUAL
 44.2 12.4 12.4 7.0 5.1 12.5 11.5 1-2.3*4*6 1-2.3*4*6
 43.8 12.5 12.5 7.0 5.1 12.5 11.5 3.1 -6.8
 199.2 42.4 42.4 22.5 16.0 42.3 38.8 2.7 -7.3
 RANGE (NM) 44.2 12.4 12.4 7.0 5.1 12.5 11.5 3.1 -6.8
 TAU (SEC) 43.8 12.5 12.5 7.0 5.1 12.5 11.5 2.7 -7.3
 RFTA (NM2SEC) 199.2 42.4 42.4 22.5 16.0 42.3 38.8 28.5 -23.6

Figure 18. Example of computer printout for flight test data. These printouts were obtained at five second intervals during each test.

The receiver outputs are listed for both systems. These outputs include signal levels, signal to noise plus interference ratio, AGC voltage, doppler frequency, and the alarm status of the receiver.

The next listing on the computer printout list geometrical, experimental, and calculated values of various geometrical parameters and warning criteria. The calculated values are given in geometrical units and also as voltages measured at the various receiver outputs. Also, in this section the percent errors are calculated for the difference between experimental and geometrical values, calculated and geometrical values, and experimental and calculated values. A description of the expressions used to calculate the values in this section is given in Appendix D .

The last section on the computer printout gives an error breakdown for 3 parameters measured by the receiver; range, tau, and beta. The first column in this section repeats the percent error between the experimental and geometrical (ground radar) values of the parameter. The second column indicates the error due to amplitude variations in the receiver doppler filter. The third column gives the percent error due to deviations of the detector characteristics from linearity. The fourth column indicates the error and measurement due to gain variations of the elevation patterns (transmitter, transponder, and receiver). The fifth column indicates the percent errors due to the complete antenna patterns, again considering all patterns in the system. The sixth column is a fixed error source due to gain calibration errors in the flight test system. That is, the calculated or simulated values of range are based on exact gain calibrations that provide a -85 dbm signal level at a range of 5 miles. During flight test it was determined that the overall gain of the warning system was down somewhat, and this error source reflects the value of range and analogous to the deficiency in system gain of the flight systems.

The last two columns in the error breakdown section indicate residual errors between the experimental and geometrical values that are unaccounted for by the error sources previously considered. The first residual column does not take into account variations in the azimuth patterns of the antennas, while the last residual column is the percent error remaining after effects of the doppler filter, detector slope, and the total antenna patterns are removed. The percent error remaining in this last

column, then, is due to system errors not subtracted out in the calculation (e.g. saturation of the transponder) and factors not considered in the simulation such as aircraft deviations from straight line, level flight.

It should be noted that the systems were calibrated over a range from 1 to 5 nautical miles, hence relatively large errors outside of this range were expected and are felt to be unimportant in system evaluation.

C. FLIGHT TEST RESULTS

Extensive analyses of the flight test data have been conducted by LRC personnel, using the results of the flight test simulation program to determine contribution to the measurement errors of various system components. Thus, in this section the major emphasis will be on documentation of the flight paths and comparison of the simulated and experimental relative range data. Since the relative velocity between aircraft is simply a frequency measurement on the doppler signal, errors in measurement of this parameter were small.

For each flight test as listed in Table 2, the following plots have been made:

- (1) the flight path of the aircrafts.
- (2) the geometrical, calculated and experimental range measurements vs. flight time.
- (3) the percent difference between calculated and experimental range measurements plotted vs. the value of geometrical range.

These curves indicate the accuracy of the simulation of the actual flights. It should be recalled that the residual differences between the calculated and experimentally measured values of range are most likely due to variations of the aircraft from straight line level flight. Computer printouts listing the data at the approximate time the alarm was received in the simulated system are given in Appendix F.

Inspection of the plots indicates that for most flights the difference between simulated and experimental values of range was within 15 percent over the calibration range of the equipment. An exception to this agreement was found in flight 8C, where the experimental and calculated values disagreed by as much as 80 percent. Although the cause for this discrepancy has not yet been determined, it is felt to be due to a mistake in calibration of the experimental data in the digitizing process.

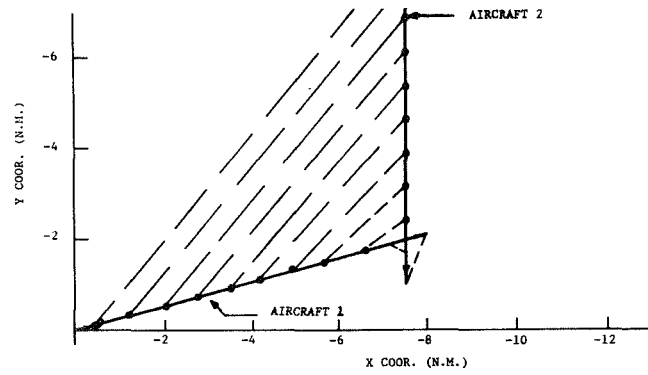


Figure 19-A. Ground tracks for flight test 7A.

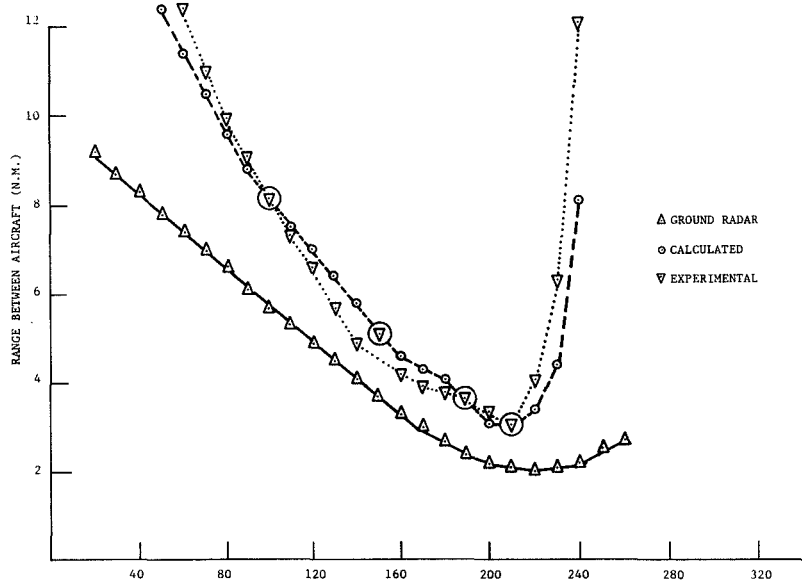


Figure 19-B. Ground radar experimental, and calculated values of relative range vs. time, test 7A.

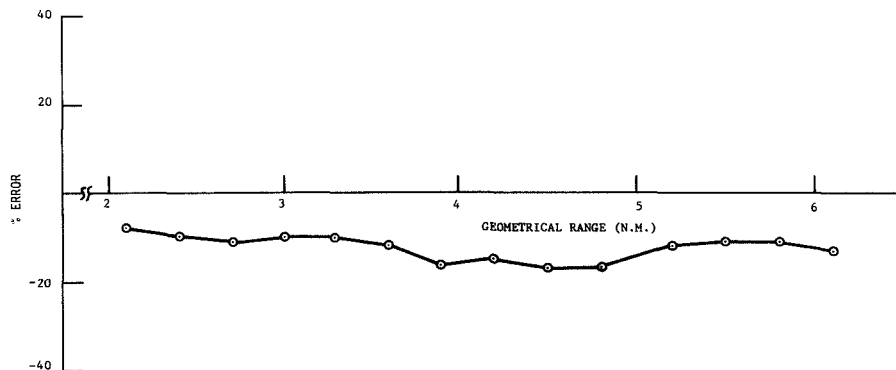


Figure 19-C. Percent error between calculated and experimental range measurements plotted vs ground radar (geometrical) range, test 7A.

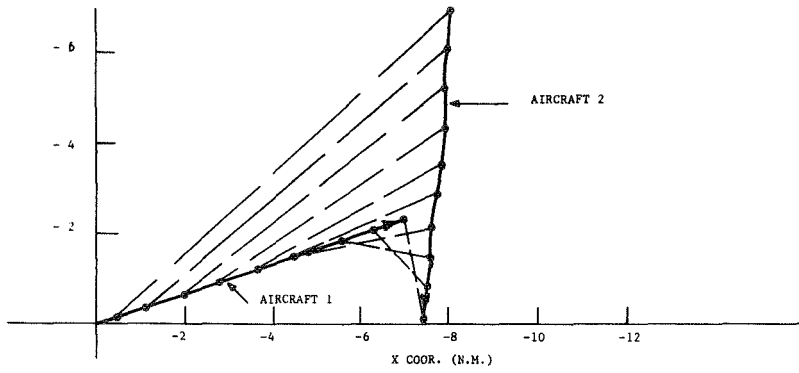


Figure 20-A. Ground tracks for flight test 7B.

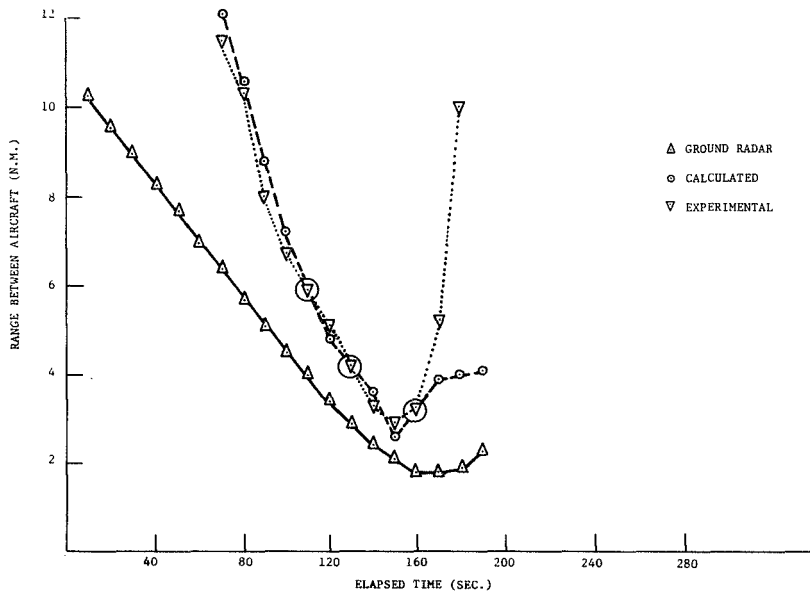


Figure 20-B. Ground radar experimental, and calculated values of relative range vs. time, test 7B.

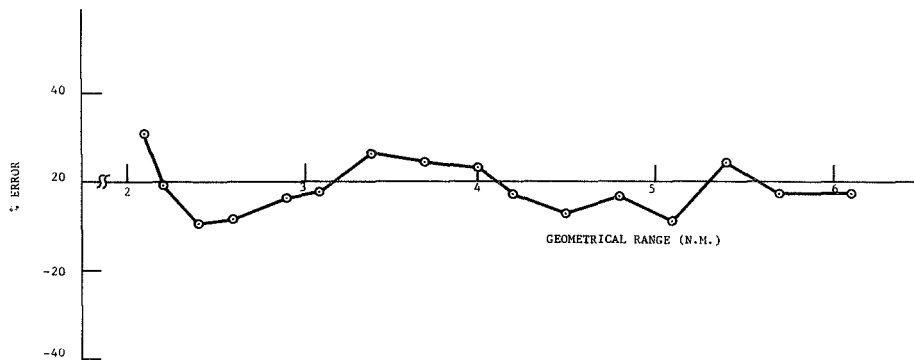


Figure 20-C. Percent error between calculated and experimental range measurements plotted vs ground radar (geometrical) range, test 7B.

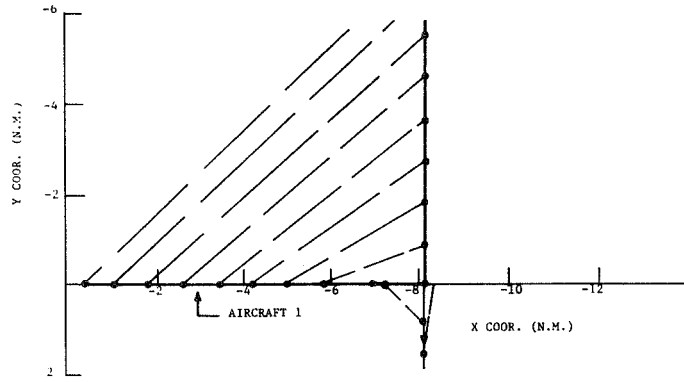


Figure 21-A. Ground tracks for flight test 7C.

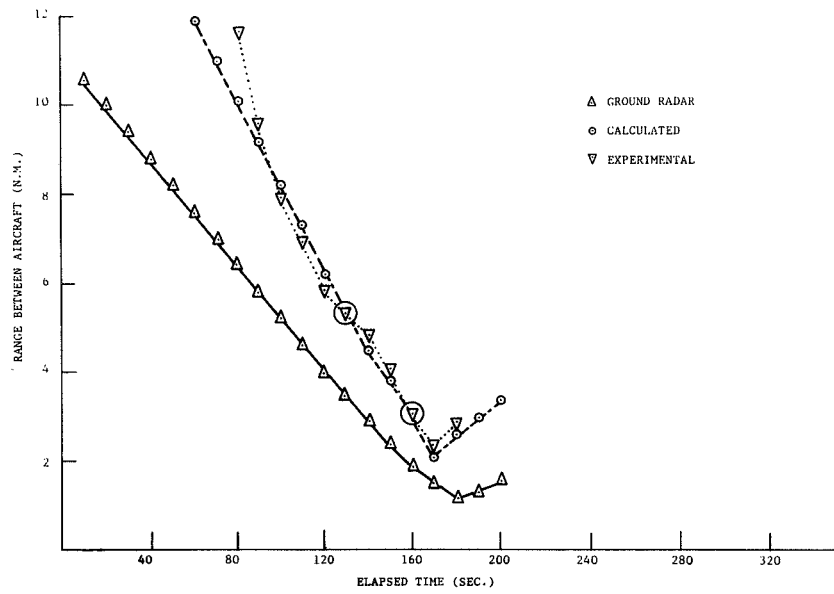


Figure 21-B. Ground radar, experimental, and calculated values of relative range vs. time, test 7C.

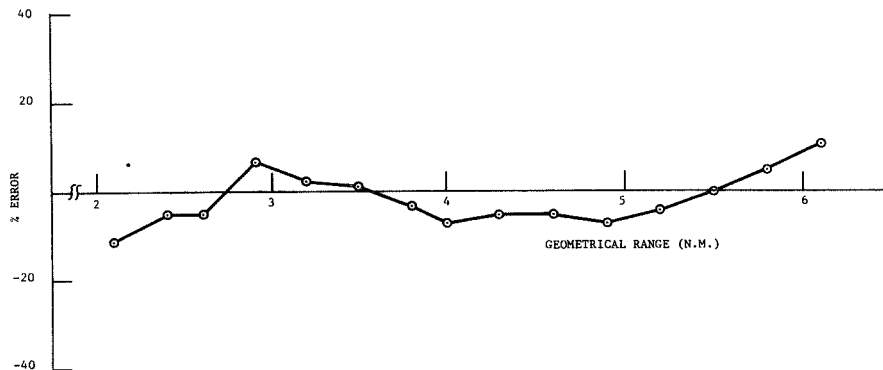


Figure 21-C. Percent error between calculated and experimental range measurements plotted vs ground radar (geometrical) range, test 7C.

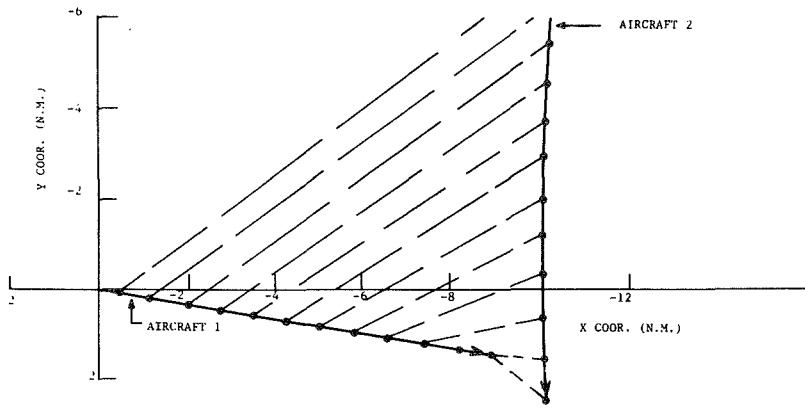


Figure 22-A. Ground tracks for flight test 7D.

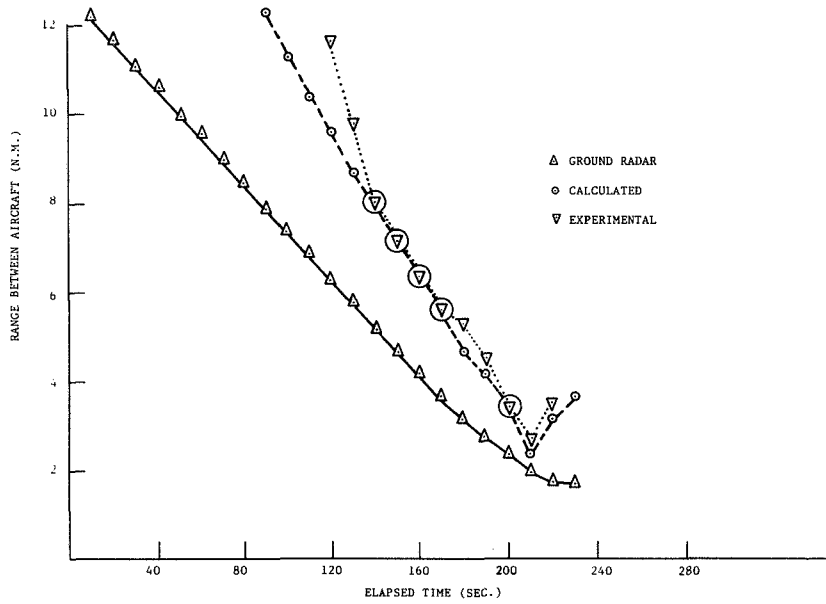


Figure 22-B. Ground radar, experimental, and calculated values of relative range vs. time, test 7D.

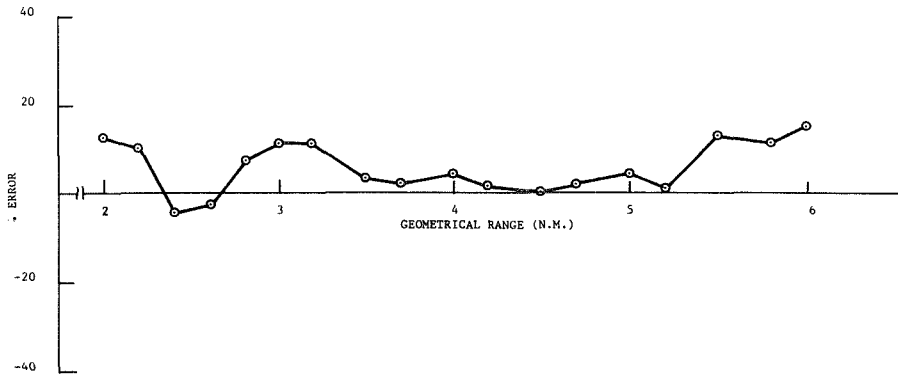


Figure 22-C. Percent error between calculated and experimental range measurements plotted vs ground radar (geometrical) range, test 7D.

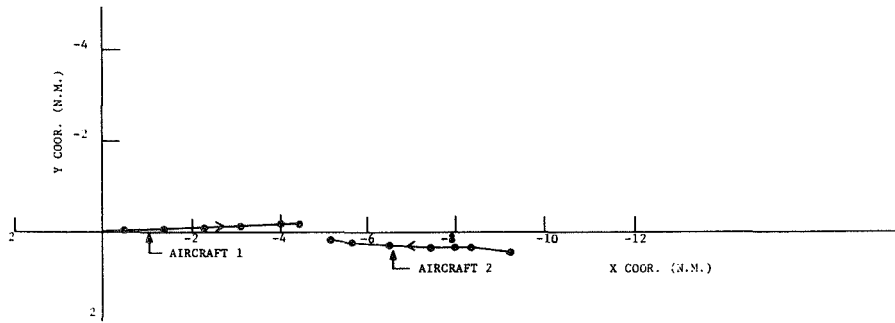


Figure 23-A. Ground tracks for flight test 8B.

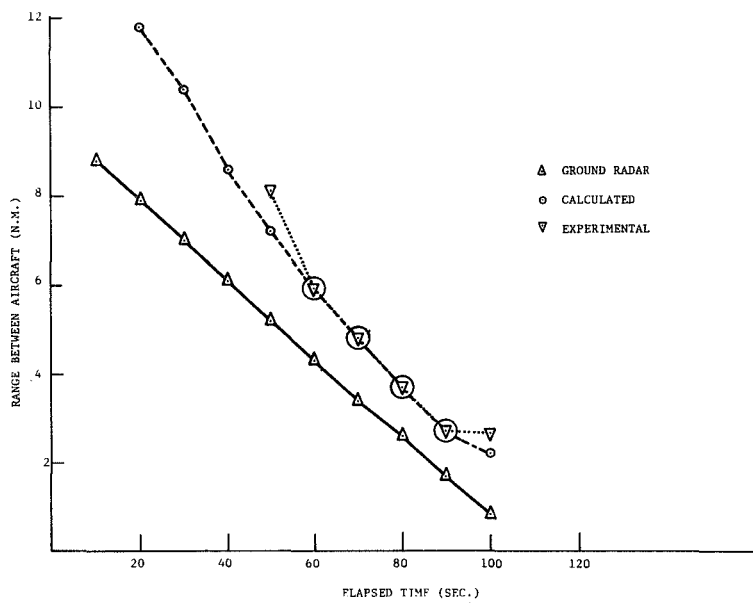


Figure 23-B. Ground radar, experimental, and calculated values of relative range vs. time, test 8B.

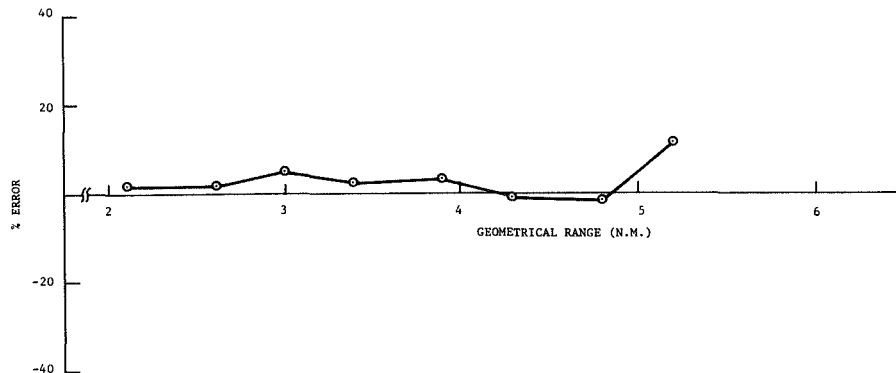


Figure 23-C. Percent error between calculated and experimental range measurements plotted vs ground radar (geometrical) range, test 8B.

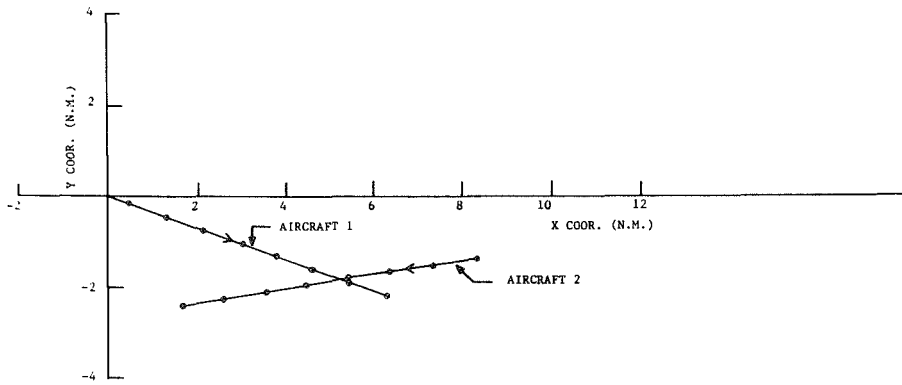


Figure 24-A. Ground tracks for flight test 8C.

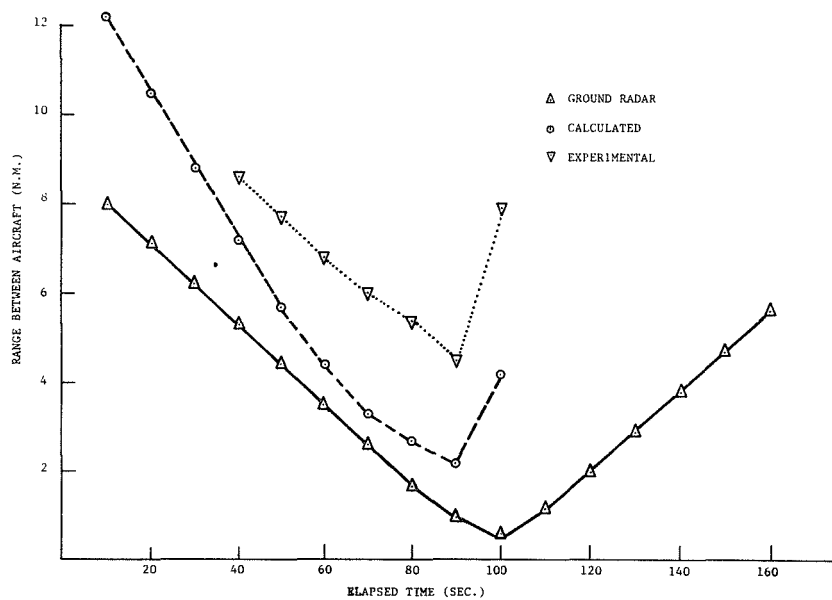


Figure 24-B. Ground radar, experimental, and calculated values of relative range vs. time, test 8C.

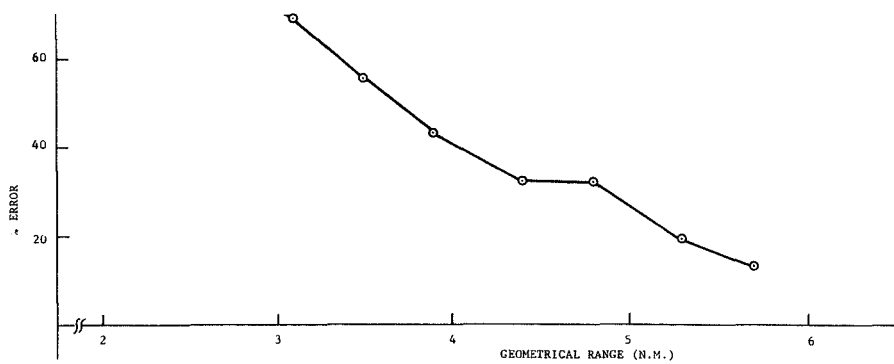


Figure 24-C. Percent error between calculated and experimental range measurements plotted vs ground radar (geometrical) range, test 8C.

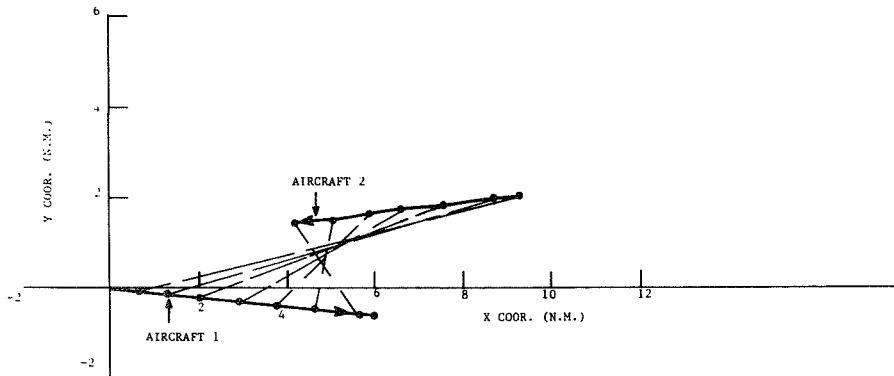


Figure 25-A. Ground tracks for flight test 9B.

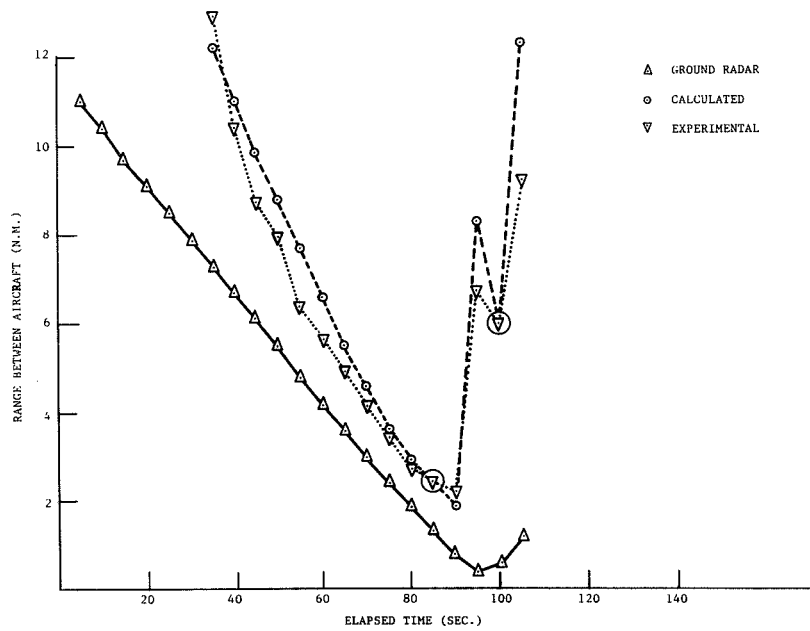


Figure 25-B. Ground radar, experimental, and calculated values of relative range vs. time, test 9B.

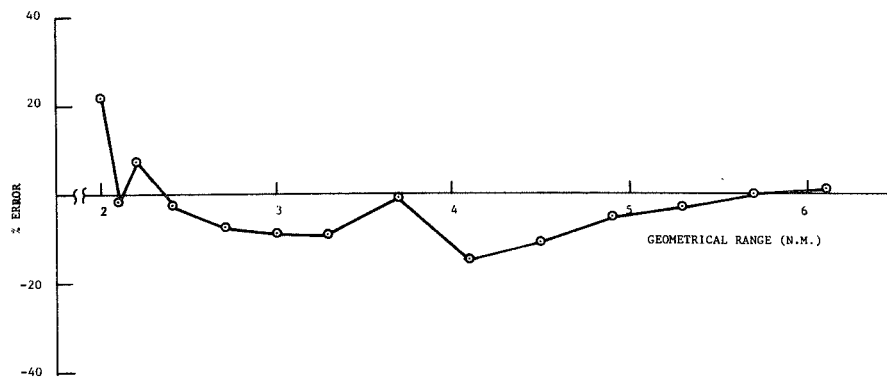


Figure 25-C. Percent error between calculated and experimental range measurements plotted vs. ground radar (geometrical) range, test 9B.

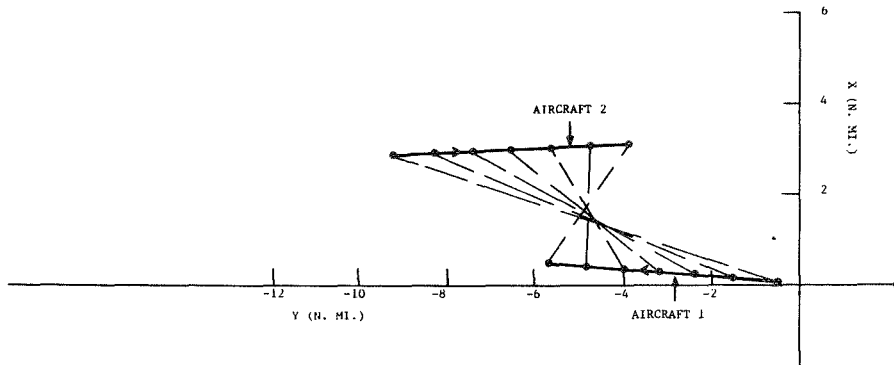


Figure 26-A. Ground tracks for flight test 9C.

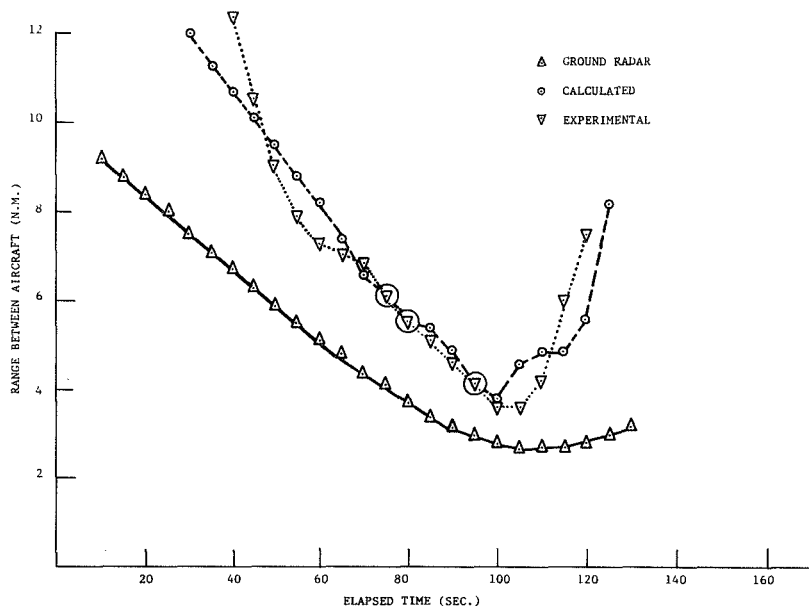


Figure 26-B. Ground radar, experimental, and calculated values of relative range vs. time, test 9C.

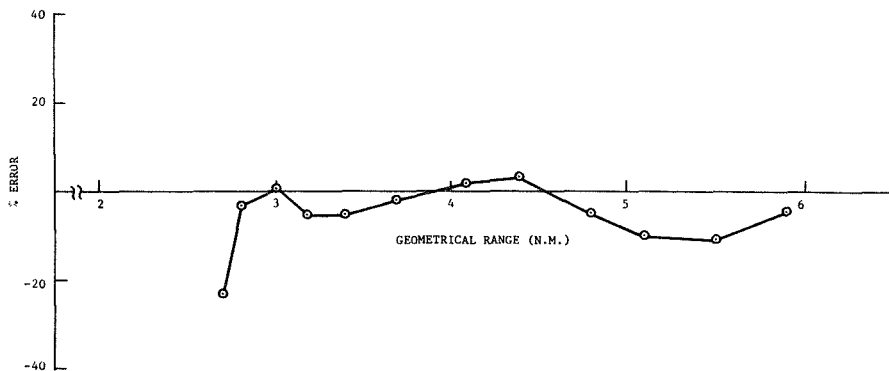


Figure 26-C. Percent error between calculated and experimental range measurements plotted vs. ground radar (geometrical) range, test 9C.

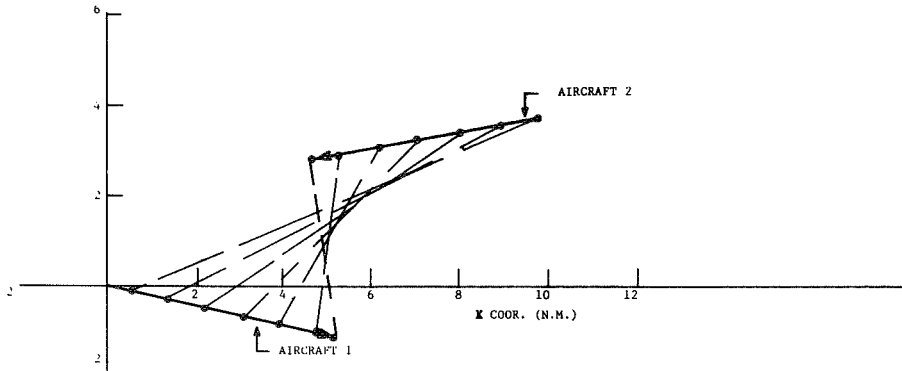


Figure 27-A. Ground tracks for flight test 9D.

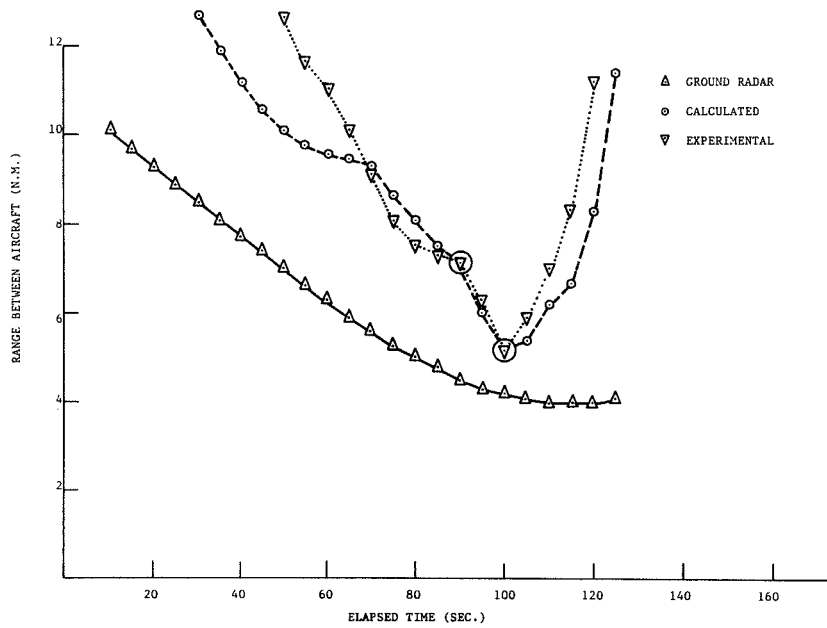


Figure 27-B. Ground radar experimental, and calculated values of relative range vs. time, test 9D.

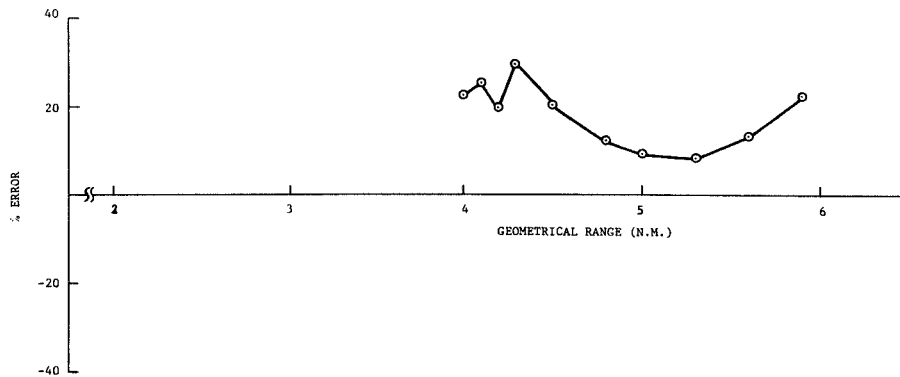


Figure 27-C. Percent error between calculated and experimental range measurements plotted vs. ground radar (geometrical) range, test 9D.

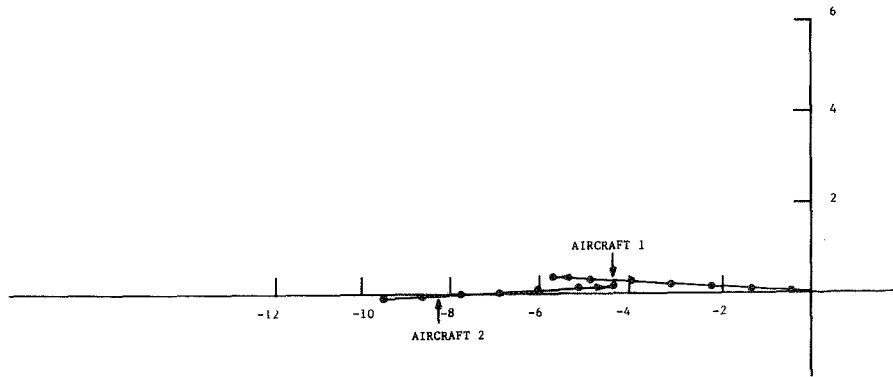


Figure 28-A. Ground tracks for flight test 9E.

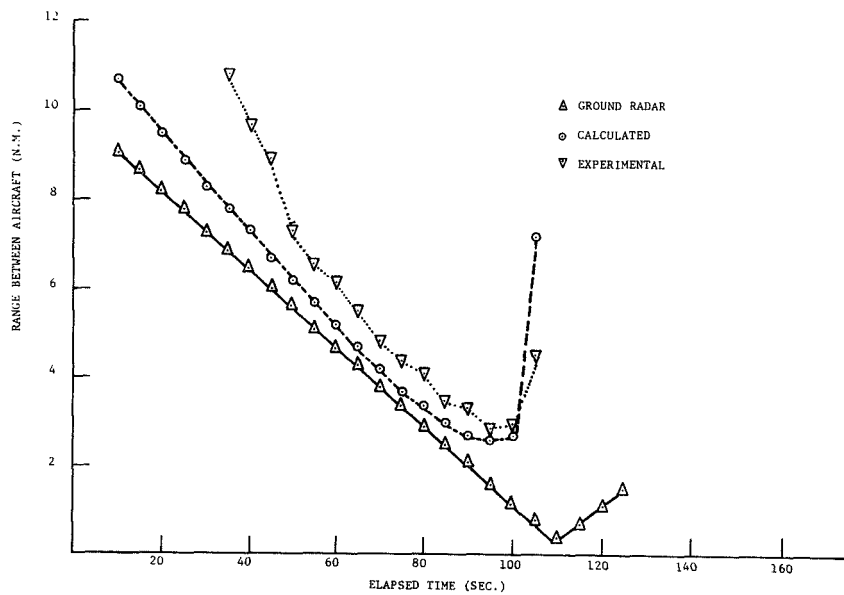


Figure 28-B. Ground radar experimental, and calculated values of relative range vs. time, test 9E.

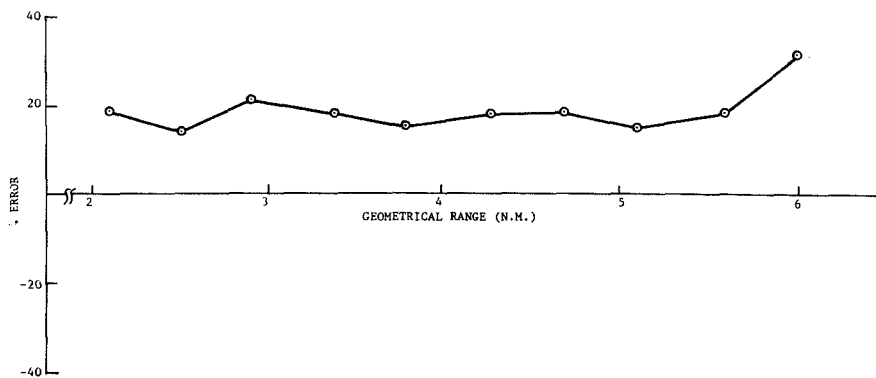


Figure 28-C. Percent error between calculated and experimental range measurements plotted vs. ground radar (geometrical range, test 9E).

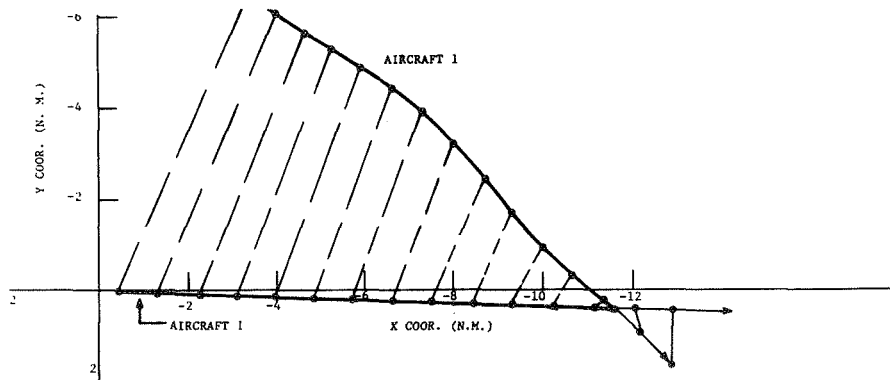


Figure 29-A. Ground tracks for flight test 10A.

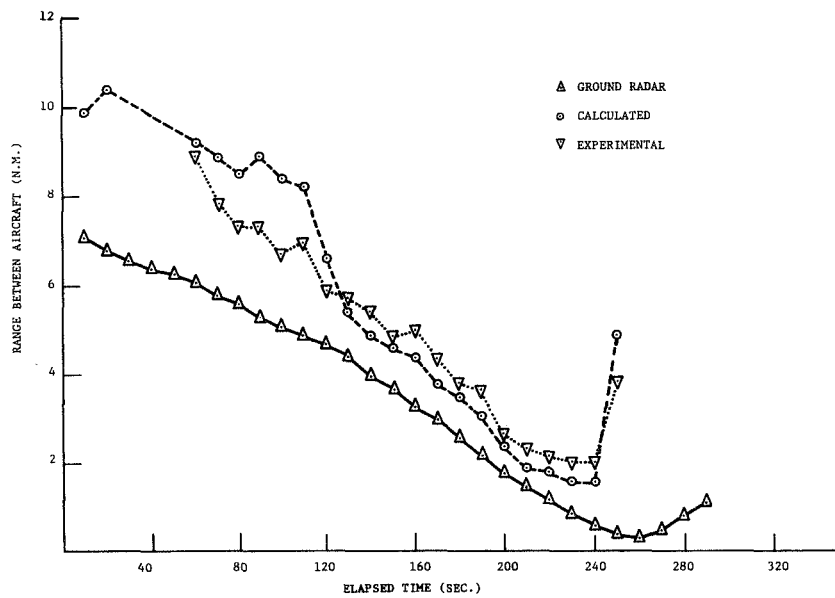


Figure 29-B. Ground radar, experimental, and calculated values of relative range vs. time, test 10A.

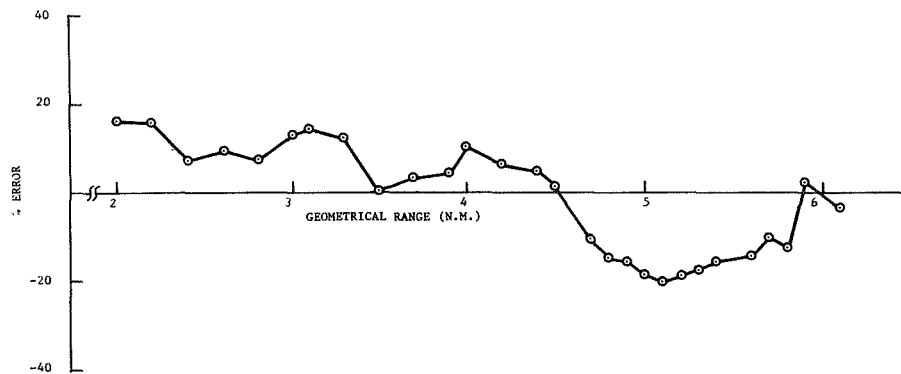


Figure 29-C. Percent error between calculated and experimental range measurements plotted vs. ground radar (geometrical) range, test 10A.

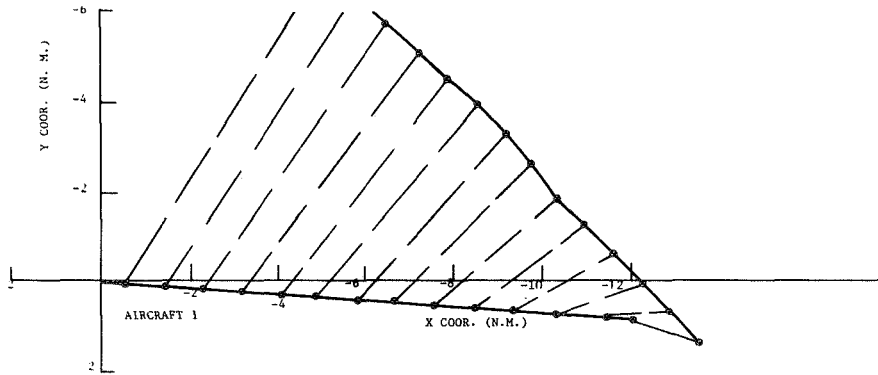


Figure 30-A. Ground tracks for flight test 10B.

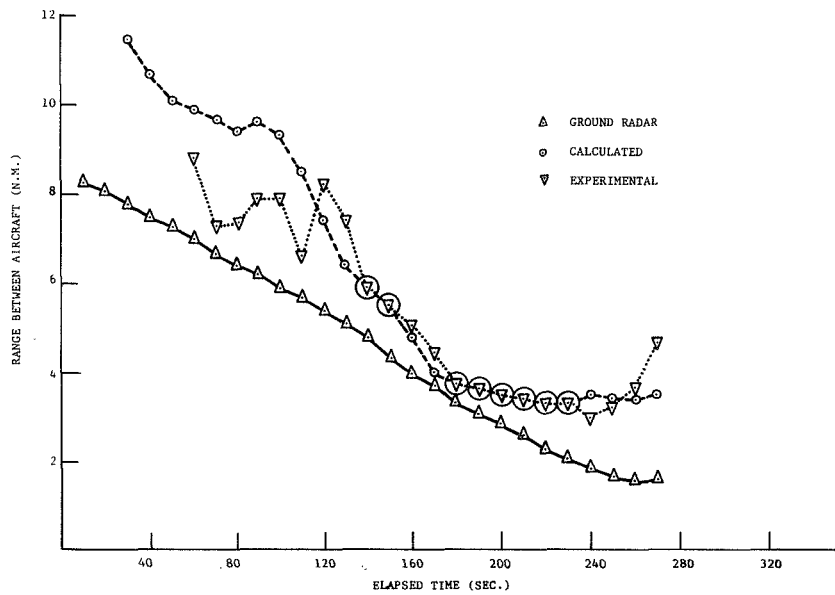


Figure 30-B. Ground radar, experimental, and calculated values of relative range vs. time, test 10B.

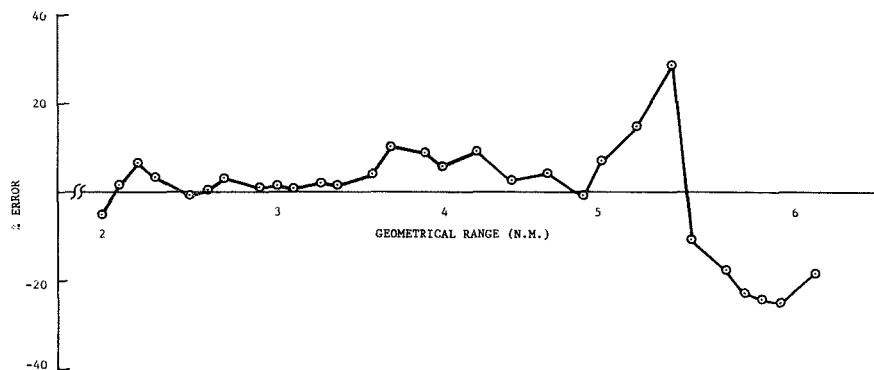


Figure 30-C. Percent error between calculated and experimental range measurements plotted vs. ground radar (geometrical) range, test 10B.

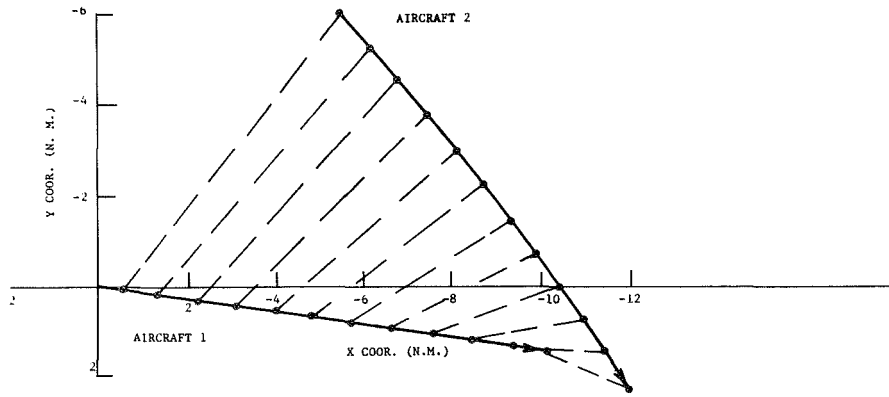


Figure 31-A. Ground tracks for flight test 10C.

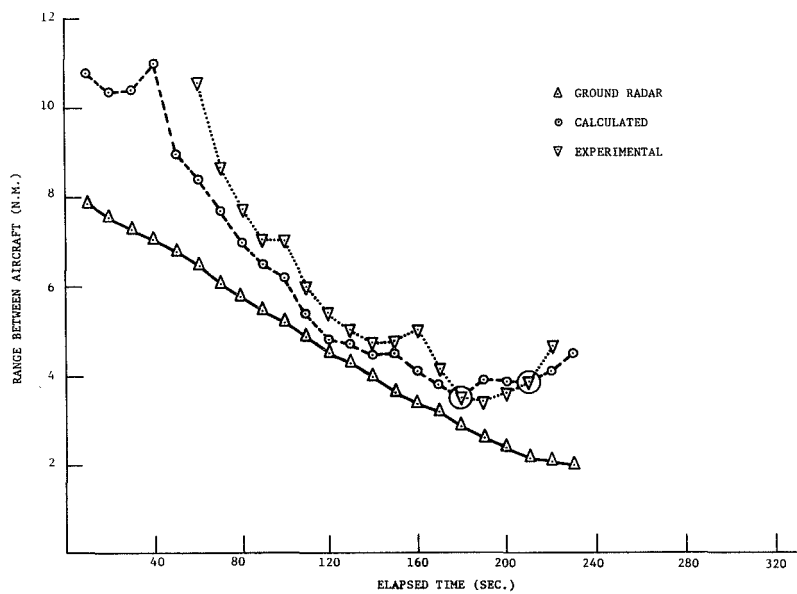


Figure 31-B. Ground radar, experimental, and calculated values of relative range vs. time, test 10C.

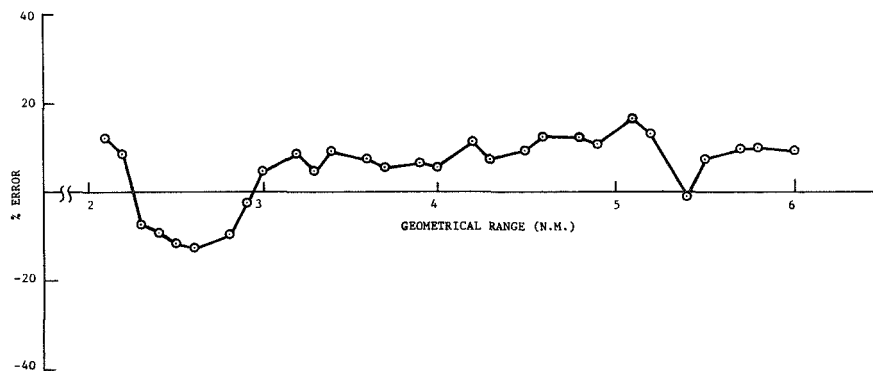


Figure 31-C. Percent error between calculated and experimental range measurements plotted vs. ground radar (geometrical) range, test 10C.

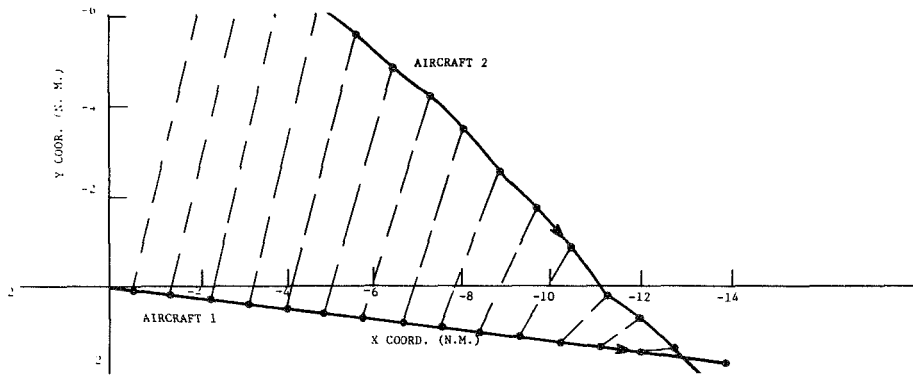


Figure 32-A. Ground tracks for flight test 10D.

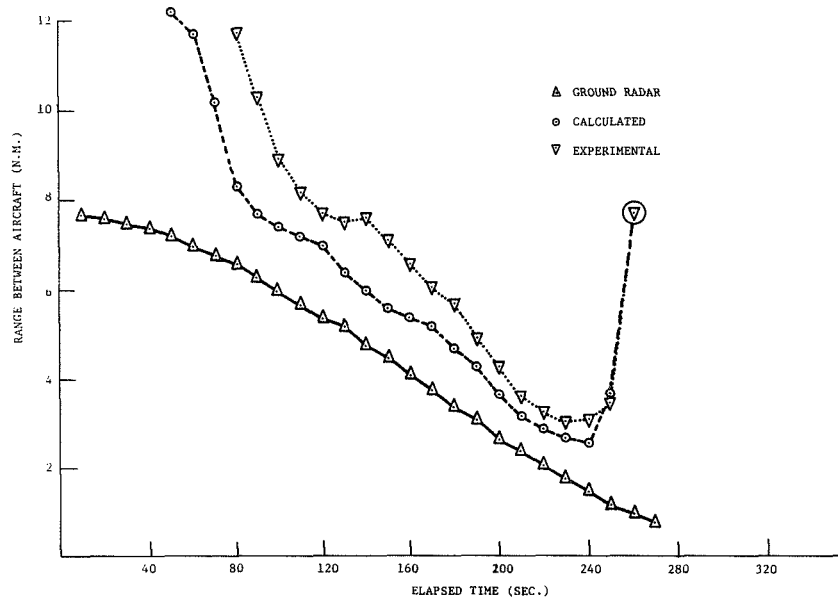


Figure 32-B. Ground radar, experimental, and calculated values of relative range vs. time, test 10D.

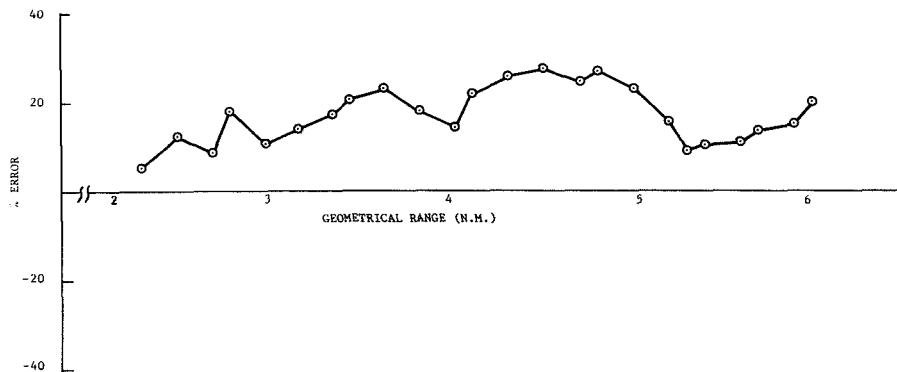


Figure 32-C. Percent error between calculated and experimental range measurements plotted vs. ground radar (geometrical) range, test 10D.

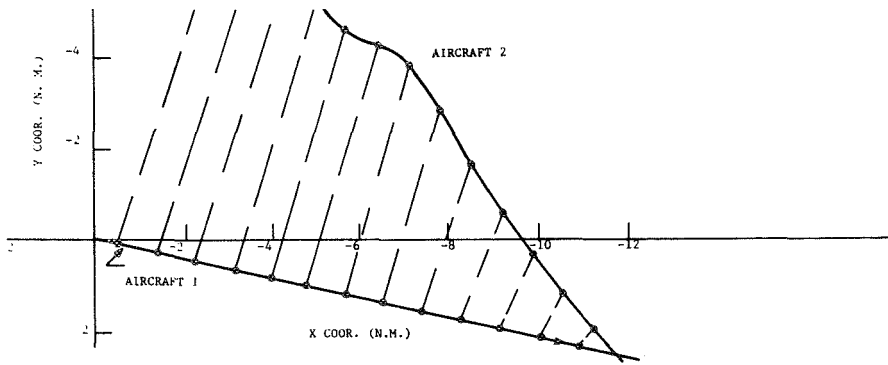


Figure 33-A. Ground tracks for flight test 10E.

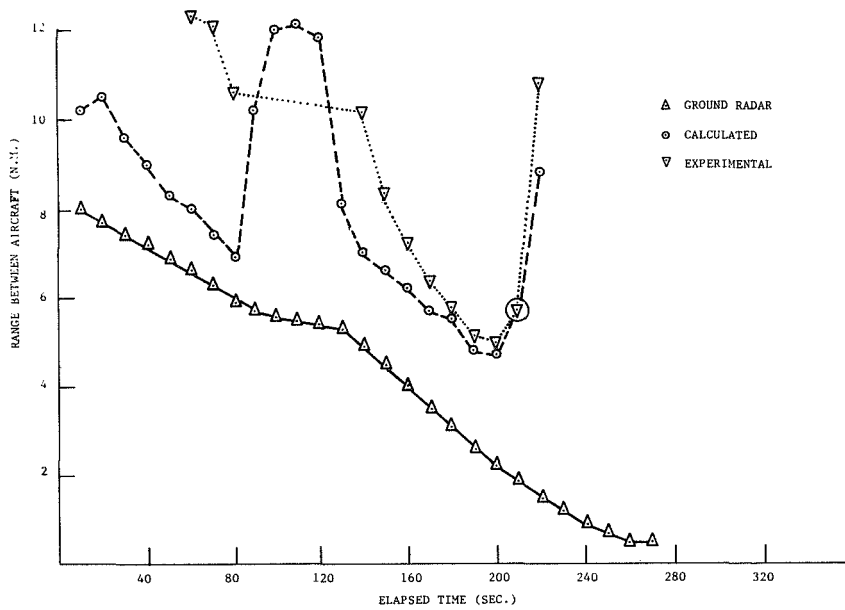


Figure 33-B. Ground radar, experimental, and calculated values of relative range vs. time, test 10E.

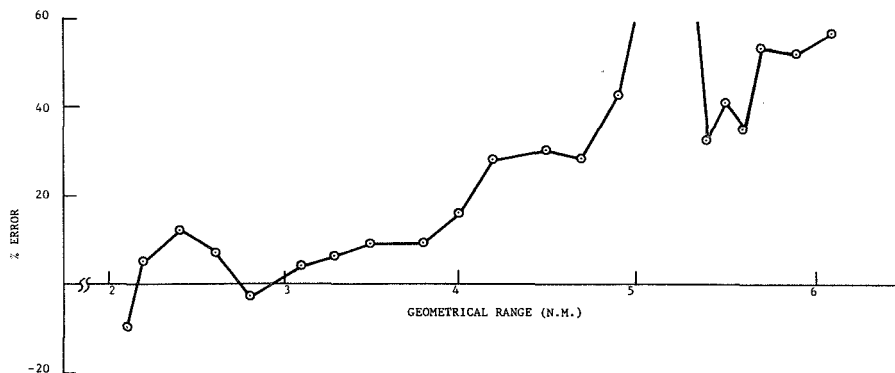


Figure 33-C. Percent error between calculated and experimental range measurements plotted vs. ground radar (geometrical) range, test 10E.

VI. MISCELLANEOUS STUDIES

A. GENERAL

During the course of the contract, several studies were undertaken that have general applicability to the collision-warning problem. These studies include: (1) common definitions of warning times for various system warning criteria, (2) the possibility of alarm suppression due to relative range acceleration threshold logic, (3) comparison of warning times of various systems with equal alarm probability, and (4) warning times required for escape maneuvers.

Other studies were concerned with extension of the "modified tau" warning criteria developed by Collins personnel, Reference [4]. The extensions involved consideration of relative aircraft accelerations as a random variable and the introduction of additional constraints on aircraft acceleration vectors. Also, general results were derived for determination of the DC output of a product detector-limiter circuit with multiple input signals. Results of these latter studies are given in Appendices A and B respectively, while the general studies on system warning times are presented in the following.

B. DEFINITION OF WARNING TIMES

Since some system warning criteria and warning times are derived based on the assumption of nonaccelerating flight, while others are based on accelerating flight with acceleration constraints, it can be misleading to speak of a warning time attained without further elaboration as to the assumptions used.

To provide a common basis for comparison of the protection afforded by the various systems, we define warning times as follows:

t_n = minimum warning time for a nonaccelerating co-altitude collision with a maximum relative velocity of V_m . (i.e. this is the time-to-collision assuming a roll-out to linear flight at the instant the alarm is received, and a subsequent collision)

t_{mh} = minimum warning time achieved for a co-altitude threat under the worst possible conditions within the assumed velocity (V_m) and acceleration (U) constraints. (i.e. this is the time-to-collision assuming flight paths subsequent to the alarm at the maximum relative acceleration and/or the maximum relative velocity until collision occurs)

t_{mv} = warning time for a nonaccelerating collision occurring in the vertical plane with a maximum relative rate of descent or ascent of \dot{h}_m .

In Section VI-C, inhibition of the alarm by range acceleration discrimination is considered. This inhibition will be shown to occur for sets (S_1) of particular trajectories, hence to distinguish warning times for these cases, we define, for systems using \dot{R} measurements for discrimination:

t_n, t_{mh} = same as previous definitions, except trajectories are assumed not in S_1

t_n^d, t_{mh}^d = same definitions as t_n, t_{mh} , except that the times are calculated using the worst-case member of the set of trajectories S_1 . (i.e. for the trajectory that provides the smallest warning time.)

Expressions for the times t_n , t_{mh} , and t_v are easily derived. Let $R(t_o)$ and $\dot{R}(t_o)$ be the relative range and closing velocity at which a given system gives an alarm. The time t_n is then

$$t_n = \min \left\{ \frac{R(t_o)}{\dot{R}(t_o)} \right\} \text{ over } C \quad (36)$$

where C is the contour in the R, \dot{R} plane defined by the system warning criteria.

The minimum warning time for a system that provides an alarm at range $R(t_0)$ and closing velocity $\dot{R}(t_0)$, assuming subsequent relative accelerations no greater than U is derived in [4] (i.e. the modified tau expression)

$$t_1 = \frac{-\dot{R}(t_0) + [\dot{R}^2(t_0) + 2UR(t_0)]^{1/2}}{U} \quad (37)$$

where t_1 designates this warning time. For the case where the trajectory providing the alarm time t_1 does not exceed the velocity constraint, we have for the time t_m ,

$$t_m = \min \{ t_1[\dot{R}(t_0), R(t_0)] \text{ over } C \} \quad (38)$$

where C is again the contour in the R, \dot{R} plane defined by the system warning criteria. If the trajectory exceeds the velocity constraint, (i.e. if $\dot{R}(t_0) - UT_1 > V_m$) graphical or approximation techniques can be used to determine t_m , assisted by the phase plane plot of trajectory slope isoclines given in Appendix C.

For those systems using altitude discrimination of the form $|\Delta A| < \Delta A_k$, the minimum warning time for closing paths in the vertical plane, assuming no acceleration in this plane, is

$$t_v = \frac{|\Delta A|}{\dot{h}_m} \quad (39)$$

Thus, by assuming a maximum closing velocity V_m , a maximum rate of ascent (or descent) of \dot{h}_m , and a maximum relative acceleration U , the defined warning times achieved by the various systems may be determined to provide a common basis of comparison of the protection afforded by the systems.

Table 3. Warning times t_n and t_m as defined in Section VI-B for various system types. The maximum closing velocity assumed is V_m , the maximum relative acceleration is U and the maximum relative rate of descent or ascent is h_m .

System Type and Threshold	Value of t_n	Value of t_m^*
1. Range $R < R_k$	$\frac{R_k}{V_m}$	$\frac{R_k}{V_m}$
2. Tau-range $\tau < \tau_k; R < R_k$	τ_k	$\frac{-R_k + [R_k^2 + 2U\tau_k^2 R_k]^{1/2}}{U\tau_k}$
3. $R^2\tau$ - range $R^2\tau < \beta_k; R < R_k$	$\left[\frac{\beta_k}{V_m} \right]^{1/3}$	smaller of $\frac{-R_k^3 + [R_k^3 + 2UR_k\beta_k^2]^{1/2}}{\beta_k U}$ or $\left[\frac{\beta_k}{V_m} \right]^{1/3}$
4. Modified tau $\tau_m < \tau_{mk}$	$\tau_{mk} + \frac{U\tau_{mk}^2}{2V_m}$	τ_m

* Note: If altitude discrimination ($|\Delta A| < \Delta A_k$) is used, the minimum warning time is the value from the expression listed, or $\Delta A_k/h_m$, whichever is smaller. The minimum warning times may also be determined by R or normal velocity discrimination as discussed in Section VI-C.

For the $R^2\tau$ and tau systems, the minimum warning time approaches zero as the relative closing velocity approaches zero. However, a supplementary (over-riding) range threshold can be used to prevent this situation. Hence, in the work that follows, we will consider these systems with a supplementary range threshold of magnitude R_k .

In Table 3, expressions are given for the defined warning times for the various systems that have been considered, in terms of the warning thresholds and the assumed constraints V_m , \dot{h}_m and U . The effect of range acceleration discrimination on the defined warning times is considered in the following section.

C. ALARM SUPPRESSION DUE TO RELATIVE RANGE ACCELERATION THRESHOLDS

For systems using discrimination based on \ddot{R} measurements (e.g. approximate miss distance thresholds assuming nonaccelerating flight), the measurements will, of course, be erroneous if accelerating flight occurs. Under accelerating conditions, we must consider the possibility that accelerations due to maneuvers will effect the measurement in the worse possible way. These worse case conditions are considered for various systems in the following.

Tau, Range, Normal Velocity System. In this system, normal velocity is estimated in accordance with [2]

$$V_n = \sqrt{R \ddot{R}} \quad (40)$$

which was derived based on nonaccelerating flight paths. The system warning criteria are

$$R/\dot{R} < \tau_k \text{ and } \sqrt{R \dot{R}} < V_{nk} \quad (41)$$

$$\text{or } R < R_k$$

where the k subscripts indicate selected threshold constants.

For closing, nonaccelerating flight, \ddot{R} is positive. For closing accelerating flight, however, \dot{R} can be either positive or negative.

If the magnitude of \dot{R} is sensed, such that the threshold condition is

$$\sqrt{R|\ddot{R}|} < V_{nk} \text{ and } R/\dot{R} < \tau_k \quad (42)$$

and if relative accelerations no greater than U are allowed, the possibility exists that measurements of $|\ddot{R}|$ will equal U . If this is the case, an alarm will be suppressed so long as

$$\sqrt{RU} \geq V_{nk} \quad (43)$$

or until a range less than

$$R_1 = \frac{V_{nk}^2}{U} \quad (44)$$

is reached. If this range is greater than the supplementary range threshold R_k , and if the worse case trajectory (within the constraints) is assumed, the alarm would occur at the maximum closing velocity V_m . The warning time at this alarm point is determined by division of R_1 by V_m , or,

$$t_{mh}^d = t_n^d = \frac{V_{nk}^2}{U V_m}, \text{ if } \frac{V_{nk}^2}{U} > R_k. \quad (45)$$

where t_{mh}^d and t_n^d were defined in Section VI.B. The situation is shown in the phase space sketch of Fig. 34.

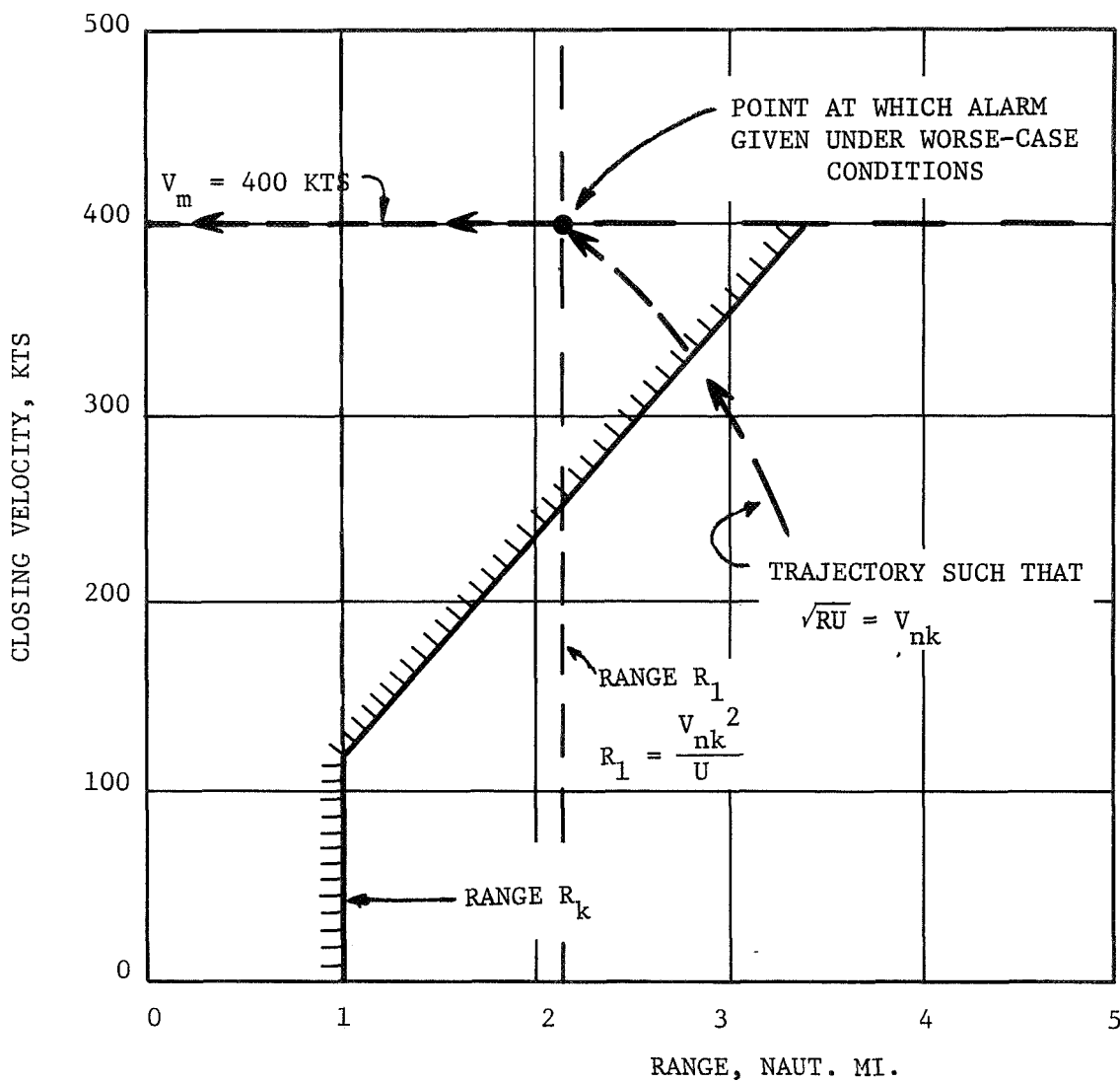


Figure 34 . Phase plane sketch for the tau-range-normal velocity system indicating possible alarm suppression due to the $\sqrt{R|\ddot{R}|} < V_{nk}$ threshold (i.e. the magnitude of \ddot{R} is used). See text for definition of the nomenclature and assumed constraints.

As an example of the numerical value of warning time suppression, we have for $V_{nk} = 120$ KTS, $U = 1/2$ g, and $V_m = 400$ KTS,

$$R_1 = .42 \text{ n. mi.} \quad (46)$$

Hence, unless the supplementary range threshold (R_k) were greater than this value, we could collide 3.8 seconds after the alarm.

If the sign of \ddot{R} is sensed, such that the threshold condition is

$$R/\dot{R} < \tau_k \text{ and } \sqrt{\frac{R}{\dot{R}}} < V_{nk} \text{ if } R > 0$$

(closing velocity decreasing)

(47)

$$R/\dot{R} < \tau_k \text{ if } \ddot{R} < 0 \text{ (closing velocity increasing)}$$

$$\text{or } R < R_k$$

the situation is not quite so severe, although the alarm can still be drastically suppressed. We could still suppress the alarm so long as the relative trajectory is such that

$$\frac{V_{nk}^2}{R} \leq \ddot{R} \quad (48)$$

In the worse case, the path is such that the equality holds, and such that the trajectory passes through a point in the R, \dot{R} plane; $(\tau_k V_m, V_m)$.

Since we allow acceleration magnitudes no greater than U , the path can suddenly change to one with acceleration of $-U$, and a collision can occur. The alarm will be given at the point of deviation from the path. Thus we are led to determine the point that provides the minimum warning time.

For a path defined by

$$\ddot{R} = \frac{V_{nk}^2}{R} \quad (49)$$

and passing through the point (τ_k, V_m, V_m) , the points in the R, \ddot{R} plane defining the trajectory can be found by dividing Equation by \dot{R} and integrating,

$$\frac{\ddot{R}}{\dot{R}} = \frac{V_{nk}^2}{R \dot{R}} = \frac{d\dot{R}}{dR} \quad (50)$$

Separation of variables and integration gives

$$\dot{R}^2 = 2V_{nk}^2 \ln \frac{R}{R_i} + \dot{R}_i^2, \quad (51)$$

where R_i, \dot{R}_i are the initial values of range and closing velocity.

The point of maximum hazard is given approximately by the point of minimum time to closest approach, or

$$\min \{\tau\} \text{ where } \tau = R/\dot{R} \quad (52)$$

(For accelerating flight, we should actually minimize t_1 as given by Equation 37, however, this minimization is more complex and graphical considerations indicate that the approximation of Equation 52 does not lead to significant error in finding the point of maximum hazard). The point on the path for maximum hazard is thus found as

$$R_1 = R_i \text{ EXP } \frac{1}{2} \left[1 - \frac{\dot{R}_i^2}{V_{nk}^2} \right]$$

$$\dot{R}_1 = V_{nk} \quad (53)$$

where the initial conditions are $R_i = \tau_k V_m$ and $\dot{R}_i = V_m$, for the worse-case trajectory.

At the point (R_1, \dot{R}_1) , the minimum time to collision is found from Equation 37 as

$$t_{mh}^d = \frac{-\dot{R}_1 + [\dot{R}_1^2 + 2UR_1]^{1/2}}{U} \quad (54)$$

which assumes an immediate trajectory change to increasing closing velocity. The situation is shown on the phase plane sketch of Figure 35. For the time t_n^d , we have

$$t_n^d = R_1 / \dot{R}_1 \quad (55)$$

If R_1 is less than the supplementary range threshold R_k , then the alarm would be given at the point

$$\begin{aligned} R_1' &= R_k \\ \dot{R}_1' &= \left[2V_{nk}^2 \ln \frac{R_k}{R_i} + \dot{R}_i^2 \right]^{1/2} \end{aligned} \quad (56)$$

Hence, if $R_1 < R_k$, we use (R_k, \dot{R}_1') in Equations 54 and 55 to determine the minimum times remaining until collision.

A complication may arise in that the minimum time trajectory used in calculating the time given by Equation 54 may result in closing velocities exceeding the assumed maximum (V_m). For velocities on the order of 2 miles, however, the actual time difference in using Equation versus the time for a nonaccelerating path (R_1 / \dot{R}_1) is small (e.g. ≈ 2.5 sec. for $U = 1/2 g$).

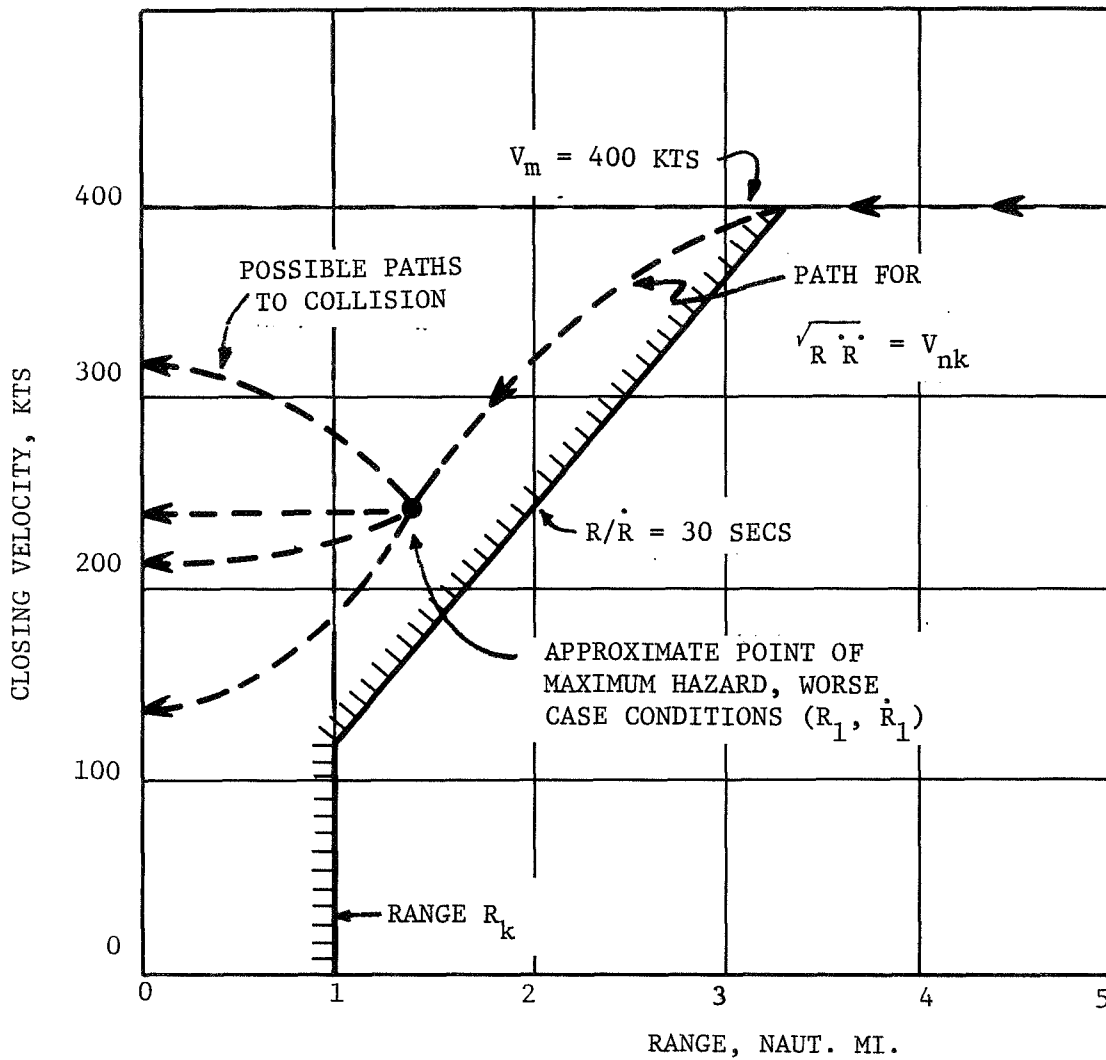


Figure 35. Phase plane plot for the tau-range-normal velocity system indicating possible alarm suppression due to a $\sqrt{R \dot{R}} < V_{nk}$ threshold when only positive \dot{R} is used (decreasing closing velocity). For the sketch, $\tau_k = 30$ secs and $V_{nk} = 240$ kts.

$R^2\tau$, Range, Normal Velocity System. In this system, the threshold conditions are

$$R^2\tau < \beta_k \text{ and } \ddot{R}/\dot{R} < \gamma_k$$

$$\text{or } R < R_k \tag{57}$$

and we will assume that only positive values of \dot{R} are used. The alarm will be suppressed for trajectories such that

$$\ddot{R} \geq \gamma_k \dot{R}. \tag{58}$$

Values of range and closing velocity for the path such that the equality holds are found by integration as,

$$\dot{R} - \dot{R}_i = \gamma_k (R - R_i), \tag{59}$$

where \dot{R}_i and R_i are the initial points.

In this case, the hazard increases continually for the worse case trajectory, and the alarm will be given when the supplementary range threshold is reached, or at,

$$R_1 = R_k$$

$$\dot{R}_1 = \gamma_k (R_k - R_i) + \dot{R}_i. \tag{60}$$

The initial conditions for the worse-case trajectory are $((\beta_k V_m)^{1/3}, V_m)$ as shown in the sketch of Figure 36 .

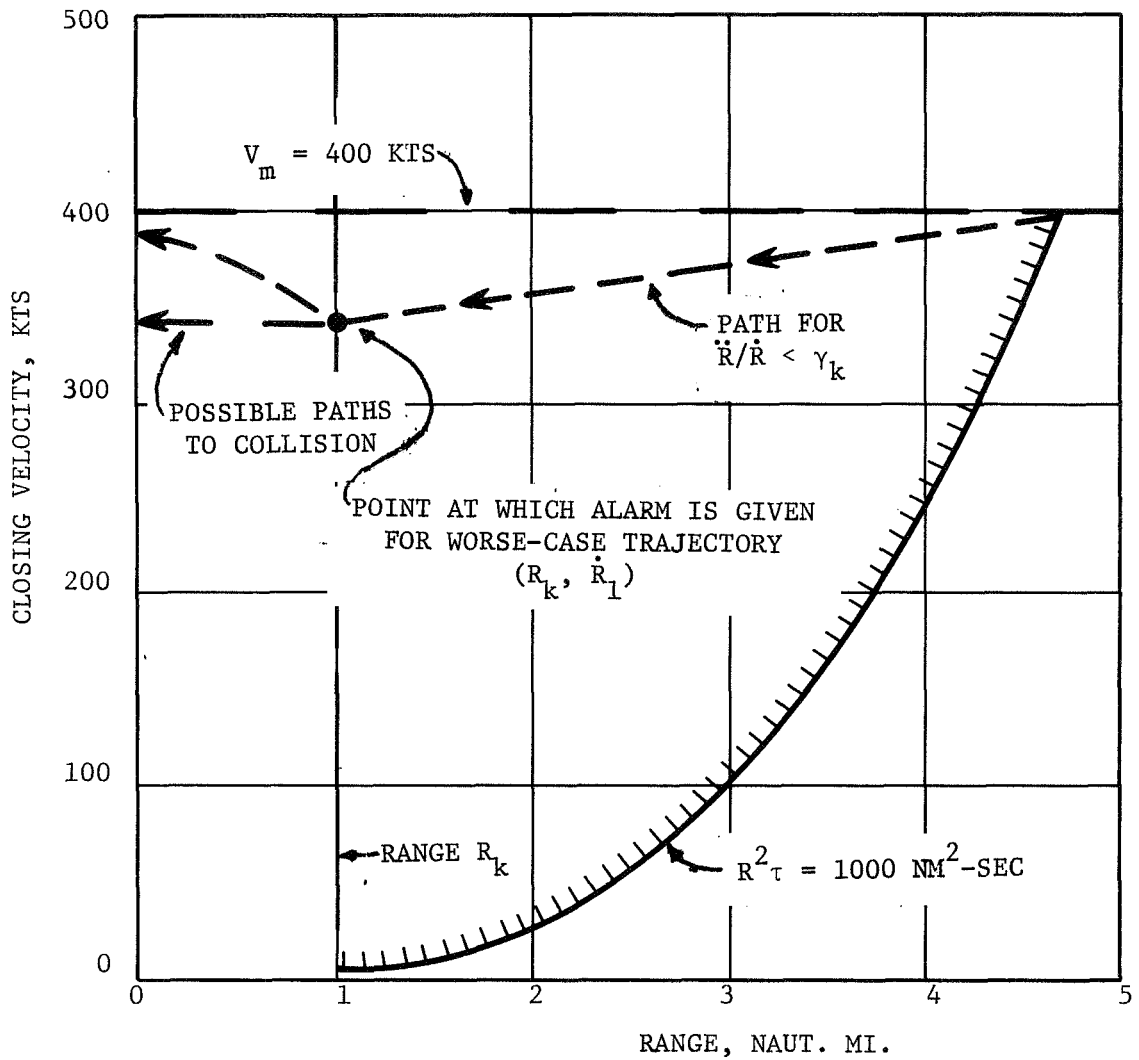


Figure 36. Phase plane plot for the $R^2\tau$ -range-normal velocity system indicating possible alarm suppression due to a $\ddot{R}/\dot{R} < \gamma_k$ threshold. For the sketch, $\gamma_k = .004 \text{ sec}^{-1}$, and $R^2\tau = 1000 \text{ nm}^2\text{-sec}$ are used.

Modified Tau, Normal Velocity System. For this system, let us assume that normal velocity measurements are made by

$$\begin{aligned} V_n &= \sqrt{R \ddot{R}} & R > 0 \\ V_n &= 0 & R \leq 0 \end{aligned} \tag{61}$$

instead of the relationship valid for accelerating paths,

$$V_n = \sqrt{V^2 - \dot{R}^2} \tag{62}$$

where V is the relative velocity.

If measurements are made in accordance with Equation 61, the alarm could be suppressed just as described for the tau-range-normal velocity system. Thus, equations derived for this system (i.e. Equations 54, 55, and 56) can be used to determine the minimum alarm time under worse case conditions.

The initial conditions for the worse case trajectory are

$$\begin{aligned} R_i &= V_m \tau_{mk} + \frac{U_{mk}^2}{2} \\ \dot{R}_i &= V_m \end{aligned} \tag{63}$$

where the nomenclature has been previously described.

D. WARNING TIMES OF VARIOUS SYSTEMS WITH EQUAL ALARM PROBABILITY

In ref. [2], several systems that have been discussed in the literature were compared to determine alarm statistics that can be expected for approximately equal levels of protection (i.e. coverage in the R, \dot{R} plane). We found unreasonably high alarm probabilities in some cases. In this

section, the type and range of measurements required and level of protection achieved are determined under constraints on the alarm statistics. In particular, the idealized systems simulated are compared using the statistical results in ref. [2] to determine warning times afforded for a given fraction of flying time in an alarm status. For the comparison, the results obtained from the most congested hour of data (hour 11) are used. For calculation of warning times, we use the results of Section VI-B.

Table 4 indicates the measurements required, detection ranges, and warning times achieved for various ideal systems that were in an alarm status 1% of the time. The applicable threshold values were taken from Figures 3 through 11 in ref. [2]. The maximum detection ranges are based on a 400 KT closing velocity, as is the warning time (t_n) as discussed in the preceding section. The smallest of the warning times t_{mh} , t_v , and t_{mh}^d indicates the minimum warning assured for closing velocities from 0 to 400 KTS, for relative aircraft accelerations not exceeding 1/2 g, and for vertical rates of descent or ascent of 25 fps.

The zero minimum warning times in the τ and $R^2\tau$ systems have been eliminated in Table 4 by using a range threshold in conjunction with the τ or $R^2\tau$ criteria. The supplementary range criteria was not investigated directly (i.e. simulated with τ and $R^2\tau$ systems using the data base), however, we see from Fig. 3 that a 1 nm range threshold will not significantly increase the percent of time in an alarm status for those criteria without altitude discrimination. For systems using altitude discrimination of ± 500 ft, a range threshold of 1.5 nm does not significantly increase the alarm probability. Hence, in Table 4 we have calculated a minimum warning time for the τ and $R^2\tau$ criteria using a range threshold of 1 nm or 1.5 nm as applicable. The warning time calculations are made using the expressions listed in Table 3 and relationships in Section VI-C as applicable for the cases where \ddot{R} discrimination is used.

E. WARNING TIMES REQUIRED FOR ESCAPE MANEUVERS

A recent analysis of warning times (in the horizontal plane) required for a CAS has been conducted by Holt and Anderson [6]. In this analysis,

Table 4. Detection range and warning times for system with equal (1%) fraction of flying time in an alarm status (from hour 11 data). Warning times are defined in Section VI-B.

SYSTEM TYPE AND MEASUREMENTS	THRESHOLDS	MAX. DETECTION RANGE (N.MI.)	WARNING TIMES*				SUPPLEMENTARY RANGE THRESHOLD (N. MI.)
			t_n	t_{mh}	t_{mv}	t_{mh}^d	
1. RANGE							
R	$R < 1.6 \text{ nm}$	1.6	14	14	--	--	---
R, ΔA	$R < 2.1 \text{ nm}, \Delta A < 500 \text{ ft}$	2.1	19	19	20	--	---
2. TAU-RANGE							
R, \dot{R}	$\tau < 37 \text{ sec}$	4.1	37	19	--	--	1.0
R, R, ΔA	$\tau < 52 \text{ sec}; \Delta A < 500 \text{ ft}$	5.8	52	25	20	--	1.5
R, \dot{R} , \ddot{R}	$\tau < 43 \text{ sec}; \sqrt{R \dot{R}} < 240 \text{ kts}$	4.8	43	20	--	21	1.0
R, \dot{R} , \ddot{R}	$\tau < 57 \text{ sec}; \sqrt{\dot{R} \ddot{R}} < 120 \text{ kts}$	6.3	57	22	--	10	1.0
3. $R^2 \tau$-RANGE							
R, \dot{R}	$R^2 \tau < 256 \text{ nm}^2 \text{ sec}$	3.1	27	27	--	--	1.0
R, \dot{R} , ΔA	$R^2 \tau < 576 \text{ nm}^2 \text{-sec}; \Delta A < 500 \text{ ft.}$	4.0	35	32	20	--	1.5
R, \dot{R} , \ddot{R}	$R^2 \tau < 900 \text{ nm}^2 \text{-sec};$ $\dot{R}/\ddot{R} < .004 \text{ sec}^{-1}$	4.6	42	27	--	9	1.0
R, \dot{R} , \ddot{R}	$R^2 \tau < 1940; \dot{R}/\ddot{R} < .001 \text{ sec}^{-1}$	6.0	54	27	--	9	1.0

Table 4. (Continued).

SYSTEM TYPE AND MEASUREMENTS	THRESHOLDS	MAX. DETECTION RANGE (N.MI.)	WARNING TIMES*				SUPPLEMENTARY RANGE THRESHOLD (N. MI.)
			t_n	t_{mh}	t_{mv}	t_{mh}^d	
4. MODIFIED TAU ($U = 1/2 g$)							
R, \dot{R}	$\tau_m < 26 \text{ sec}$	3.7	34	26	--	--	----
$R, \dot{R}, \Delta A$	$\tau_m < 32; \Delta A < 500 \text{ ft.}$	4.9	44	32	20	--	----
R, \dot{R}, \ddot{R}	$\tau_m < 27; V_n < 240 \text{ kts}$	3.9	36	27	--	--	----
R, \dot{R}, V_n	$\tau_m < 32; V_n < 152 \text{ kts}$	4.9	44	32	--	--	----

* Note: The minimum alarm time in the vertical plane is calculated using $h_m = 25 \text{ fps}$. See Table 4 for nominal rates of descent and ascent. The remaining warning times assume a relative velocity no greater than 400 KTS and a relative acceleration no greater than $1/2 g$. (i.e., a 27° bank angle for one aircraft). See Section 6.2.1 for definition of warning times.

reasonable statistical distributions were assumed for altimeter errors, pilot reaction time, data processing time, and aircraft servo system delays. A computer simulation approach was then used to determine the statistical distribution of the time required for execution of an altitude separation maneuver to assure a 150 ft altitude separation.

To execute the altitude evasive maneuver, where the pilot has been previously alerted and is in straight line, level flight, a warning time of 25 seconds is recommended as a result of the above study.

For a roll-out alarm (i.e. if in a turn, stop turning) a warning time of 30 seconds is recommended.

For a pilot alert, a warning time of 41 seconds is recommended. This allows an average pilot reaction time of 2.5 seconds and then 10 seconds to level-off prior to execution of a possible evasive maneuver. (All times assume only one aircraft maneuvers).

In the vertical plane, it is estimated by Perkinson [7], that for most aircraft, altitude rate can be reduced to zero within 15 seconds after warning. Hence, if descending or ascending aircraft level off after warning, a 21 second warning of an aircraft above or below would assure safe clearance of 150 ft for a maximum rate of descent (or ascent) of 25 fps, assuming no vertical accelerations.

For a pilot warning indicator that depends upon visual acquisition to evaluate the threat and to determine the required maneuver, further study is necessary to evaluate the time required to visually acquire the target and evaluate the threat. This is presently under study by the FAA .

F. SUMMARY

Comparison of the minimum assured warning time for systems that were found to be in an alarm status 1% of the time (Table 4) with the desired pilot alert time on the order of 40 seconds indicates that none of the systems provide this minimum warning time. Although the 1% alarm probability is quite arbitrary, it is felt to be a reasonable upper bound.

If we assume an average alarm duration of 10 seconds, Equation indicates that the probability of an alarm during a thirteen minute flight is $\approx .5$ under hour 11 conditions. Hence, we are reluctant to relax this constraint.

The systems operating on range alone and range-range rate measurements only should be eliminated from further consideration as not feasible. The data clearly indicate that added discrimination in altitude and possibly in (true) normal velocity is desirable if the required warning times are to be achieved without excessive alarms under normal operational conditions.

Discrimination based on range acceleration measurements is effective in increasing the maximum warning time for fixed levels of alarm probability. Unfortunately, as indicated in Table 4 and Section VI-C, discrimination based on \dot{R} measurements has an adverse effect on the minimum warning times achieved under certain worse-case trajectories, when accelerating flight is considered. The effect is particularly bad when measuring \ddot{R}/\dot{R} in the $R^2\tau$ -range system. Thus, \dot{R} measurements do not appear desirable for use in alarm logic, although this measurement may prove useful for indications of the effectiveness of avoidance maneuvers after an alarm is received.

Normal velocity discrimination is effective in the modified tau system, providing (under the conditions discussed) a minimum warning time of 32 seconds as compared to 26 seconds obtained without this form of discrimination. Derivation of true normal velocity, however, requires an exchange of velocity vector data between aircraft, and adds considerably to the system complexity.

We thus conclude that, unless an unduly high alarm rate is accepted, the minimum measurements required are relative range, closing velocity, and altitude. With these measurements, minimum alarm times on the order of 30 seconds can be obtained using the modified tau or $R^2\tau$ -range warning criteria (see Table 4) under the acceleration and velocity constraints assumed. For longer warning times and/or reduced false alarms, it appears necessary to exchange velocity vector data between aircraft.

Under the velocity and acceleration constraints assumed, the required detection range is on the order of 5 miles for the modified tau - altitude system providing a 32 second warning time.

VII. CONCLUSIONS

The simulation of the system using the most congested hour (hour 11) of the Atlanta data base indicated that interference levels from all sources were small in comparison to the signal from a potentially hazardous aircraft. Transponder saturation by multiple aircraft interrogations does not appear to be any problem with the system parameters now used. The probability, under hour 11 conditions, that the transponder saturation factor will exceed a value of 1.4 (i.e. a gain reduction of 1.45 db) is on the order of .01. The probability that the total output of the transponder will exceed 16 dbm is of this same order (.01). Thus, the transponder is operating well within its designed values under congested conditions, and appears to be somewhat conservatively designed.

In the receiver, a dynamic range of 45 db should be adequate to prevent saturation, with high probability. There is a low probability (4×10^{-5}) that the noise plus the interference power will exceed a threshold level providing a 60 second warning at a 240 knot closing velocity. Thus, alarms caused by interfering signals are expected to be negligible under the conditions represented during the simulation. The cross-product power term is the most significant interference source.

Using the threshold level mentioned above, the system was in an alarm status 2.4 percent of the time. The probability that the second largest received signal will exceed the threshold level is on the order of 4×10^{-4} under hour 11 conditions. While the receiver is an alarm status, the probability that the largest signal to noise plus interference ratio will exceed 20 db is on the order of .9. No cases were observed in which the signal to noise plus interference ratio was less than 10 db for the signal causing the alarm.

Detailed study of the distribution of power levels from the aircraft in the population indicated that the power levels are approximately distributed normally. Actual distributions were found for the five closest aircraft to a randomly selected aircraft, and knowledge of the theoretical distributions permits extrapolation to higher density terminal area models.

In the flight tests, comparison of simulated and experimental values of range measurements indicated differences on the order of 10-15 percent over the calibration range of the equipment. This degree of accuracy permitted the determination of the sources of the measurement errors in the flight systems. Analyses of these sources of error were conducted by LRC personnel, using the results of the flight tests simulation.

A comparison of idealized systems on the basis of warning times achieved for a given probability of alarm indicates that achieving the required protection without excessive alarms is an extremely difficult task. Systems based on proximity alone and on range and range rate measurements only are felt to be not feasible. As a minimum, altitude difference data should be used in the warning logic.

Use of approximate miss distance discrimination is effective in reducing the number of false alarms, however, it was found that dangerous suppression of the warning time can occur under accelerating conditions, and that discrimination based on relative range acceleration should not be used in warning logic. The use of approximate miss distance measurements as assistance to the pilot in evasive maneuvers should be investigated further in future work.

The extended modified tau criteria developed in Appendix A should have a beneficial effect on the false alarm performance, while not adversely effecting the system protection. This extended criterion, when simulated using the hour 11 data base, reduced the percent of time in alarm status from 2.2% to 1.4% for the criterion $\tau_m < 35$ secs. and alt. diff. < 500 ft.

In summary, we can conclude that saturation and interference is not a problem with the system as presently designed, and under the flight conditions represented by the most congested hour of the data base. Simulations of the flight tests indicate that, in most cases, the sources of measurement error in the system are well known and can be accounted for satisfactorily. Comparisons of idealized systems indicate that the alarm threshold should be set to provide an alarm on the order of 30 seconds and that the modified tau (or extended modified tau) criterion should be used in warning logic, along with altitude discrimination on the order of ± 500 feet.

VIII. LIST OF REFERENCES

- [1] Britt, C. L., D. F. Palmer, W. H. Ruedger, R. C. Haws, and E. H. Young, "Investigation of the Performance Characteristics of a Doppler Radar Technique for Aircraft Collision Hazard Warning," Phase I Report, Contract No. NAS1-7537, March 22, 1968.
- [2] Britt, C. L., W. H. Ruedger, K. W. Poole, R. C. Haws, and E. H. Young, "Statistical Evaluation of Aircraft Collision - Hazard Warning System Techniques in the Terminal Area," Phase II Interim Report, Contract No. NAS1-7537, July 15, 1969.
- [3] Schrader, J. H., C. P. Hearn, R. H. Couch, and E. S. Bradshaw, "An Aircraft Collision Warning System Employing a Cooperative C.W. Doppler Radar, Working Paper No. 361, NASA, Langley Research Center, Hampton, Va.
- [4] Holt, J., L. Belden, and W. Jameson, "Computer Simulation Study of Air-Derived Separation Assurance Systems in Multiple Aircraft Environments," Third Interim Report, Contract FA-WA-4598, Collins Radio Company, Cedar Rapids, Iowa, 1968.
- [5] Aitchison, J. and J.A.C. Brown, "The Lognormal Distribution," Cambridge University Press, New York, 1968.
- [6] Holt, J. M. and R. M. Anderson, "Analysis of Warning Times for Collision Avoidance Systems, IEEE Trans. on Aerospace and Electronic Systems, Vol. AES-4, No.2: 305-314, 1968.
- [7] Perkinson, R. E., "CAS Message Format," IEEE Trans. on Aerospace and Electronic Systems, Vol. AES-4, No. 2: 273-277, 1968.
- [8] Rice, S. O., In Noise and Stochastic Processes, edited by N. Wax, Dover Publications Inc., New York, N. Y., 1954.
- [9] Middleton, David, An Introduction to Statistical Communication Theory, McGraw-Hill Book Company, Inc., New York, N. Y. 1960.

IX. APPENDICES

APPENDIX A
EXTENSIONS OF THE "MODIFIED TAU" WARNING CRITERIA

The "modified tau" criteria provides a warning based on the measurement of range (R) and range rate (\dot{R}), and an alarm is sounded if

$$\tau_m = \frac{-R + [\dot{R}^2 + 2UR]^{1/2}}{U} < \tau_{mk} \quad (A-1)$$

where U and τ_{mk} are selected constants. The criteria, as shown in Appendix A, indicates that it may be possible for the two aircraft to collide within τ_m seconds if they make the worse possible maneuvers with a constant relative acceleration of U.

This is a "worse case" criteria that requires relatively large regions in the R, \dot{R} plane to assure reasonable warning times τ_{mk} .

To obtain a more realistic idea of the warning time to be expected using this criteria, and assuming that pilot intent is unknown, it seems that probabilistic description should be used for the acceleration constraint U. That is, we consider the maximum relative acceleration as a random variable, and determine the expected or average value of the time-to-collision, again assuming that the aircrafts make the worse possible maneuvers.

The value of this approach is that a more realistic estimate of the degree of hazard is obtained, and hence smaller regions in the R, \dot{R} plane are required to provide sufficient protection. The fact that the worse possible maneuver is still assumed provides an additional margin of safety.

We find the expected or average value of τ_m by use of the expression.

$$E\{\tau_m\} = \int_{-\infty}^{\infty} \tau_m(u) f(u) du \quad (A-2)$$

where $f(u)$ is the probability density function of maximum acceleration, considered now as a random variable. $\tau_m(u)$ is given by Equation A-1 with $U = u$. As an example of the calculation, assume that any value of u is equally likely, $0 < u < U$, so that the probability density of u is

$$f(u) = \frac{1}{U}, \quad 0 < u < U \quad (A-3)$$

The expected value of τ_m is then

$$E\{\tau_m\} = \frac{R}{U} \int_0^{\infty} \left(\left[1 + \frac{2uR}{R^2} \right]^{1/2} - 1 \right) \frac{du}{u} \quad (A-4)$$

This integral is evaluated to give

$$\tau_{em} = E\{\tau_m\} = \frac{2\dot{R}}{U} \left\{ (\phi(U) - 1) + \log \frac{2}{\phi(U) + 1} \right\} \quad (A-5)$$

where

$$\phi(U) = \left[1 + \frac{2UR}{R^2} \right]^{1/2}$$

and τ_{em} is used to designate the expected value of time-to-collision under the assumptions made. Curves of constant τ_{em} have been plotted in the R, \dot{R} plane in Figure A-1 for comparison with values of τ_m . As may be seen, the curves have the same general shape of the τ_m curves except for the region where closing velocity is small. For a given measured value of R and \dot{R} , we find, as would be expected, that values of τ_{em} are considerably less than value of τ_m .

The reliability of the estimated value τ_{em} could be improved if the assumption as to the density function of U could be removed.

Further Extensions

The modified tau criteria contains an unrealistic feature in that no distinction is made between normal and axial accelerations of the individual aircrafts involved. Axial (along path) acceleration components are known to be small in comparison to the normal acceleration components,

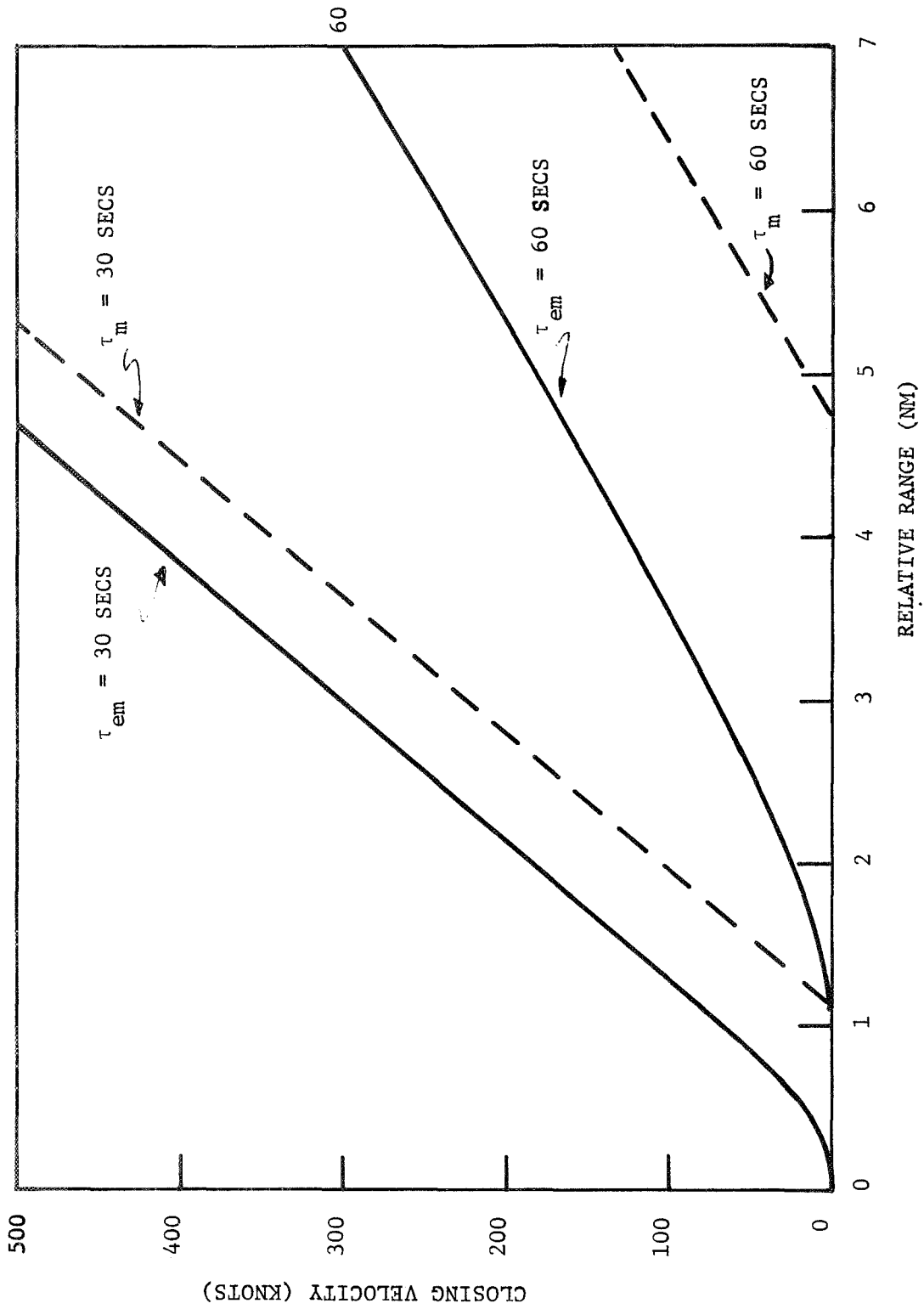


Figure A-1. Curves of constant τ_{em} and τ_m in the range-range rate plane.

particularly in the terminal area with imposed speed limits. Also, one feels intuitively that hazards due to aircraft accelerations become less important as the measured closing velocity increases. That is, if a large closing velocity is measured, a near head-on encounter is indirectly implied.

Thus, we are led to formulate mathematically a criteria that takes into account additional constraints on the allowable relative acceleration profile.

Consider the diagram of Figure A-2. Here the present positions of the protected and intruding aircrafts are indicated by 0 and $\bar{p}_2(T)$ respectively (i.e. aircraft 1 is at the origin of coordinates defined by unit vectors \bar{i}_r and \bar{i}_n , with \bar{i}_r in the direction of $\bar{p}_2(T)$). The positions of the aircrafts at some time t later are given by

$$\int_T^{T+t} \int_T^s \ddot{\bar{P}}_1(\tau) d\tau ds = \int_T^{T+t} \int_T^s \bar{A}_1(\tau) d\tau ds \quad (A-6)$$

and

$$\int_T^{T+t} \int_T^s \ddot{\bar{P}}_2(\tau) d\tau ds = \int_T^{T+t} \int_T^s \bar{A}_2(\tau) d\tau ds \quad (A-7)$$

where $\bar{A}_1(\tau)$ and $\bar{A}_2(\tau)$ are the acceleration functions of aircrafts 1 and 2, respectively.

Evaluations of the integrals on the left hand side gives

$$\bar{p}_1(T + t) = \dot{\bar{p}}_1(T) t + \int_T^{T+t} \int_T^s A_1(\tau) d\tau ds \quad (A-8)$$

$$\bar{p}_2(T + t) = \bar{p}_2(T) + \dot{\bar{p}}_2(T) t + \int_T^{T+t} \int_T^s A_2(\tau) d\tau ds \quad (A-9)$$

Now, since if a point can be reached in a given time by any sort of acceleration profile, it can also be reached by a constant acceleration of no greater magnitude, we assume a constant acceleration to obtain

$$\bar{p}_1(T + t) = \dot{\bar{p}}_1(T) t + \bar{A}_1 t^2/2 \quad (A-10)$$

$$\bar{p}_2(T + t) = \bar{p}_2(T) + \dot{\bar{p}}_2(T) t + \bar{A}_2 t^2/2 \quad (A-11)$$

These equations define the sets of points reachable by the aircrafts in a time t_e where \bar{A} varies over all allowable constant vectors and t varies from 0 to t_e .

For the set of allowable \bar{A}_1 and \bar{A}_2 vectors, we assume that axial components are negligible and that the relative magnitude is limited to U . Thus the acceleration constraints are

$$\begin{aligned} \bar{A}_1 \cdot \dot{\bar{p}}_1(T) &= 0 \\ \bar{A}_2 \cdot \dot{\bar{p}}_2(T) &= 0 \end{aligned} \quad (A-12)$$

and

$$|\bar{A}_2 - \bar{A}_1| < U$$

For a collision to take place within a time t_e , we must have

$$\bar{p}_2(T + t) = \bar{p}_1(T + t) \quad (\text{A-13})$$

for some t , $0 < t < t_e$. Using Equations A-10 and A-11, we obtain

$$\bar{r}(T) + \dot{\bar{r}}(T) t + (\bar{A}_2 - \bar{A}_1) t^2/2 = 0$$

where $\bar{r}(T) = \bar{p}_2(T)$ and $\dot{\bar{r}}(T) = \frac{d}{dt}\bar{p}_2(T) - \frac{d}{dt}\bar{p}_1(T)$. (A-14)

Now resolve Equation A-14 into components normal to and along the relative range vector.

$$\bar{1}_r \left[\bar{R}(T) + \dot{\bar{R}}(T)t - A_2 t^2/2 \sin \theta_2 - A_1 t^2/2 \sin \theta_1 \right] = 0 \quad (\text{A-15})$$

$$\bar{1}_\theta \left[\bar{V}_n(T) t - A_2 t^2/2 \cos \theta_2 + A_1 t^2/2 \cos \theta_1 \right] = 0$$

where, dropping the T notation for simplicity, $\bar{R} = \bar{1}_r \cdot \bar{r}$, $\dot{\bar{R}} = \dot{\bar{1}}_r \cdot \dot{\bar{r}}$, $\bar{V}_n = \bar{1}_\theta \cdot \dot{\bar{r}}$, $A_2 = |\bar{A}_2|$, $A_1 = |\bar{A}_1|$, $\sin \theta_1 = \frac{\bar{1}_r \cdot \bar{A}_1}{A_1}$ and $\sin \theta_2 = \frac{\bar{1}_r \cdot \bar{A}_2}{A_2}$.

Each vector component must equal zero, and squaring and adding the components gives (A-16)

$$(\bar{R} + \dot{\bar{R}}t)^2 + (\bar{V}_n t)^2 = \left[\frac{(A_1^2 + A_2^2)}{4} - \frac{A_1 A_2}{2} \cos(\theta_2 + \theta_1) \right] t^4.$$

The term in the brackets is, of course, the square of the magnitude of the relative acceleration vector. We desire to place additional constraints on the magnitude of this vector based on the fact that only components of acceleration normal to the velocity vectors are being considered. This appears impossible in general unless the relative headings of each aircraft is known, or unless additional assumptions are made. Following the latter course, we assume that

$$|\dot{p}_1(T)| = |\dot{p}_2(T)| \quad (A-17)$$

and that $V_n(T) = 0$. The first assumption is reasonable in the terminal area with imposed speed limits, while the latter assumption is equivalent to that assumed in the derivation of the "modified tau" criteria.

With these assumptions, we note that $\theta_1 = \theta_2$ and that the maximum relative acceleration vector that will provide a solution is obtained when $A_1 = A_2$. In reference [4], it is shown that if a solution to Equation A-16 exists for some $|\bar{A}_2 - \bar{A}_1|$ and some t , $0 < t < t_e$, it also exists for all greater values of $|\bar{A}_2 - \bar{A}_1|$. We have

$$\text{max. effective } |\bar{A}_2 - \bar{A}_1|^2 < \frac{A_1^2}{2} (1 - \cos 2\theta) \quad (A-18)$$

and since $2A_1 < U$ if $A_1 = A_2$ and $|\bar{A}_2 - \bar{A}_1| < U$, we have also

$$\frac{A_1^2}{2} (1 - \cos 2\theta) < \frac{U^2}{8} (1 - \cos 2\theta) \quad (A-19)$$

Thus, under our assumption, a hazard will exist if

$$(R + \dot{R}t)^2 = \frac{U^2}{8} (1 - \cos 2\theta) t^4 \quad (\text{A-20})$$

for some t , $0 < t < t_e$. Taking the square root of both sides gives

$$R + \dot{R}t = \frac{U}{2\sqrt{2}} [1 - \cos 2\theta]^{1/2} t^2 \quad (\text{A-21})$$

or

$$R + \dot{R}t = \frac{Ut^2}{2} \sin \theta \quad (\text{A-22})$$

The remaining task in developing this criteria is to estimate $\sin \theta$ from potentially measurable data. If we assume a reasonable maximum relative velocity exists, say V_{\max} , (e.g. about 400 KTS in the terminal area), then an estimate of $\sin \theta$ based on a range rate measurement is

$$\begin{aligned} \sin \theta &\approx [1 - \left(\frac{\dot{R}}{V_{\max}}\right)^2]^{1/2} && \dot{R} < V_{\max} \\ &\approx 0 && \dot{R} > V_{\max} \end{aligned} \quad (\text{A-23})$$

Since $\cos \theta \approx \frac{\dot{R}}{V_{\max}}$ (when $|V_1| = |V_2|$ and $\theta_1 = \theta_2$ as assumed).

Thus, we have developed a criteria that has the desired behavior as initially discussed. At low values of \dot{R} , the criteria behaves as "modified tau," while at large value of \dot{R} , the criteria reduces to the "tau" criteria ($\tau = R/\dot{R}$). The criteria is summarized as: a hazard exists if there exists a t , $0 < t < t_e$ such that,

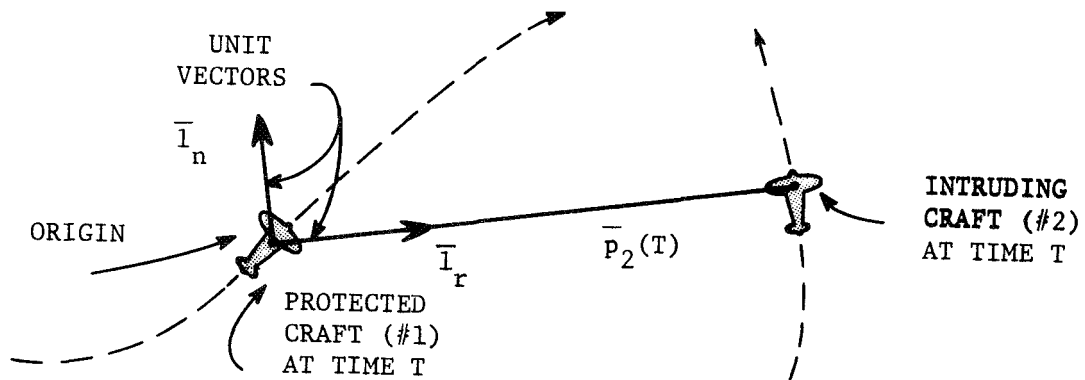


Figure A-2. Coordinate system.

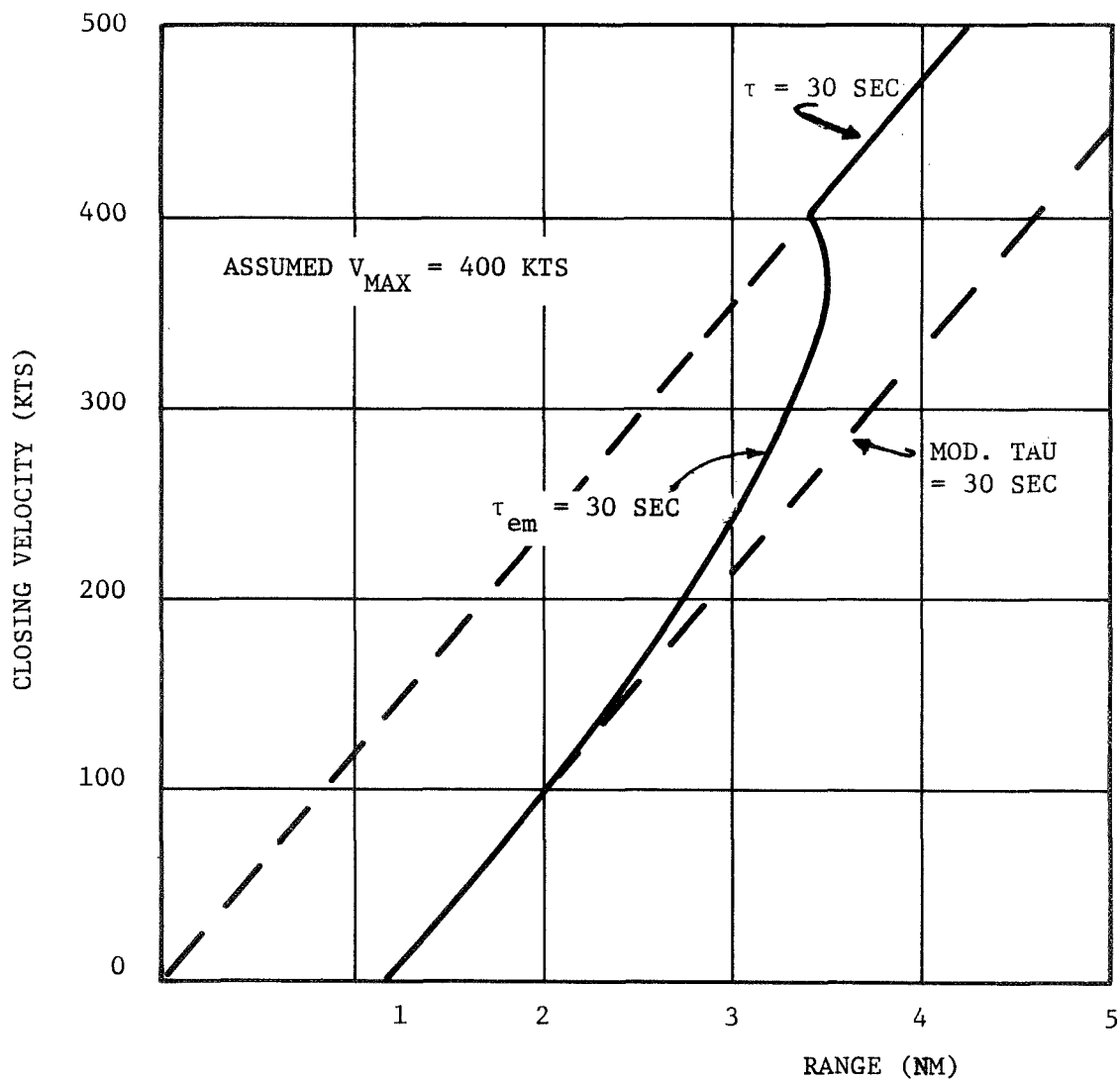


Figure A-3. Plot of the extended modified tau criteria (assumes acceleration components normal to the velocity vectors).

$$R + \dot{R}t = \frac{Ut^2}{2} \left[1 - \left(\frac{\dot{R}}{V_{\max}} \right)^2 \right]^{1/2} \quad \text{if } \dot{R} < V_{\max}$$

(A-24)

$$R + \dot{R}t = 0 \quad \text{if } \dot{R} > V_{\max}.$$

This criteria is plotted in Figure A-3 for several values of t_e for comparison with the modified tau and tau criteria.

APPENDIX B

THE D.C. OUTPUT OF A PRODUCT DETECTOR-LIMITER CIRCUIT WITH MULTIPLE INPUT SIGNALS

Introduction

The detector circuit used in the collision warning receiver has a configuration as shown in Figure B-1. The Doppler tone signal is differentiated and split into two parts, one of which passes through a limiter and thence is combined with the other in the product detector. A low pass filter is used to eliminate high-order harmonics and smooth the output voltage.

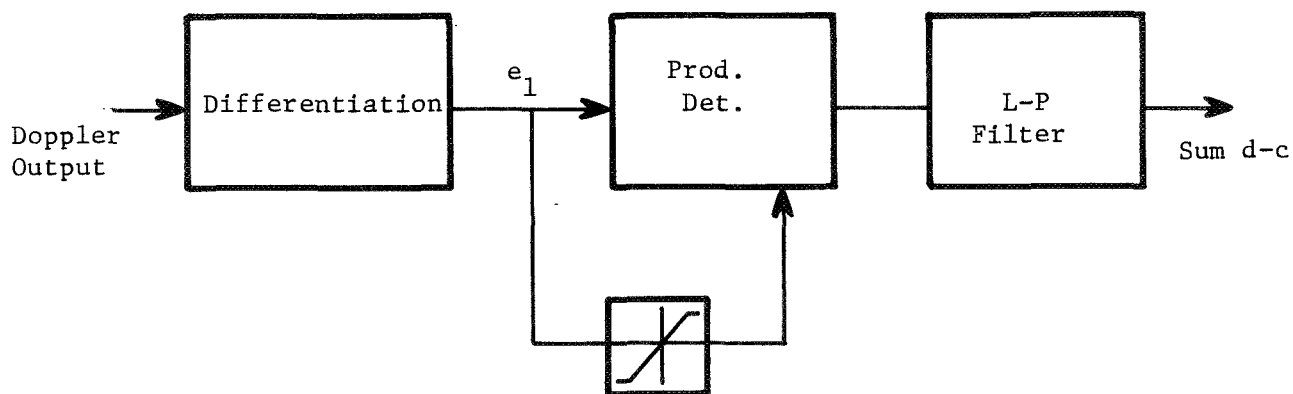


Figure B-1. Detection block diagram.

Analysis

Assume that four doppler signals of magnitudes $P, Q, R,$ & S and noise $n(t)$, are present at the doppler output, i.e.

$$e(t) = P \cos pt + Q \cos qt + R \cos rt + S \cos st + N(t) \quad (B-1)$$

where $p, q, r, & s$ are the doppler frequencies. The output of the differentiator $e_1(t)$ is

$$e_1(t) = P p \sin pt + Q q \sin qt + Rr \sin rt + Ss \sin st + \dot{n}(t) \quad (B-2)$$

$$p, q, r \text{ or } s \leq 2\pi \times 10^4$$

note that the derivative of the noise term is indicated only. Additional comments will be made in the subsequent analysis, for the case in which $n(t)$ corresponds to white noise.

The signal $e_1(t)$ is also the input to the limiter. The output of the limiter will now be derived, based on an extension of the results given by Rice [2]. The auto-correlation of the output from the limiter $\phi_L(T)$ is

$$\phi_L(T) = \int_{-\infty}^{\infty} \int_{-\infty}^{\infty} f(e_a) f(e_b) p(e_a, e_b) de_a de_b \quad (B-3)$$

in which the output voltage of the nonlinear element is $e_2 = f(e_1)$ and $p(e_a, e_b)$ is the joint probability-density function of e_2 , that is $e_b(t) = e_a(t + \tau)$ for the ergodic case. This equation will now be expressed in terms of the transform of $f(e)$, which is defined as

$$F(ju) = \int_{-\infty}^{\infty} f(e) e^{-jue} de \quad (B-4)$$

Substituting (4) into (3) and interchanging the order of integration gives

$$\phi_L(T) = \frac{1}{4\pi^2} \int_{-\infty}^{\infty} F(ju) du \int_{-\infty}^{\infty} F(jv) dv \int_{-\infty}^{\infty} \int_{-\infty}^{\infty} P(e_a, e_b) e^{jue_a + jve_b} de_a de_b \quad (B-5)$$

(the constant term arises from inversion of (4)). The last term in this equation may be recognized as the characteristic function of v_a and v_b , i.e.,

$$M(ju, jv, \tau) \stackrel{d}{=} \int_{-\infty}^{\infty} \int_{-\infty}^{\infty} P(e_a, e_b) e^{jue_a + jve_b} de_a de_b . \quad (B-6)$$

Thus (5) can be written as

$$\Phi_L(\tau) = \frac{1}{4\pi^2} \int_{-\infty}^{\infty} F(ju) du \int_{-\infty}^{\infty} F(jv) M(ju, jv, \tau) dv . \quad (B-7)$$

Assuming that the individual terms in (2) are independent, the characteristic function can be written in terms of the component sinusoidal and noise terms,

$$M(ju, jv, \tau) = M_p(ju, jv, \tau) M_Q(ju, jv, \tau) M_R(ju, jv, \tau) M_S(ju, jv, \tau) M_n(ju, jv, \tau) . \quad (B-8)$$

Consider a typical term such as $M_R(ju, jv, \tau)$, by use of the ergodic hypothesis,

$$M_R(ju, jv, \tau) = \lim_{T \rightarrow \infty} \frac{1}{T} \int_0^T \exp[ju R \cos rt + jv R \cos r(t+\tau)] dt$$

and by use of the relationship,

$$u \cos r t + v \cos r (t+\tau) = \sqrt{u^2 + v^2 + 2uv \cos r\tau} (\cos r t + \theta)$$

(where θ is the phase angle), then integration yields

$$M_R(ju, jv, \tau) = J_0(R\Gamma_R) . \quad (B-9)$$

The notation Γ used in the above equation is defined by the expression,

$$\Gamma_i = \sqrt{u^2 + v^2 + 2uv \cos i\tau} .$$

One other result is needed at this point. The characteristics function for the gaussian noise voltage is given by,

$$M_u(ju, jv, \tau) = \exp \left[-\frac{\psi_0}{2} (u^2 + v^2) - \psi_\tau uv \right]. \quad (\text{B-10})$$

In this equation ψ_τ is the correlation function of $n(t)$ and ψ_0 is the mean-square noise. The autocorrelation function, in terms of the above quantities, is

$$\begin{aligned} \phi_L(\tau) = & \frac{1}{4\pi^2} \int_{-\infty}^{\infty} F(ju) e^{-\frac{\psi_0}{2} u^2} du \int_{-\infty}^{\infty} F(jv) e^{-\frac{\psi_0}{2} v^2} \\ & \times e^{-\psi_\tau uv} J_0(P\Gamma_p) J_0(Q\Gamma_q) J_0(R\Gamma_r) J_0(S\Gamma_s) dv \end{aligned} \quad (\text{B-11})$$

By use of the expansion

$$M_R(ju, jv, \tau) = \sum_{n=0}^{\infty} \epsilon_n (-1)^n J_n(Ru) J_n(Rv) \cos n\tau,$$

the autocorrelation function (11) can be written as

$$\begin{aligned} \phi_L(\tau) = & \sum_{f=0}^{\infty} \sum_{g=0}^{\infty} \sum_{h=0}^{\infty} \sum_{i=0}^{\infty} \sum_{k=0}^{\infty} \frac{1}{k!} \psi_\tau^k h^2 \epsilon_n \\ & \times \cos f p\tau \cos g q\tau \cos hr\tau \cos i s\tau. \end{aligned} \quad (\text{B-12})$$

The H_{fghik} term in this equation is given by

$$H_{fghik} = \frac{j^{f+g+h+i+k}}{2\pi} \int_{-\infty}^{\infty} F(ju) u^k J_f(Pu) J_g(Qu) J_h(Ru) J_i(Su) e^{-\frac{\psi_0}{2} u^2} du. \quad (B-13)$$

As Rice has pointed out, the dc and periodic terms in this expression are obtained by letting $T \rightarrow \infty$.

$$\phi_{L\tau} \rightarrow \infty = \sum_{f=0}^{\infty} \sum_{g=0}^{\infty} \sum_{h=0}^{\infty} \sum_{i=0}^{\infty} \epsilon_n H_{fghi}^2 \cos fp\tau \cos gq\tau \times \cos hr\tau \cos is\tau \quad (B-14)$$

This equation represents the autocorrelation function for the signal at the output of the limiter. Specific terms will be examined following analysis of the product detector. Note that the above expressions assumed an input of the same form as (1), for an input such as (2) each of the P, Q, R, and S terms should be replaced by Pp, Qq, etc.

The next task to be discussed is that of deriving an expression for the dc output of the product detector. The terms related to the dc output

can be identified by considering the following analysis. For a signal

$$K_1 w_d \cos w_d t$$

acting as an input to the product detector, and a square wave switching voltage

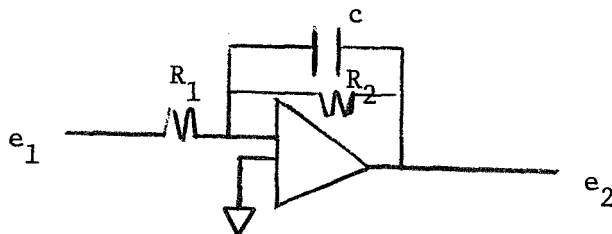
$$2K_2 \sum_{n=1}^{\infty} \frac{\sin n\pi/2}{n\pi/2} \cos nw_d t,$$

the output will comprise the product of these terms. The only term contributing to the dc component is

$$\begin{aligned} & 2K_1 K_2 w_d \frac{\sin \pi/2}{\pi/2} [\cos nw_d t]^2 \\ &= \frac{4}{2\pi} K_1 K_2 w_d (1 - \cos 2 w_d t). \end{aligned}$$

The dc output of a product detector, in which the input and switching voltage consists of incommensurable sinusoidal terms, is the sum of fundamental coefficient products. The expressions for the harmonic and cross product (fluctuating) terms is extremely messy. These terms will not be considered since the present purpose is to evaluate distortion in the detected doppler signal arising from multiple targets.

The low-pass filter, shown in Figure B-1, uses the circuit shown below



The transfer function of this filter is

$$\frac{e_2(S)}{e_1(S)} = \frac{\frac{R_2}{sC} \frac{1}{R_2 \frac{1}{sC}}}{R_1} = \frac{R_2}{R_1} \frac{1}{sCR_2 + 1} \quad (B-15)$$

The transfer function for a limiter may be found in Middleton p. (639)[9],
i.e.

$$F(ju) = 2\beta \frac{1 - e^{-uR_0}}{-u^2}$$

The symbols used in this equation are shown in the following sketch.

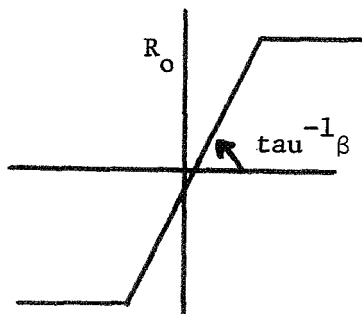
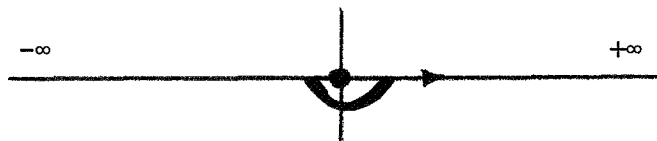


Figure B-2. Definition of β

Returning to (14), the fundamental terms in the output of the limiter can be seen to result from equating one of the fghi indices to unity and the others to zero. Thus the magnitude, for the input sinusoidal $P_p \cos pt$, of the output fundamental term is

$$H_p = \frac{i}{\pi} \int_c 2\beta \frac{1 - e^{-uR_o}}{-u^2} J_1(pPu) J_0(qQu) J_0(rRu) J_0(sSu) du \quad (B-16)$$

This equation also assumes that $\psi_o \ll R_o^2$. The contour for this integration is shown below.



The dc output of the product detector (using k_e as the detector proportionality factor) is the product of the input signal and the coefficient of the fundamental terms, i.e.,

$$E_{dc} = k_d [pPH_p + qQH_q + rRH_r + sSH_s]. \quad (B-17)$$

This equation represents the dc output of the sum channel. The outputs from the other channels are obtained by substituting the proper channel voltages for the P, Q, R, and S terms in the above equation (e.g., page 9 of ref [3]).

Integration of Equation B-16 is accomplished as follows.

$$2H = \frac{i}{\pi} \int_c 2\beta \frac{1 - e^{-iuR_o}}{-u^2} \underbrace{J_1(P_u) J_0(Q_u) J_0(R_u) J_0(S_u)}_{F(PQRSU)} du$$

$$= \frac{2i\beta}{\pi} \int_c \frac{1 - (\cos u R_o - i \sin u R_o)}{-u^2} F(P, Q, R, S, U) du$$

$$u = \sigma + j \delta$$

$$= \frac{2\beta i}{\pi} \left[\int_{-\infty}^{\infty} \frac{F(PQRS\sigma) d\sigma}{-u^2} - \int_{-\infty}^{\infty} \frac{\cos R_o \sigma F(PQRS\sigma) d\sigma}{-u^2} + i \int_{-\infty}^{\infty} \frac{\sin R_o \sigma F(\sigma) d\sigma}{-u^2} \right]$$

$\begin{matrix} \swarrow & & \swarrow \\ = 0 \text{ since } J_1 \text{ is odd} & & = 0 \text{ since } J_1 \text{ is odd} \end{matrix}$

$$2H = \frac{2\beta}{\pi} \int_{-\infty}^{\infty} \frac{\sin R_o u}{u^2} J_1(Pu) J_0(Qu) J_0(Ru) J_0(Su) du$$

$$= \frac{4\beta}{\pi} \int_0^{\infty} \frac{\sin R_o u}{u^2} J_1(Pu) J_0(Qu) J_0(Ru) J_0(Su) du \quad (B-18)$$

Note that the terms such as qQ have been abbreviated simply as Q in this integration.

Numerical Calculations

Computer programs have been written to solve the integral given in Equation B-18. This integral calculates the fundamental output of the limiter, or

normalized gain for the particular input of interest. Curves have been calculated for various values of input signal level as shown in Figures B-3 and B-4. Figure B-3 represents the case for two input signals and Figure B-4 shows the normalized limiter gain for the case when a third signal is present.

In the computer simulation, the dc voltage from the product detector is calculated using Equation B-17, with Equation B-17 generalized to include all significant signals.

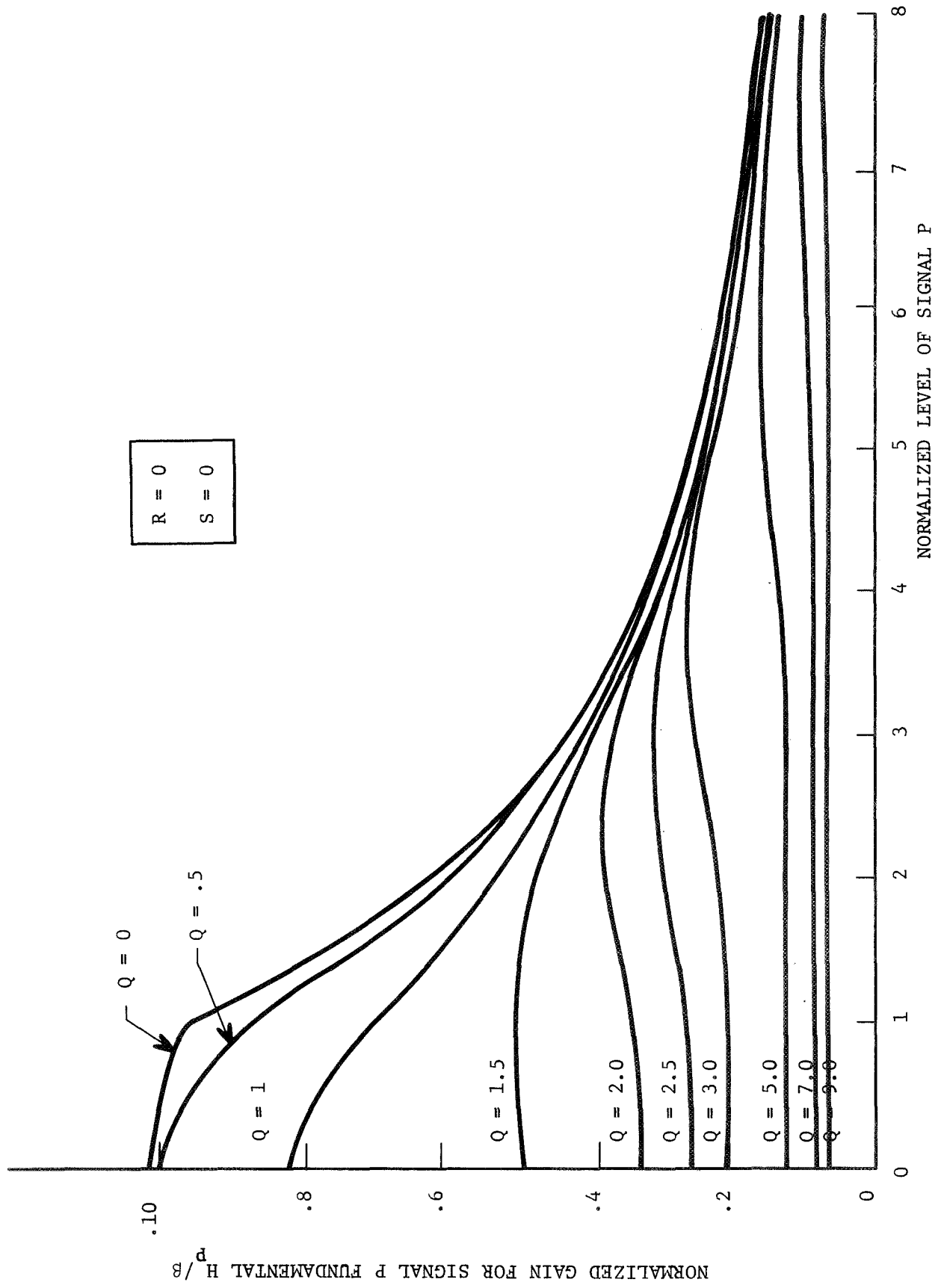


Figure B-3. Normalized gain of limiter for fundamental component of input signal (P) for various levels of signals P and Q.

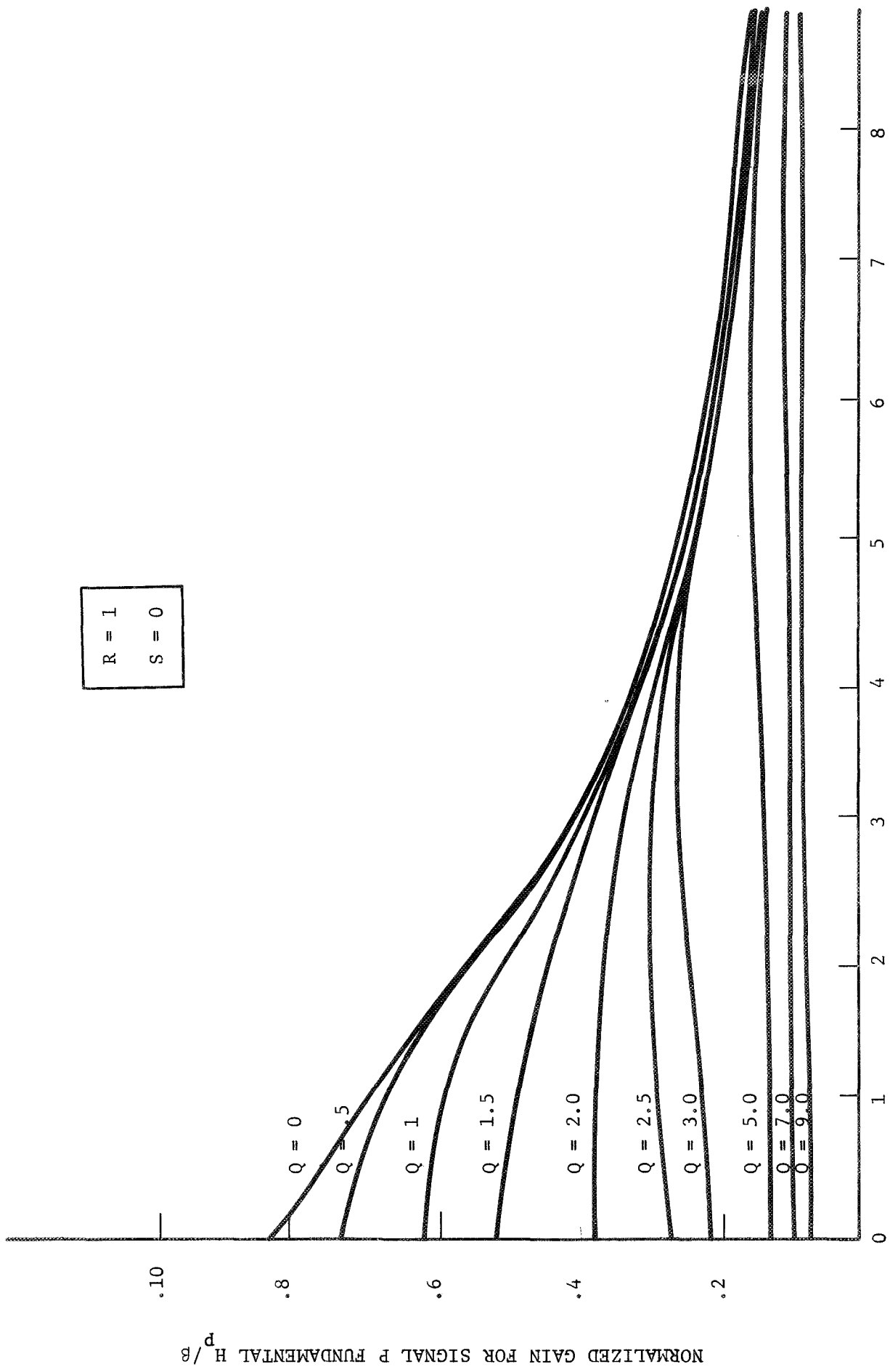


Figure B-4. Normalized gain of limiter for fundamental component of input signal (P) for various levels of signals P and Q for third signal (R) of unity level.

APPENDIX C
PHASE PLANE PLOT OF A SET OF COLLISION TRAJECTORIES
UNDER AN ACCELERATION CONSTRAINT

It is informative, in investigation of the protection afforded by various systems, to visualize the relative trajectories in the phase (R, \dot{R}) plane.

For acceleration limited trajectories, we have

$$|\ddot{R}| < U \text{ or } -U < \ddot{R} < U \quad (\text{C-1})$$

where \dot{R} is range acceleration. Hence, the slopes of the trajectories in phase space are given by,

$$-\frac{U}{\dot{R}} < \alpha < \frac{U}{\dot{R}} \quad (\text{C-2})$$

A set of allowable trajectories are sketched in Figure C-1, for the specific case of $U = 1/2 \text{ g}$. (Corresponding to an aircraft bank angle of about 27° for one aircraft turning)

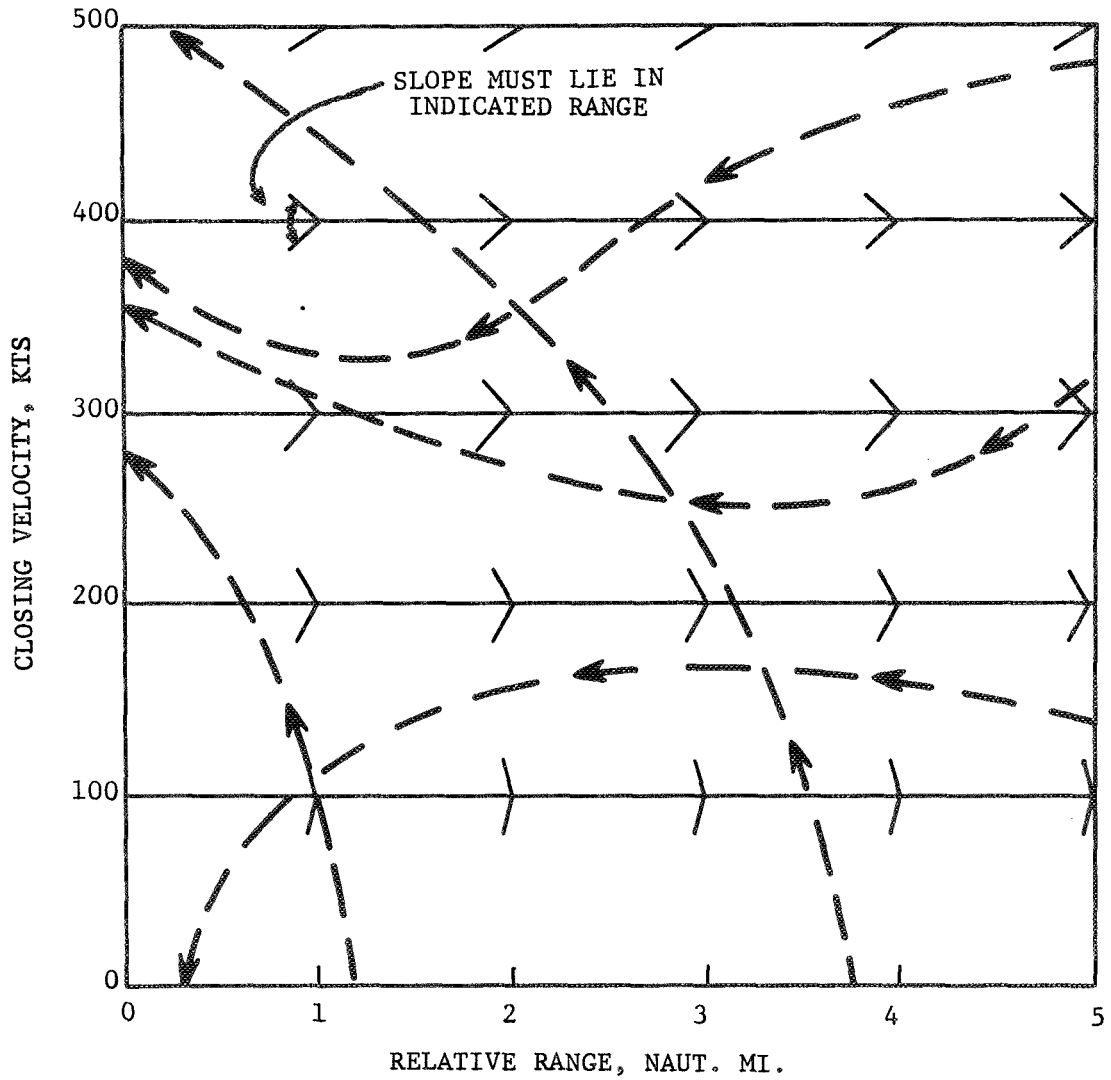


Figure C-1. Phase plane plot indicating slope isoclines for trajectories with accelerations not exceeding $\pm 1/2$ g. A set of allowable trajectories is also sketched.

APPENDIX D
RECEIVER DATA PROCESSING

General Description

The following documents the calculations for voltages from the receiver that are analogs of range, range rate, range acceleration, normal velocity, tau, beta, miss distance, and modified tau. All of these voltage levels are calculated from the received power levels and frequencies. The calculations are based on both theoretical models and empirical data derived during the receiver calibrations at LRC.

After calculation of the voltage analogs, a conversion is made to the corresponding geometrical value and the errors relative to the ground based radar values and experimental values are calculated. The inputs to this part of the simulation program include the received power levels and frequencies, the geometrical and experimental values of parameters, and the applicable system parameters.

Input Parameters

Inputs used in this section of the program include the following:

Δt	= Calculation time increment
τ_a	= AGC loop time constant
τ_{d1}	= Discrimination time constant
τ_{d2}	= Differentiator time constant
$f(P, f_d)$	= Receiver response characteristic as a fraction of IF amplifier input power level (P) and doppler frequency (f_d) (experimentally determined)

Experimental (determined from reduction of flight records) values of range, range rate, etc.

Geometrical (derived from ground-based radar) values of range, range rate, etc.

Calculations

Using the values of doppler frequency and power at the IF amplifier input, the voltage from the receiver-detector is calculated from the function $f(P, f_d)$. This experimentally determined receiver calibration function is shown in Fig. D-1. Figure D-2 indicates the detected voltage versus power at the IF amplifier input for a particular frequency (1600 Hz). The output of the detector is a voltage analogous to range in nautical miles. It should be noted that the function shown in Fig. D-1 is introduced into the computer as points at 100 Hz intervals of frequency, and linear interpolation is used to calculate values at intermediate frequencies.

The time response characteristics are introduced into the calculation by the following technique: The detector low-pass filter output voltage is given by the equation

$$\hat{V}_o = \hat{V}_i \left[\frac{1}{\tau_a S + 1} \right] \quad (D-1)$$

where V_i is the input voltage, τ_a is the filter time constant, and S is the Laplace variable. In differential equation form,

$$\tau_a \frac{dv_o}{dt} + v_o = v_i \quad (D-2)$$

Approximating the derivative gives

$$\tau_a \frac{v_o^n - v_o^{n-1}}{\Delta t} + v_o^n = v_i^n \quad (D-3)$$

where the superscripts indicate the calculation increment. Solving for the current (nth) value of output voltage gives

$$v_o^n = \frac{v_i^n + \frac{\tau_a}{\Delta t} v_o^{n-1}}{\left(1 + \frac{\tau_a}{\Delta t} \right)} \quad (\text{volts}) \quad (D-4)$$

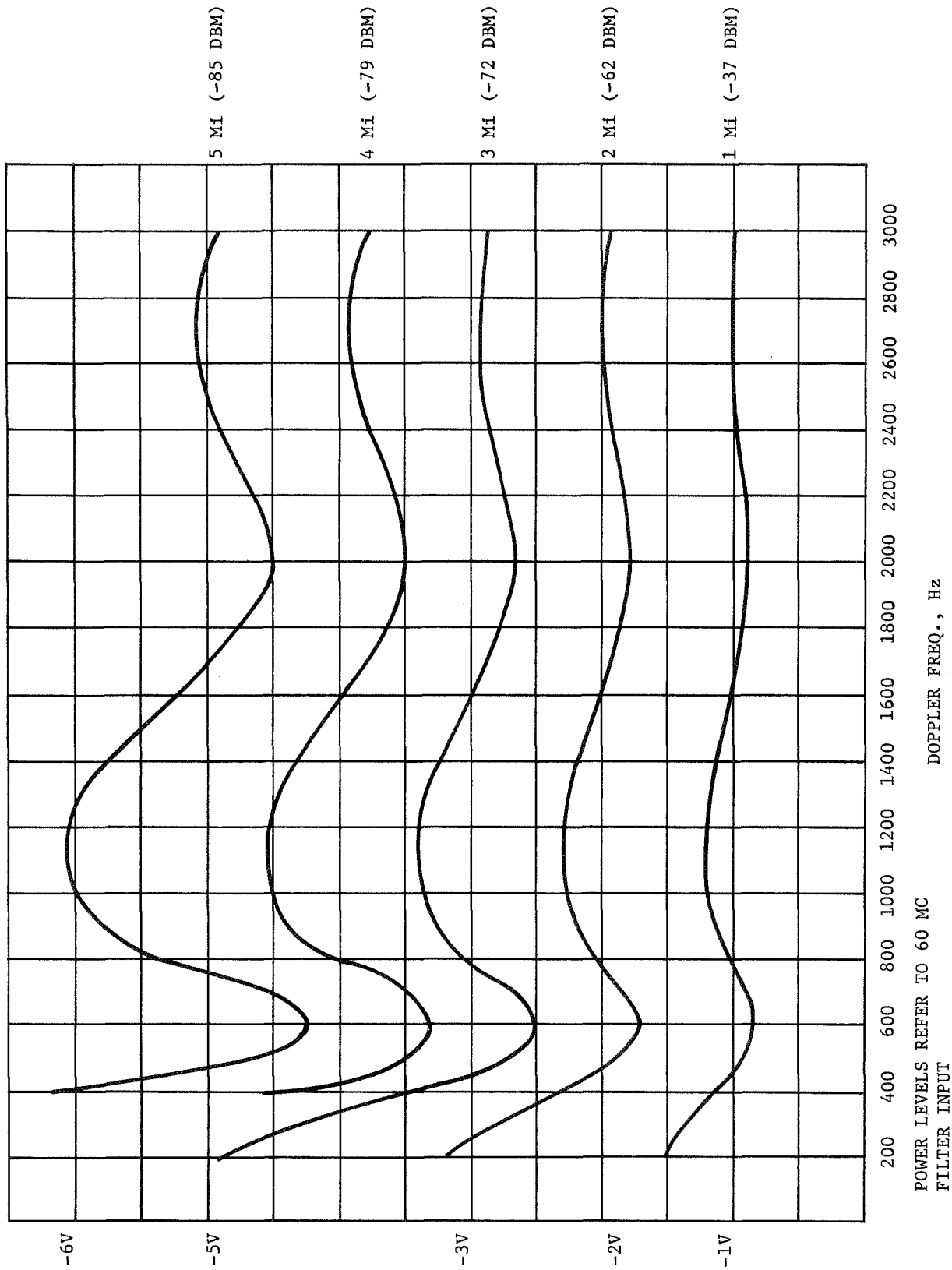


Figure D-1. Receiver detector and doppler filter characteristics.

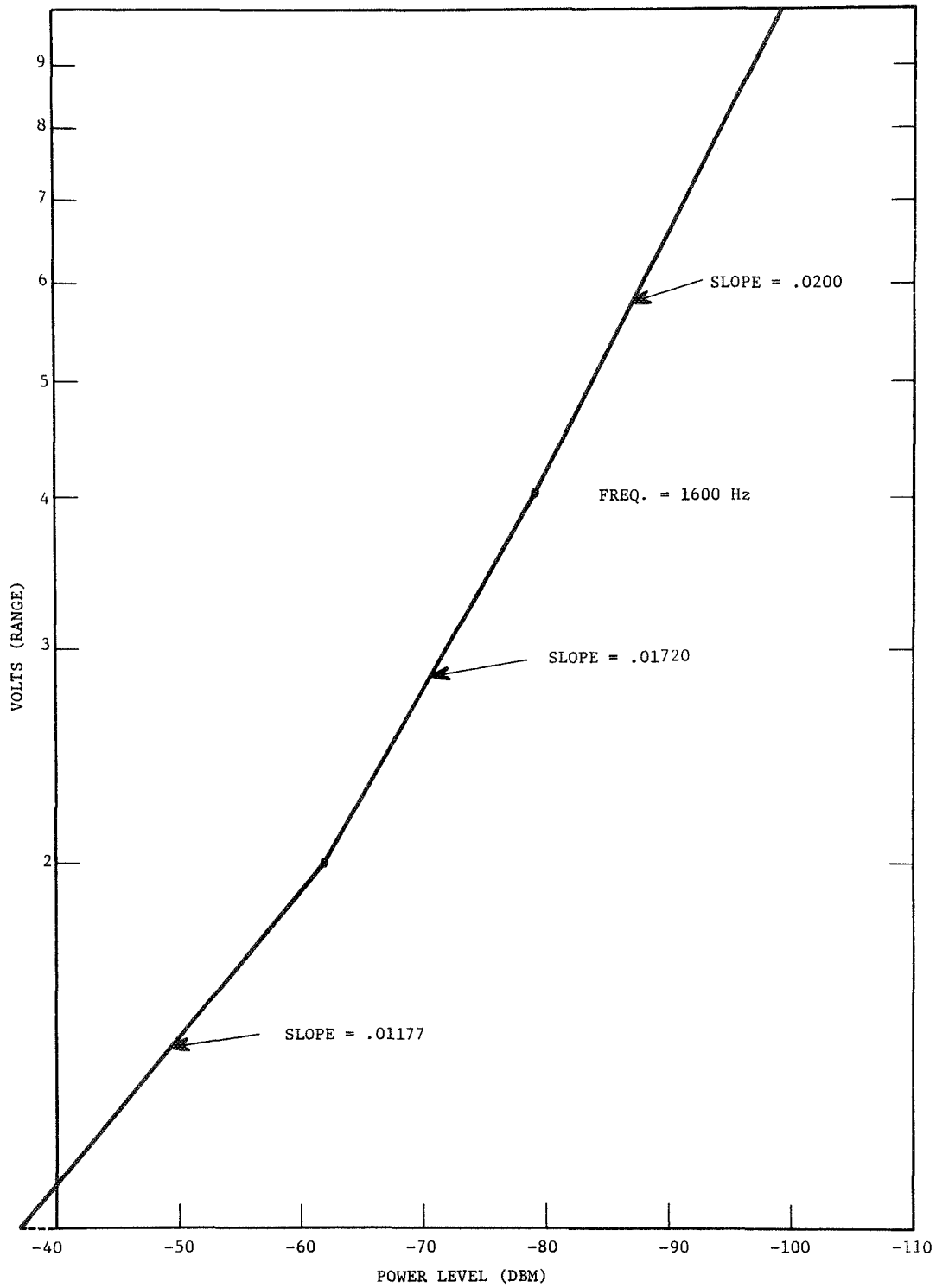


Figure D-2. Power at IF amp input (DBM).

Equation D-4 is then used to calculate the detector output (range) voltage. Provisions are, of course, made to assure the proper initial conditions to prevent transients. Similar expressions are used for the discriminator and differentiator filter voltage outputs.

The percentage errors between measured, geometrical and experimental values (see printout of Fig. 18) are calculated as, for example,

$$\% \text{ error EXP-GEO} = \frac{\text{Exp. range} - \text{Geo. range}}{\text{Geo. range}} \times 100. \quad (\text{D-5})$$

Percentage errors due to power variations (e.g. gain calibration and antenna pattern characteristics) are calculated from expressions such as,

$$\% \text{ error (antenna pattern)} = K (\Delta G) \quad (\text{D-6})$$

where ΔG is the antenna gain variation in db and K is a constant reflecting the detector slope (i.e. the "range" voltage per DBM power at the IF amplifier input) and a conversion from base 10 logs to base e logs. The derivation of Equation D-6 is as follows: The detector characteristics at 1600 cps are given by

$$\log R = .02 P_{\text{dbm}} + C_1 \quad (\text{D-7})$$

where R is the range in n. mi. and C is a constant. Differentiation gives

$$\frac{dR}{R} = \frac{.02}{\log_{10} e} dP_{\text{dbm}}, \quad (\text{D-8})$$

and Equation D-6 follows immediately since a change in gain is equivalent to a change in power level.

The residual errors are calculated as indicated by the numbers on the printout sheet. For example,

$$\text{Residual (1 - 2 * 3 * 4 * 6) =}$$

$$\left[\frac{(\text{EXP-GEO \% error} + 100)}{100} - \frac{(\text{dop. fil. \% error} + 100)}{100} \times \frac{(\text{det. slope \% error} + 100)}{100} \times \frac{(\text{el. pattern \% error} + 100)}{100} \times \frac{(\text{gain calib. \% error} + 100)}{100} \right] \times 100 - 100.$$

APPENDIX E
SYSTEM PARAMETERS

System parameters form an input to the simulation program, and are a punched card input. Following is a list of the system parameters used.

<u>No.</u>	<u>Parameter</u>	<u>Units</u>	<u>Value</u>
1	Transmitted Power	DBM	30.00
2	High Transmitter Freq.	MC	4252.50
3	Low Transmitter Freq.	MC	2702.50
4	Oscillator Deviation Del	MC	2.50
5	Oscillator Deviation Del	MC	.50
6	Bal. Mixer Bias Power	DBM	-22.00
7	Transponder Output Sat. Power	DBM	30.00
8	Transponder Gain Constant	DB	176.50
9	Transponder Input to Bal. Mixer Gain	DB	49.50
10	Transponder Input Channel Bandwidth	MC	12.00
11	Transponder Output Channel Bandwidth	MC	2.00
12	Transponder Noise Figure	DB	8.50
13	Transmitter-Transponder Isolation	DB	-150.00
14	Receiver Noise Figure	DB	6.30
15	Doppler Filter Bandwidth	KC	3.00
16	Power Gain Constant-Rec. Input to I.F. Amp Input	DB	28.50
17	Transponder-Receiver Isolation	DB	-150.00
18	Spare	--	0.00
19	Spare	--	0.00
20	AGC Time Constant	SECS	3.00
21	Discriminator Time Constant	SECS	1.00
22	Differentiator Time Constant	SECS	1.00
23	Spare	--	0.00

<u>No.</u>	<u>Parameter</u>	<u>Units</u>	<u>Value</u>
24	4.25 Transmitter Antenna Gain	DB	3.90
25	4.25 Transponder Antenna Gain	DB	-1.50
26	2.70 Transmitter Antenna Gain	DB	5.20
27	2.70 Transponder Antenna Gain	DB	-1.00
28	1.55 Receiver Antenna Gain	DB	1.80
29	1.55 Transponder Antenna Gain	DB	.50
30	Spare	--	0.00

*

Note: Antenna gain values are adjusted for loss factors in some cases.

APPENDIX F
FLIGHT TEST DATA

In this Appendix, computer printouts for the flight tests discussed in Section V are presented. Although the printouts were obtained every 5 seconds during each flight test, the printouts are given only for the first point at which the alarm was received in order to conserve space. In cases where no alarm was received (in the simulated flight) a printout near the point of minimum R^2_{τ} is given. For interpretation of the printouts, see the discussion in Section V-B.

It should be noted that during the flight test, the systems in the aircrafts were slightly different. For simulation purposes, however, both systems were assumed to be configured as was the prime system. Thus the simulated systems (system 1 and system 2) are identical. System 1 was the prime test aircraft, and the aircraft on which the experimental data were obtained.

FLIGHT NO. 78, PAGE 25, ELAPSED TIME 145.07 SEC; GREENWICH TIME 16 HRS 49 MIN 53.30 SEC

GEOMETRICAL PARAMETERS

AIRCRAFT 1 AIRCRAFT 2
 X Y X Y R V/C V/D V/C V/W I TAU D R0 BETA TM A7 EL
 (NM) (NM) (NM) (NM) (KTS) (FT/S2) (KTS) (FT/S2) (KTS) (NM) (NM) (NM) (NM) (NM) (NM) (DEG) (DEG)
 -5.40 -1.75 .82 -7.62 -1.67 .57 2.2 133. 6.6 1.77 177. 22. 61. 3.0 1.8 302. 30. 22. 104. -4.

TRANSPONDER OUTPUTS

NOISE POWER (DBM) SYSTEM 1 SYSTEM 2
 -23. -23.
 SIGNAL POWER (DBM) 11. 7.
 SATURATION FACTOR 1.18 1.11

ANTENNA GAIN VARIATIONS (DB)

SYSTEM 1 SYSTEM 2
 4.25 TRANSMITTER -2.1 1.4
 4.25 TRANSPONDER -2.2 -1.1
 2.70 TRANSMITTER -2.6 -1.3
 2.70 TRANSPONDER -2.2 -1.1
 1.55 TRANSPONDER -2.2 -1.1
 1.55 RECEIVER .1 -2.7
 TOTAL -5.2 -3.0

RECEIVER OUTPUTS

SYSTEM 1 SYSTEM 2
 SIGNAL LEVEL AT I.F. AMP (DBM) -72.5 -70.5
 SNR AT DOPPLER FILTER OUTPUT (DB) 34.4 36.4
 AGE VOLTAGE (VOLTS) -1.7 -1.8
 VOLTAGE AT L.P. FILTER OUTPUT (VOLTS) -3.2 -2.8
 DOPPLER FREQUENCY (CPS) 708.4 708.4
 ALARM STATUS ON ON

MEASURED PARAMETERS

	1	2	3	4	5	6
RANGE (NM)	2.2	3.1	3.2	-1.00	40.8	41.5
RANGE RATE (KTS)	133.		137.	-1.23		3.1
RANGE ACCEL (FT/S2)	6.6		6.0	-0.53		-8.9
NORMAL VEL (KTS)	177.		271.	.92		13.5
TAU (SEC)	61.	43.	93.	1.04	36.4	37.3
BETA (NM2SEC)	302.	815.	829.	1.77	170.0	174.9
MISS DISTANCE (NM)	3.0		4.6	1.96		55.8
MODIFIED TAU (SEC)	30.		40.			37.2

CALCULATED % ERROR BREAKDOWN

	1	2	3	4	5	6
EXP-GF1	40.8	-1.9	4.2	5.1	19.9	11.5
EXP-GF2	36.4	-1.9	4.3	5.1	19.9	11.5
EXP-GF3	170.1	-5.6	13.3	16.0	72.4	38.8
TOTAL PATTERN						
GAIN CALIB						1-2*3*4*6 1-2*3*5*6
% ERROR						20.9
% ERROR EXP-GF1						16.6
% ERROR EXP-GF2						174.1
% ERROR EXP-GF3						40.0

Figure F-2. Computer printout of flight test simulation for Flight 78.

GEOMETRICAL PARAMETERS

AIRCRAFT 1	AIRCRAFT 2	X (NM)	Y (NM)	Z (NM)	R (NM)	VC (KTS)	VCD (FT/SQ)	VN (KTS)	T (SEC)	TAU (NM)	D (NM)	BETA (DEG)	TM (SEC)	AZ (DEG)	EL (DEG)	
2.52	-0.87	0.2	5.91	-1.73	0.63	3.5	321.	0.2	0.2	39.	0.4	0.6	481.	28.355	355.	-3.

TRANSPONDER OUTPUTS

NOISE POWER (DBM)	SIGNAL POWER (DBM)	SATURATION FACTOR	SYSTEM 1	SYSTEM 2
-22.	-22.	1.08	1.08	1.08

ANTENNA GAIN VARIATIONS (DB)

4.25 TRANSMITTER	4.25 TRANSDUCER	2.70 TRANSMITTER	2.70 TRANSDUCER	1.55 TRANSDUCER	1.55 RECEIVER	TOTAL	SYSTEM 1	SYSTEM 2
-4	-4	-4	-4	-1	-1	-1.3	-1.4	-1.4

RECEIVER OUTPUTS

SIGNAL LEVEL AT I.F. AMP (DBM)	SAR AT DOPPLER FILTER OUTPUT (DB)	AGC VOLTAGE (VOLTS)	VOLTAGE AT L.P. FILTER OUTPUT (VOLTS)	DOPPLER FREQUENCY (CPS)	ALARM STATUS	SYSTEM 1	SYSTEM 2
-80.2	-26.7	-1.5	4.4	1713.	ON	-80.3	-80.3

MEASURED PARAMETERS

RANGE (NM)	RANGE RATE (KTS)	RANGE ACCEL (FT/SQ)	NORMAL VEL (KTS)	TAU (SEC)	ETA (NM/SEC)	MISS DISTANCE (NM)	MODIFIED TAU (SEC)	EXP VALUE	CAL VALUE	DIFFERENCE	% ERROR	EXP-REF	CAL-REF	% ERROR	EXP-CALI
3.5	321.	0.2	39.	39.	481.	28.355	355.	6.8	3.2	3.6	52.9	95.4	25.4	55.8	55.8

CALCULATED % ERROR BREAKDOWN

RANGE (NM)	TAU (SEC)	BETA (NM/SEC)	EXP-GEO	DOPPLER	FI	TOTAL	GAIN	RESIDUAL
95.4	39.4	67.3	643.2	11.9	4.1	6.1	13.8	68.0

Figure F-6. Computer printout of flight test simulation for Flight 80.

FLIGHT NO. 9D, PAGE 21, ELAPSED TIME 110.00 SEC, GREENWICH TIME 16 HRS 35 MIN 32.20 SEC

GEOMETRICAL PARAMETERS

AIRCRAFT 1		AIRCRAFT 2		R		VC		VCD		VN		T		TAU		D		RO		BETA		TM		AZ		EL			
(NM)	(NM)	(NM)	(NM)	(NM)	(NM)	(KTS)	(KTS)	(F/S2)	(F/S2)	(KTS)	(KTS)	(SEC)	(SEC)	(NM)	(NM)	(NM)	(NM)	(NM)	(NM)	(NM)	(NM)	(NM)	(NM)	(NM)	(NM)	(NM)	(NM)	(NM)	
4.78	-1.02	.82	5.27	2.95	.71	4.0	33.	11.8	12.64	317.	5.	433.	38.2	4.0	6913.	52.	265.	280.	-2.										

TRANSPONDER OUTPUTS

NOISE POWER (DBM)	SIGNAL POWER (DBM)	SATURATION FACTOR	SYSTEM 1	SYSTEM 2
-22.	-23.	1.06	1.10	5.

ANTENNA GAIN VARIATIONS (DB)

SYSTEM 1		SYSTEM 2	
4.25	TRANSMITTER	1.2	-1.9
4.25	TRANSPONDER	-0.	-0.
2.70	TRANSMITTER	1.8	.2
2.70	TRANSPONDER	-0.	-0.
1.55	TRANSPONDER	-0.	-0.
1.55	RECEIVER	.1	.1
	TOTAL	2.9	-1.7

RECEIVER OUTPUTS

SYSTEM 1		SYSTEM 2	
	SIGNAL LEVEL AT I.F. AMP (DBM)	-79.5	-84.0
	SNR AT DOPPLER FILTER OUTPUT (DB)	27.5	23.0
	AGC VOLTAGE (VOLTS)	-1.5	-1.2
	VOLTAGE AT L.P. FILTER OUTPUT (VOLTS)	-6.2	-7.5
	DOPPLER FREQUENCY (CPS)	200.	200.
	ALARM STATUS	OFF	OFF

MEASURED PARAMETERS

GEO VALUE	EXP VALUE	CAL VALUE	LOG VALUE	% ERROR EXP-GED	% ERROR CAL-GED	% ERROR EXP-CAL
RANGE (NM)	4.0	7.0	6.2	74.9	54.7	12.9
RANGE RATE (KTS)	33.	44.	-2.22	31.9	31.9	
RANGE ACCEL (F/S2)	11.8	10.4	-1.1	-11.5	-11.5	
NORMAL VEL (KTS)	317.	371.	.27	17.0	17.0	
TAU (SEC)	433.	508.	-53	32.4	17.3	12.9
BETA (NM2SEC)	6913.	27963.	19405.	304.5	180.7	44.1
MISS DISTANCE (NM)	38.2	52.4	-26		37.2	
MODIFIED TAU (SEC)	52.	375.			625.8	

CALCULATED % ERROR BREAKDOWN

SYSTEM 1		SYSTEM 2		SYSTEM 3		SYSTEM 4		SYSTEM 5		SYSTEM 6	
EXP-GEO	DOPPLER	FIL	SLOPE	DETECTOR	EL	PATTERN	TOTAL	GAIN	RESIDUAL	CALIB	RESIDUAL
74.9	41.4	8.1	1.1	1.1	1.1	-13.4	-13.4	13.8	-0.9	1-2*3*4*6	1-2*3*5*6
32.4	41.4	8.1	1.1	1.1	1.1	-13.4	-13.4	13.8	-43.4	24.4	24.4
304.5	182.5	26.4	3.2	3.2	3.2	-35.2	-35.2	47.4	-116.7	103.1	103.1

Figure F-9. Computer printout of flight test simulation for Flight 9D.

GEOMETRICAL PARAMETERS

AIRCRAFT 1 AIRCRAFT 2
 X Y Z X Y Z R VC VCD VCN VN T TAU D RO BETA TH AZ EL.
 (NM) (NM) (NM) (NM) (NM) (NM) (KTS) (FT/S2)(1/M)(KTS)(SEC) (SEC) (NM) (NM) (NM2SEC)(SEC) (DEG) (DEG) (DER)
 -7.92 1.11 .82-10.71 .34 .70 2.9 96. .14 .15 50. 56. 109. 1.5 2.0 909. 38. 336. 129. -2.

TRANSPONDER OUTPUTS

	SYSTEM 1	SYSTEM 2
NOISE POWER (DBM)	-22.	-23.
SIGNAL POWER (DBM)	-31.	4.
SATURATION FACTOR	1.00	1.09

ANTENNA GAIN VARIATIONS (DB)

	SYSTEM 1	SYSTEM 2
4.25 TRANSMITTER	-2.0	-15.0
4.25 TRANSPONDER	-1	-1
2.70 TRANSMITTER	-1.1	-24.2
2.70 TRANSPONDER	-1	-0
1.55 TRANSMITTER	-1.1	-0
1.55 RECEIVER	.5	-10.9
TOTAL	-3.1	-50.2

RECEIVER OUTPUTS

	SYSTEM 1	SYSTEM 2
SIGNAL LEVEL AT I.F. AMP (DBM)	-77.0	-123.8
SNR AT DOPPLER FILTER OUTPUT (DB)	29.9	-16.9
AGC VOLTAGE (VOLTS)	-1.0	-1.0
VOLTAGE AT L.P. FILTER OUTPUT (VOLTS)	-3.6	-26.9
DOPPLER FREQUENCY (CPS)	512.	512.
ALARM STATUS	OFF	OFF

MEASURED PARAMETERS

	GED VALUE	EXP VALUE	CAL VALUE	VOLTS (LOG)	% ERROR EXP-GED	% ERROR CAL-GED	% ERROR EXP-CAL
RANGE (NM)	2.9	3.5	3.6	-1.88	22.1	25.3	-2.5
RANGE RATE (KTS)	96.		96.	-1.53		.5	
RANGE ACCEL (FT/S2)	4		4	-3.15		.8	
NORMAL VEL (KTS)	50.		56.	2.02		12.3	
TAU (SEC)	109.	132.	135.	.62	21.4	24.6	-2.6
BETA (NM2SEC)	909.	1641.	1776.	1.11	80.6	95.5	-7.6
MISS DISTANCE (NM)	1.5		2.1	2.64		40.0	
MODIFIED TAU (SEC)	38.		75.			97.6	

CALCULATED % ERROR BREAKDOWN

	1	2	3	4	5	6
EXP-GEO	22.1					
DOPPLER FIL	-4.0					
DETECTOR SLOPE	2.4					
TOTAL PATTERN	21.4					
GAIN CALIB	80.6					
RESIDUAL						
EL						
PATTERN						
TOTAL PATTERN						
GAIN CALIB						
RESIDUAL						
EL						
PATTERN						
TOTAL PATTERN						
GAIN CALIB						
RESIDUAL						
EL						
PATTERN						
TOTAL PATTERN						
GAIN CALIB						
RESIDUAL						
EL						
PATTERN						
TOTAL PATTERN						
GAIN CALIB						
RESIDUAL						
EL						
PATTERN						
TOTAL PATTERN						
GAIN CALIB						
RESIDUAL						
EL						
PATTERN						
TOTAL PATTERN						
GAIN CALIB						
RESIDUAL						
EL						
PATTERN						
TOTAL PATTERN						
GAIN CALIB						
RESIDUAL						
EL						
PATTERN						
TOTAL PATTERN						
GAIN CALIB						
RESIDUAL						
EL						
PATTERN						
TOTAL PATTERN						
GAIN CALIB						
RESIDUAL						
EL						
PATTERN						
TOTAL PATTERN						
GAIN CALIB						
RESIDUAL						
EL						
PATTERN						
TOTAL PATTERN						
GAIN CALIB						
RESIDUAL						
EL						
PATTERN						
TOTAL PATTERN						
GAIN CALIB						
RESIDUAL						
EL						
PATTERN						
TOTAL PATTERN						
GAIN CALIB						
RESIDUAL						
EL						
PATTERN						
TOTAL PATTERN						
GAIN CALIB						
RESIDUAL						
EL						
PATTERN						
TOTAL PATTERN						
GAIN CALIB						
RESIDUAL						
EL						
PATTERN						
TOTAL PATTERN						
GAIN CALIB						
RESIDUAL						
EL						
PATTERN						
TOTAL PATTERN						
GAIN CALIB						
RESIDUAL						
EL						
PATTERN						
TOTAL PATTERN						
GAIN CALIB						
RESIDUAL						
EL						
PATTERN						
TOTAL PATTERN						
GAIN CALIB						
RESIDUAL						
EL						
PATTERN						
TOTAL PATTERN						
GAIN CALIB						
RESIDUAL						
EL						
PATTERN						
TOTAL PATTERN						
GAIN CALIB						
RESIDUAL						
EL						
PATTERN						
TOTAL PATTERN						
GAIN CALIB						
RESIDUAL						
EL						
PATTERN						
TOTAL PATTERN						
GAIN CALIB						
RESIDUAL						
EL						
PATTERN						
TOTAL PATTERN						
GAIN CALIB						
RESIDUAL						
EL						
PATTERN						
TOTAL PATTERN						
GAIN CALIB						
RESIDUAL						
EL						
PATTERN						
TOTAL PATTERN						
GAIN CALIB						
RESIDUAL						
EL						
PATTERN						
TOTAL PATTERN						
GAIN CALIB						
RESIDUAL						
EL						
PATTERN						
TOTAL PATTERN						
GAIN CALIB						
RESIDUAL						
EL						
PATTERN						
TOTAL PATTERN						
GAIN CALIB						
RESIDUAL						
EL						
PATTERN						
TOTAL PATTERN						
GAIN CALIB						
RESIDUAL						
EL						
PATTERN						
TOTAL PATTERN						
GAIN CALIB						
RESIDUAL						
EL						
PATTERN						
TOTAL PATTERN						
GAIN CALIB						
RESIDUAL						
EL						
PATTERN						
TOTAL PATTERN						
GAIN CALIB						
RESIDUAL						
EL						
PATTERN						
TOTAL PATTERN						
GAIN CALIB						
RESIDUAL						
EL						
PATTERN						
TOTAL PATTERN						
GAIN CALIB						
RESIDUAL						
EL						
PATTERN						
TOTAL PATTERN						
GAIN CALIB						
RESIDUAL						
EL						
PATTERN						
TOTAL PATTERN						
GAIN CALIB						
RESIDUAL						
EL						
PATTERN						
TOTAL PATTERN						
GAIN CALIB						
RESIDUAL						
EL						
PATTERN						
TOTAL PATTERN						
GAIN CALIB						
RESIDUAL						
EL						
PATTERN						
TOTAL PATTERN						
GAIN CALIB						
RESIDUAL						
EL						
PATTERN						
TOTAL PATTERN						
GAIN CALIB						
RESIDUAL						
EL						
PATTERN						
TOTAL PATTERN						
GAIN CALIB						
RESIDUAL						
EL						
PATTERN						
TOTAL PATTERN						
GAIN CALIB						
RESIDUAL						
EL						
PATTERN						
TOTAL PATTERN						

FLIGHT NO. 10D, PAGE 42, ELAPSED TIME 215.00 SEC, GREENWICH TIME 22 HRS 46 MIN 40.50 SEC

GEOMETRICAL PARAMETERS

X (NM)	Y (NM)	Z (NM)	AIR(CRAFT 1)	X (NM)	Y (NM)	Z (NM)	R (NM)	VC (KTS)	VCD (FT/S2)	VN (KTS)	VM (KTS)	I (SEC)	TAU (NM)	D (NM)	RD (NM)	BETA IN (NM/SEC)	IN (SEC)	AZ (DEG)	EL (DEG)
-9.48	1.16	.82-10.64	-7.73	.52	2.2	115.	1.4	.43	82.	58.	70.	1.6	.9	352.	31.294	88.	-9.		

TRANSPONDER OUTPUTS

NOISE POWER (DBM)	SIGNAL POWER (DBM)	SATURATION FACTOR	SYSTEM 1	SYSTEM 2
-25.	6.	1.10		

ANTENNA GAIN VARIATIONS (DB)

4.25 TRANSMITTER	4.25 TRANSPONDER	2.70 TRANSMITTER	2.70 TRANSPONDER	1.55 TRANSMITTER	1.55 TRANSPONDER	TOTAL
-2.9	-1.4	-1.4	-1.4	-1.4	-1.4	-6.6

RECEIVER OUTPUTS

SIGNAL LEVEL AT I.F. AMP (DBM)	SNR AT DOPPLER FILTER OUTPUT (DB)	AGC VOLTAGE (VOLTS)	VOLTAGE AT L.F. FILTER OUTPUT (VOLTS)	DOPPLER FREQUENCY (CPS)	ALARM STATUS
-75.4	31.6	-1.8	-3.0	613.	ON

MEASURED PARAMETERS

RANGE (NM)	RANGE RATE (KTS)	RANGE ACCEL (FT/S2)	NORMAL VEL (KTS)	TAU (SEC)	BETA (NM/SEC)	MISS DISTANCE (NM)	MODIFIED TAU (SEC)	% ERROR CAL-EXP	% ERROR CAL-GE0	% ERROR EXP-CAL
2.2	115.	1.4	82.	70.	352.	1.6	31.	55.1	42.4	5.3

CALCULATED & ERROR BREAKDOWN

EXP-GE0	DOPPLER	FIL	SLOPE	DETECTOR	EL	TOTAL	PATTERN	CALIB	RESIDUAL
42.4	-14.9	3.2	20.8	30.8	11.5	14.3	24.1	14.3	111.7

Figure F-14. Computer printout of flight test simulation for Flight 10D.

GEOMETRICAL PARAMETERS

AIRCRAFT 1 AIRCRAFT 2
 X Y Z X Y Z R VC VCD VCN VN T TAU D RO BETA TM AZ EL
 (NM) (NM) (NM) (NM) (NM) (NM) (KTS) (KTS) (FT/S2) (1/M) (KTS) (SEC) (SEC) (NM) (NM) (NM) (NM) (NM) (DEG) (DEG)
 -8.26 1.76 .82 -9.25 -.61 .34 2.56 148. 9.6 2.31 231. 61. 64. 4.1 .5 433. 32. 281. 80. -11.

TRANSPONDER OUTPUTS

TRANSPONDER OUTPUTS
 SYSTEM 1 SYSTEM 2
 PULSE POWER (DBM) -22. -22.
 SIGNAL POWER (DBM) -6. 2.
 SATURATION FACTOR 1.04 1.07

ANTENNA GAIN VARIATIONS (DB)
 SYSTEM 1 SYSTEM 2
 4.25 TRANSMITTER -1.6 -6.7
 4.25 TRANSPONDER -1.9 -1.2
 2.70 TRANSMITTER -1.5 -6.7
 2.70 TRANSPONDER -1.9 -6.8
 1.55 TRANSPONDER -1.4 -9
 1.55 RECEIVER -1.9 -1.0
 TOTAL -9.5 -17.3

RECEIVER OUTPUTS

RECEIVER OUTPUTS
 SYSTEM 1 SYSTEM 2
 SIGNAL LEVEL AT I.F. AMP (DBM) -80.5 -88.3
 SNR AT DOPPLER FILTER OUTPUT (DB) 26.5 18.6
 AGC VOLTAGE (VOLTS) -1.4 -1.3
 VOLTAGE AT L.P. FILTER OUTPUT (VOLTS) -4.8 -6.3
 DOPPLER FREQUENCY (CPS) 787. 787.
 ALARM STATUS OFF OFF

MEASURED PARAMETERS

MEASURED PARAMETERS
 GEO. VALUE EXP. VALUE CAL. VALUE VOLTS (LOG)
 RANGE (NM) 2.6 5.1 4.8 -1.14
 RANGE RATE (KTS) 148. 152. 6.7 -52
 RANGE ACCEL (FT/S2) 9.6 262. 58
 NORMAL VEL (KTS) 231. 113. 78
 TAU (SEC) 64. 122. 113. 78
 BETA (NM/SEC) 483. 3226. 2577. 79
 MISS DISTANCE (NM) 4.1 8.2 1.36
 MODIFIED TAU (SEC) 32. 75.

CALCULATED % ERROR BREAKDOWN

CALCULATED % ERROR BREAKDOWN
 SYSTEM 1 SYSTEM 2 SYSTEM 3 SYSTEM 4 SYSTEM 5 SYSTEM 6
 EXP-GEO DOPPLER FIL SLOPE PATTERN EL
 RANGE (NM) 97.3 4.1 9.2 34.9 42.8 13.8
 TAU (SEC) 91.1 4.2 9.1 34.9 42.8 13.8
 BETA (NM/SEC) 645.5 13.1 4.50.0 145.5 191.1 47.4
 % ERROR CAL-GEO EXP-CAL RESIDUAL RESIDUAL
 83.2 3.3 3.3 3.3 3.3 3.3
 -29.7 13.4 13.4 13.4 13.4 13.4
 77.3 7.8 7.8 7.8 7.8 7.8
 495.6 25.2 25.2 25.2 25.2 25.2
 101.2 136.0 136.0 136.0 136.0 136.0

Figure F-15. Computer printout of flight test simulation for Flight 10E.

APPENDIX G
ANTENNA PATTERN MODELS

Pattern Models for Statistical Studies

For the statistical studies, the actual antenna patterns supplied RTI by NASA-LRC were represented by analytical expressions. Figures 1 through 7 show the static patterns with a broken line superimposed to indicate the corresponding analytical expression. Equations 1 through 9 below are the corresponding analytical expressions (note that the expressions indicate absolute voltage gain and are converted to power gain in db in the program).

Transmitter-Azimuth
(4252.5 & 2702.5 MHz)

$$\begin{aligned} A &= 1 - e^{-0.479(130 - \theta)^{0.314}} && ; 0 \leq \theta \leq 130^\circ \\ A &= 0.039 && ; 130^\circ \leq \theta \leq 180^\circ \end{aligned} \tag{G-1}$$

Transmitter-Azimuth
(4252.5 & 2702.5 MHz)

$$\begin{aligned} A &= 1 && ; 0 \leq \theta \leq 1^\circ \\ A &= \frac{\sin 9\theta}{0.162 \theta} && ; 1^\circ \leq \theta \leq 180^\circ \end{aligned} \tag{G-2}$$

Transponder-Elevation
(4252.5 MHz)

$$\begin{aligned} A &= \cos 3.83 \theta && ; 0 \leq \theta \leq 10^\circ \\ A &= \frac{\sin 4.87 \theta}{0.00972 \theta} && ; 10^\circ \leq \theta \leq 90^\circ \end{aligned} \tag{G-3}$$

Transponder-Elevation
(2702.5 MHz)

$$\begin{aligned} A &= \cos 3.74 \theta && ; 0 \leq \theta \leq 10^\circ \\ A &= \frac{\sin 4\theta}{0.0301 \theta^{1.43}} && ; 10^\circ \leq \theta \leq 90^\circ \end{aligned} \quad (G-4)$$

Transponder-Elevation
(1550 MHz)

$$\begin{aligned} A &= 1 && ; 0 \leq \theta \leq 1^\circ \\ A &= \frac{\sin 4\theta}{0.0722 \theta} && ; 1^\circ \leq \theta \leq 90^\circ \end{aligned} \quad (G-5)$$

Receiver-Azimuth

$$\begin{aligned} A &= 1 - e^{-0.0371(156-\theta)^{0.847}} && ; 0 \leq \theta \leq 156 \\ A &= 0.056 && ; 156^\circ \leq \theta \leq 180^\circ \end{aligned} \quad (G-6)$$

Receiver-Elevation

$$A = \cos 2.34 \theta \quad ; 0 \leq \theta \leq 20^\circ \quad (G-7)$$

$$A = \frac{\sin 3.75\theta}{0.00773 \theta^{1.76}} \quad ; 20^\circ < \theta \leq 180^\circ \quad (G-8)$$

Pattern Models for Flight Test Simulation

This section describes the antenna pattern models used for the flight test analysis. The horizontal and vertical plane patterns were subjected to a Fourier analysis to determine the Fourier coefficients for each of the

patterns supplied RTI by NASA-LRC. The gain at a desired aspect (θ, ϕ) was then reconstructed from the series representation (ref. G-1),

$$\begin{aligned}
 G(\theta, \phi)_{db} &= G(\theta)_{db} + G(\phi)_{db} \\
 &= \sum_{p=0}^{20} \left[\alpha_p^\theta \cos \frac{2\pi\theta p}{2N+1} + \beta_p^\theta \sin \frac{2\theta p}{2N+1} \right] \\
 &+ \sum_{\rho=0}^{20} \left[\alpha_\rho^\phi \cos \frac{2\pi\phi\rho}{2N+1} + \beta_\rho^\phi \sin \frac{2\phi\rho}{2N+1} \right]
 \end{aligned}
 \tag{G-9}$$

where,

- θ is azimuth in degrees ($0 \leq \theta \leq 360$) pos. CW
- ϕ is elevation in degrees ($0 \leq \theta \leq 360$) pos. up from nose
- α_ρ, β_ρ are the fourier coefficients
- N is no. of data points/2 (=180)

A brief analysis was conducted to indicate the total number of harmonics required to accurately describe the pattern signature. It was observed that 10 harmonics did not adequately describe the null regions while it was felt that in excess of 20 harmonic would introduce computing errors of sufficient extent to actually degrade the pattern. For the purpose of flight test analysis, 20 harmonics were used in the calculation of the gains.

The reconstructed patterns (see Fig. G-8 for an example) were observed to reproduce the static patterns within approximately two db over the major portion of the lobing structure and suffered some degradation in the null regions due to lack of high frequency components. This accuracy is considered adequate for the analysis

Ref. G-1 Goertzel, G., "Fourier Analysis," Mathematical Methods for Digital Computers, Wiley 1964

Az. 4252.5 MHz
Transmit

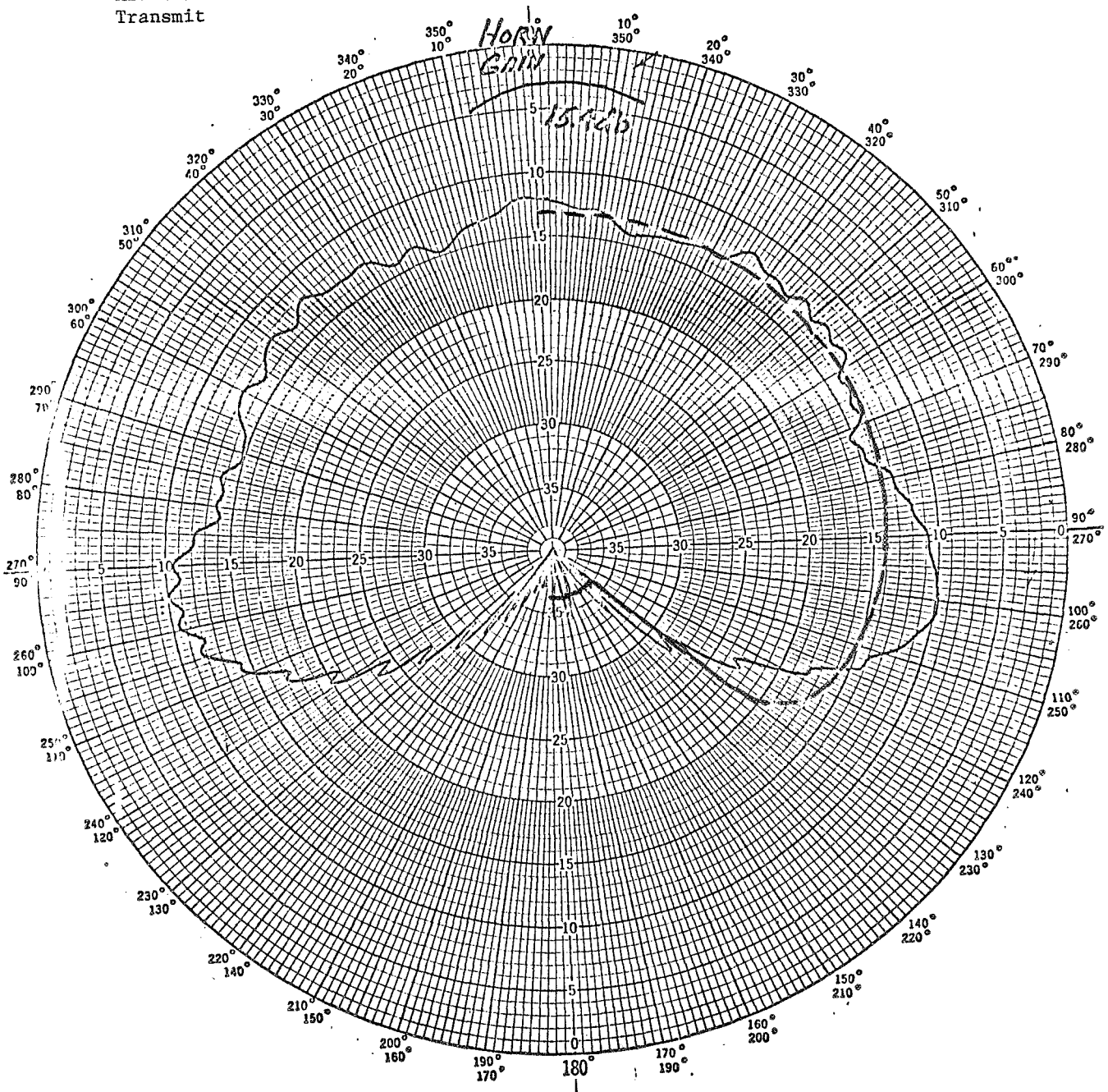


Figure G-1. Transmitter azimuth pattern (4.252 GHz).

El. 4252.5 MHz
Transmit

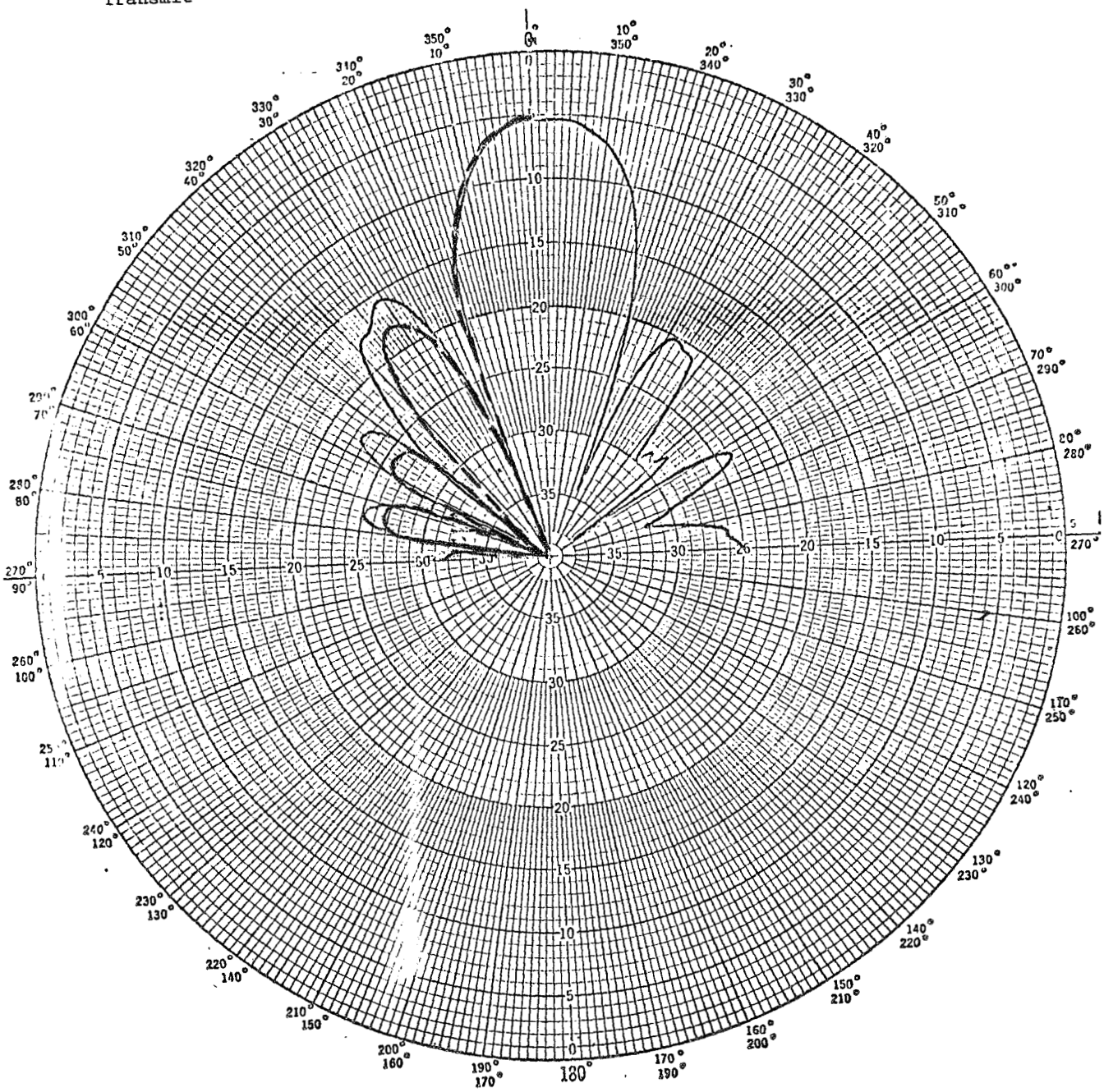


Figure G-2. Transmitter elevation pattern (4.252 GHz).

El. 4252.5 MHz
Transponder
Receive

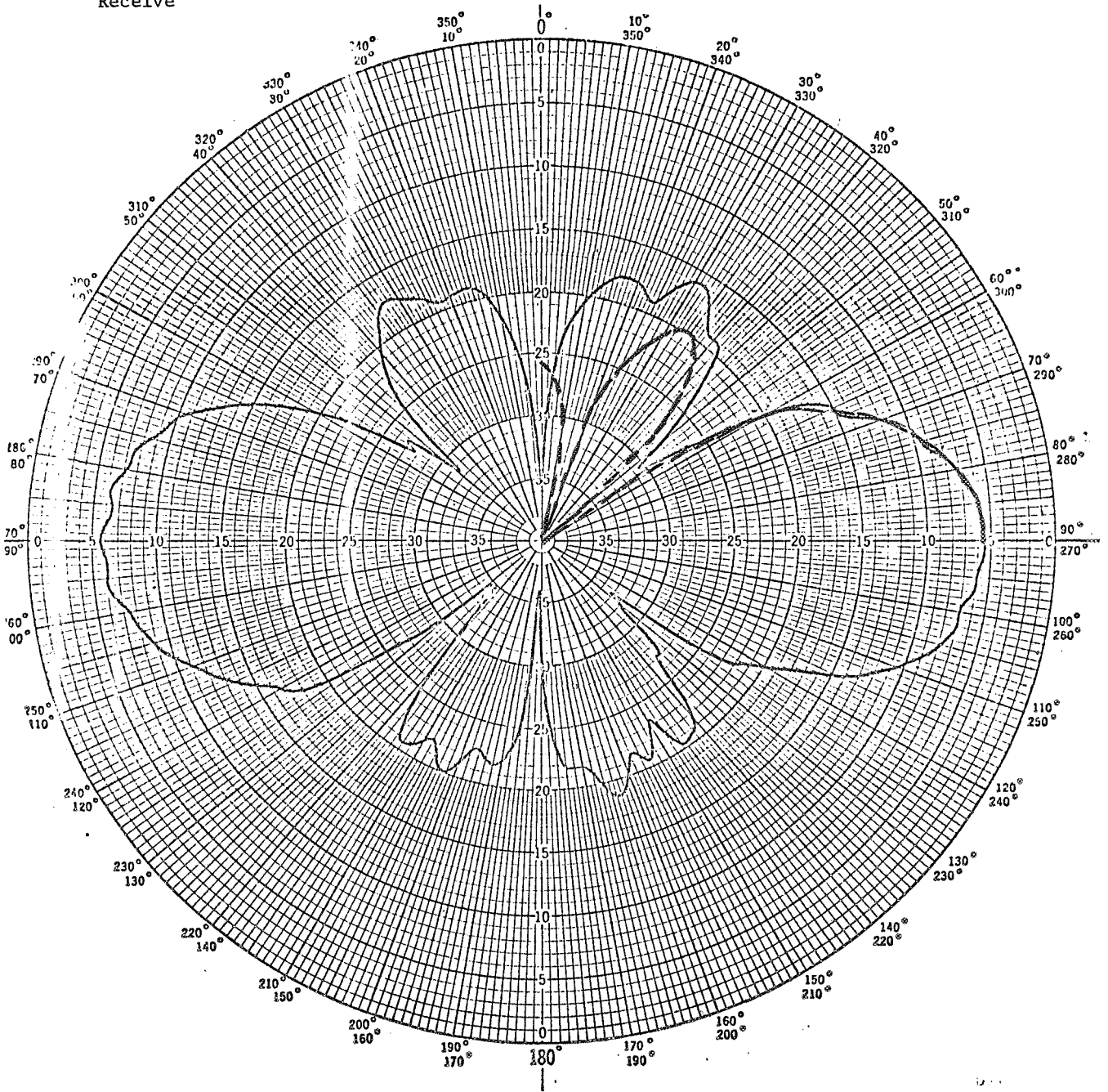


Figure G-3. Transponder receiver, elevation (4.252 GHz).

El. 2702.5 MHz
Transponder
Receive

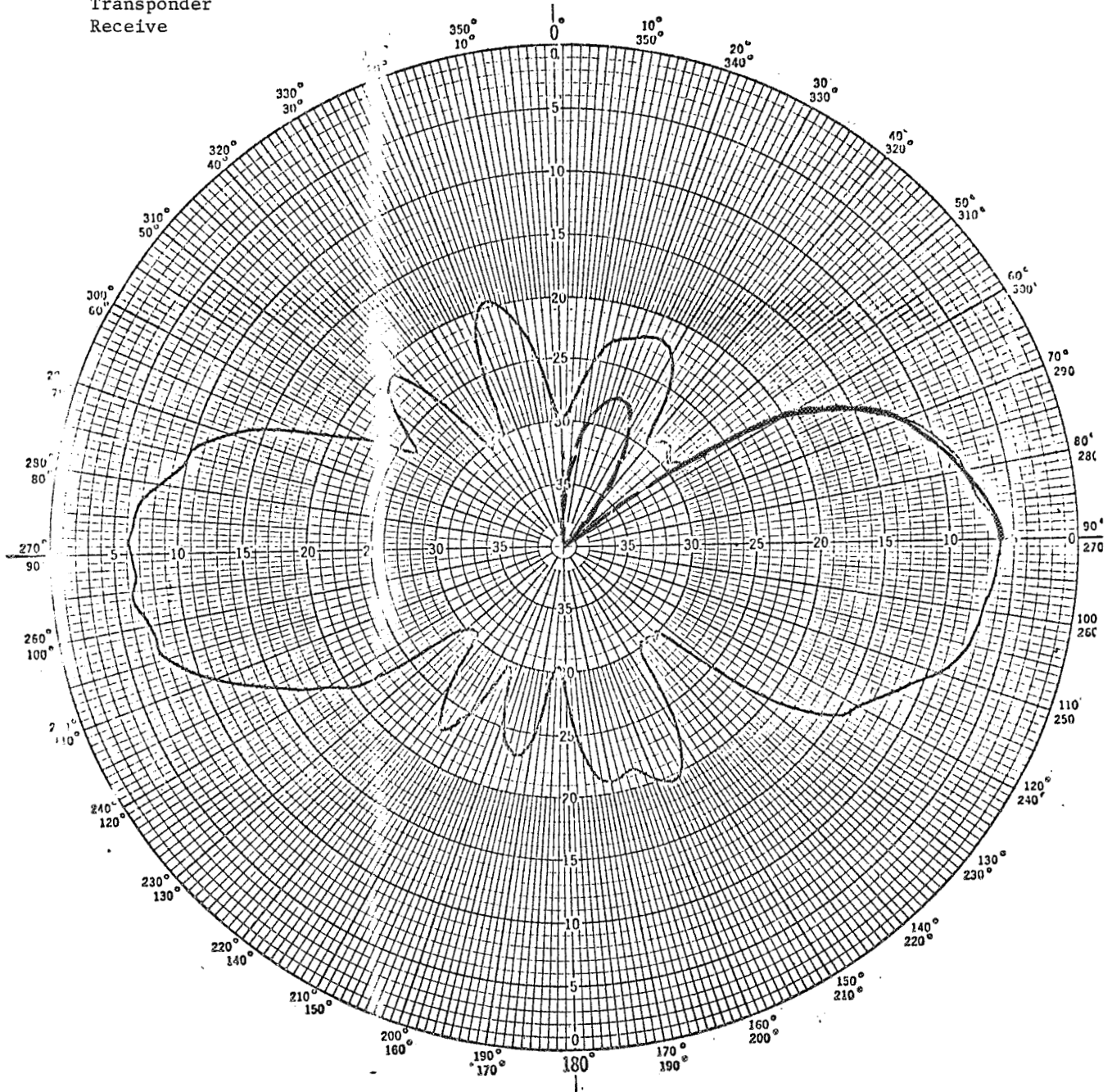


Figure G-4. Transponder receiver, elevation (2.702 GHz).

El. 1550 MHz
Transponder
Transmit

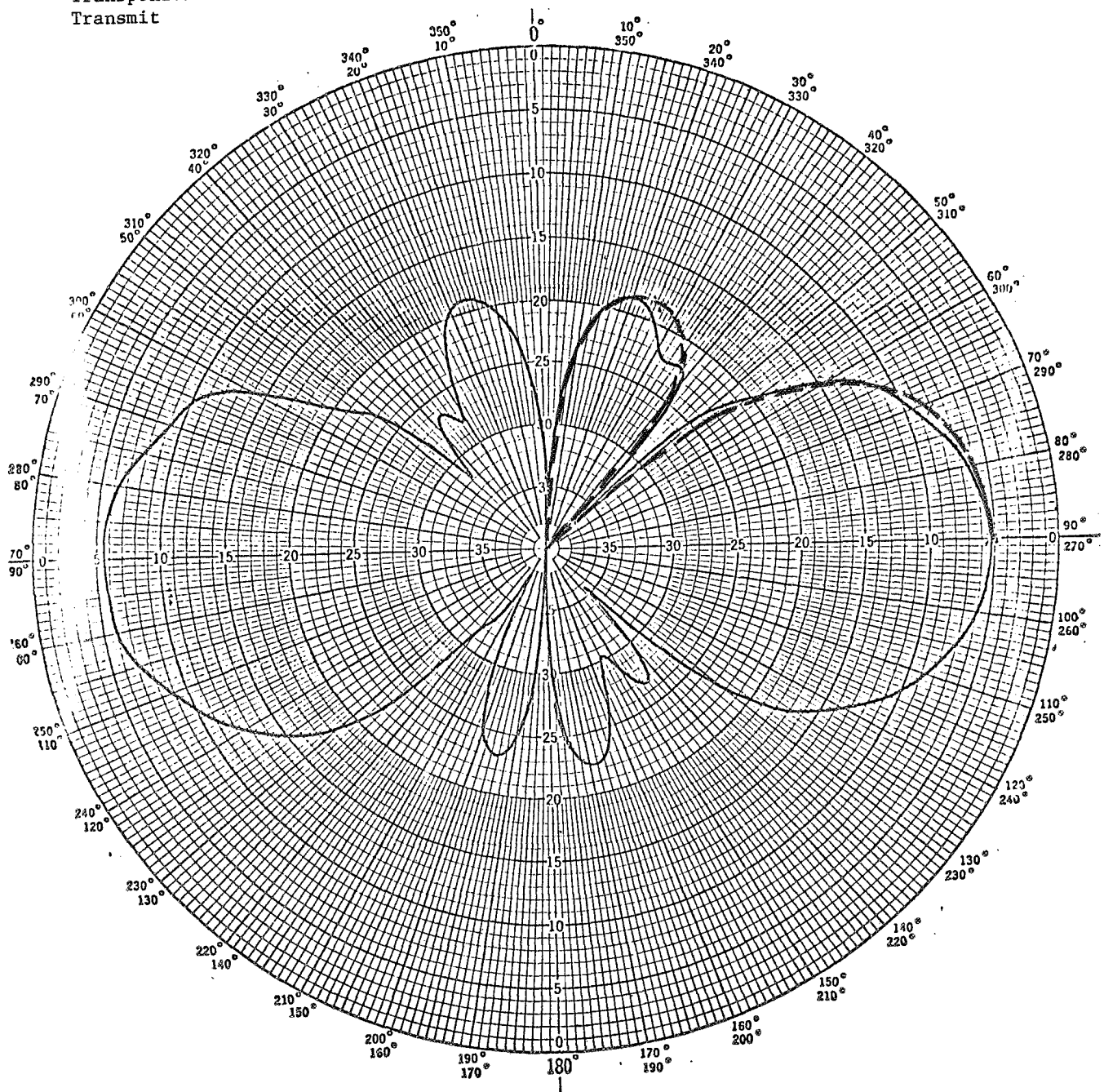


Figure G-5. Transponder transmitter, elevation (1.5 GHz)

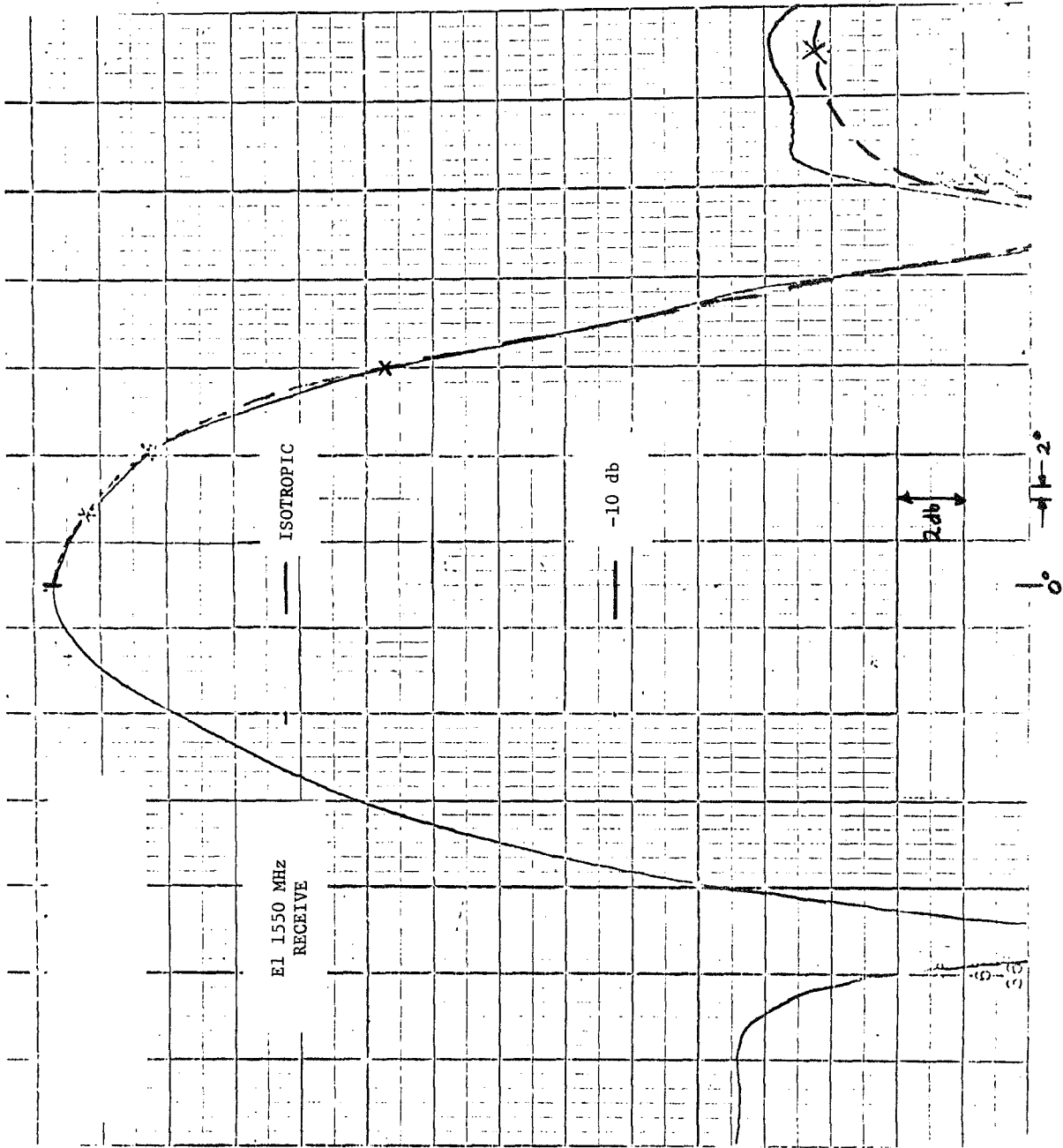


Figure G-6. Receiver elevation (1.5 GHz).

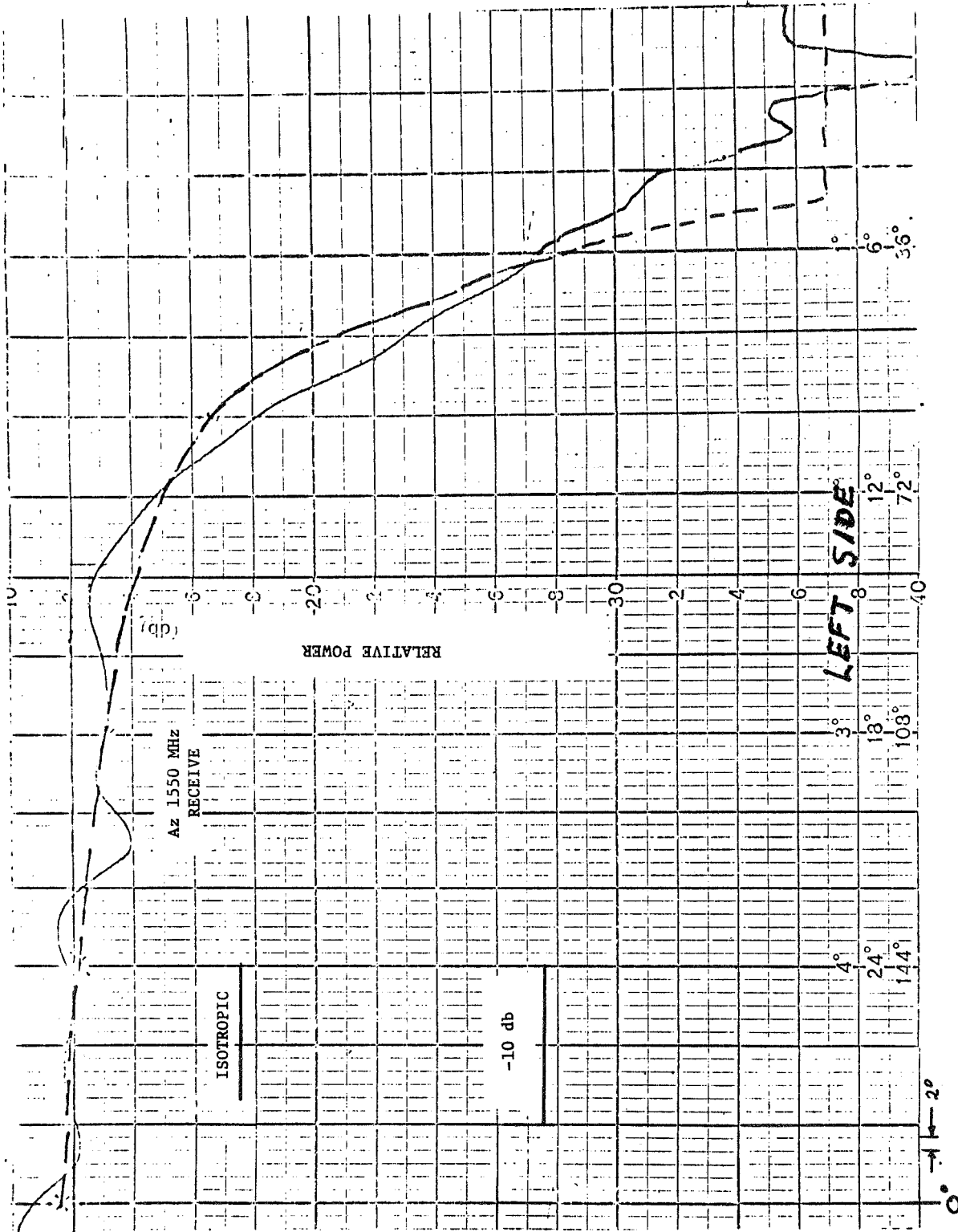


Figure G-7. Receiver azimuth (1.5 GHz).

DEGREES -
 0 4 8 12 16 20 24 28 32 36 40 44 48 52 56 60 64 68 72 76 80 84 88 92 96 100 104 108 112 116 120 124 128 132 136 140 144 148 152 156 160 164 168 172 176 180 184 188 192 196 200 204 208 212 216 220 224 228 232 236 240 244 248 252 256 260 264 268 272 276 280 284 288 292 296 300 304 308 312 316 320 324 328 332 336 340 344 348 352 356

----- TRANSDUCER (1550) WITH RADOME - ELEVATION
 CARPAT 10-9-68
 10 HARMONICS

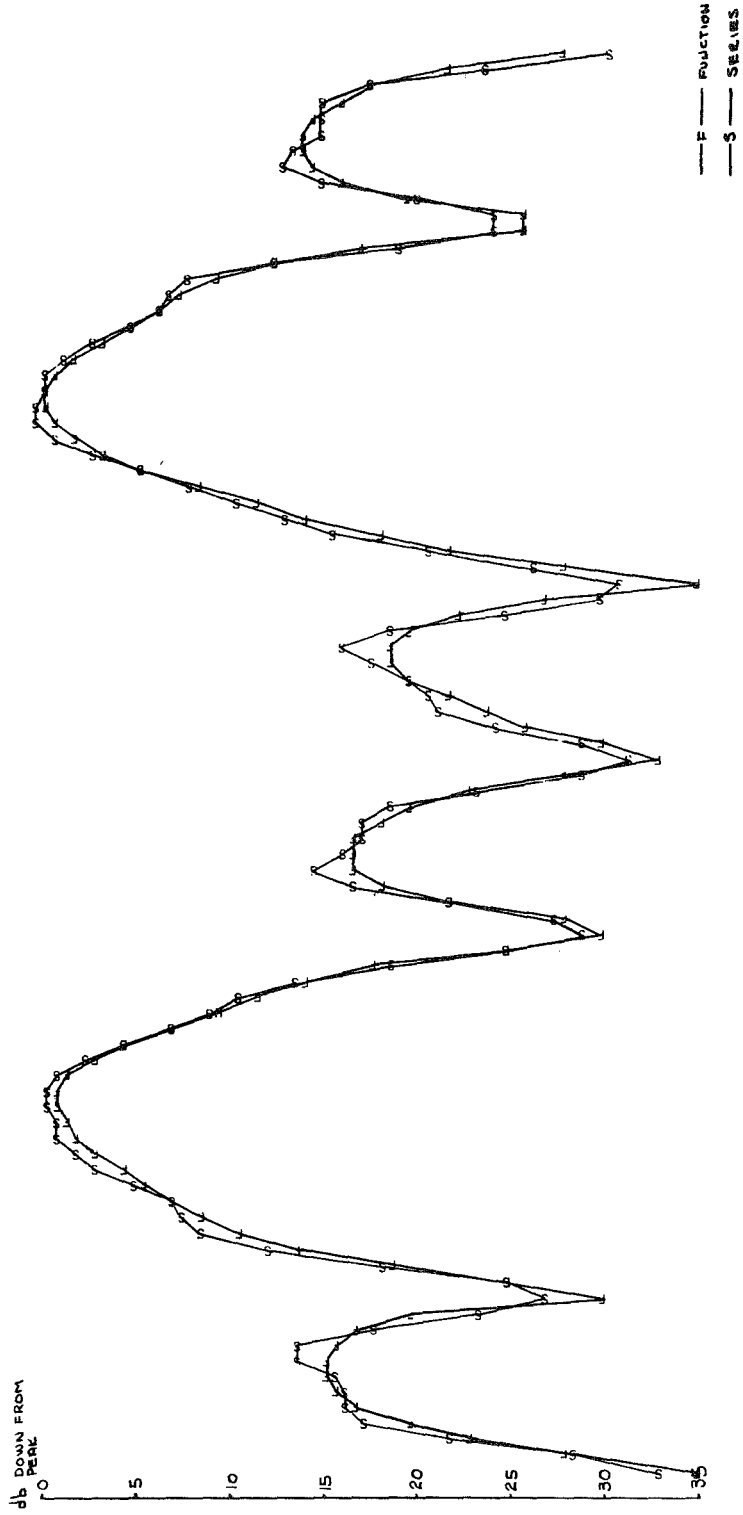


Figure G-8. Example of Fourier fit.

APPENDIX H
ANTENNA GAIN VARIATION WITH RELATIVE
ELEVATION ANGLE

To determine the variation of measured range with elevation angle, the antenna patterns obtained in the LRC anechoic chamber have been used to derive the curve of Figure H-1. This curve shows the ratio of measured range to actual range as a function of the elevation angle of the intruder. The curve takes into account the gain variation with elevation of all antennas in the system.

As may be seen from the curve, the ratio of measured range to actual range remains relatively constant over a ± 10 degree interval, and then rapidly deteriorates.

$\frac{\text{RANGE MEASURED}}{\text{RANGE ACTUAL}}$

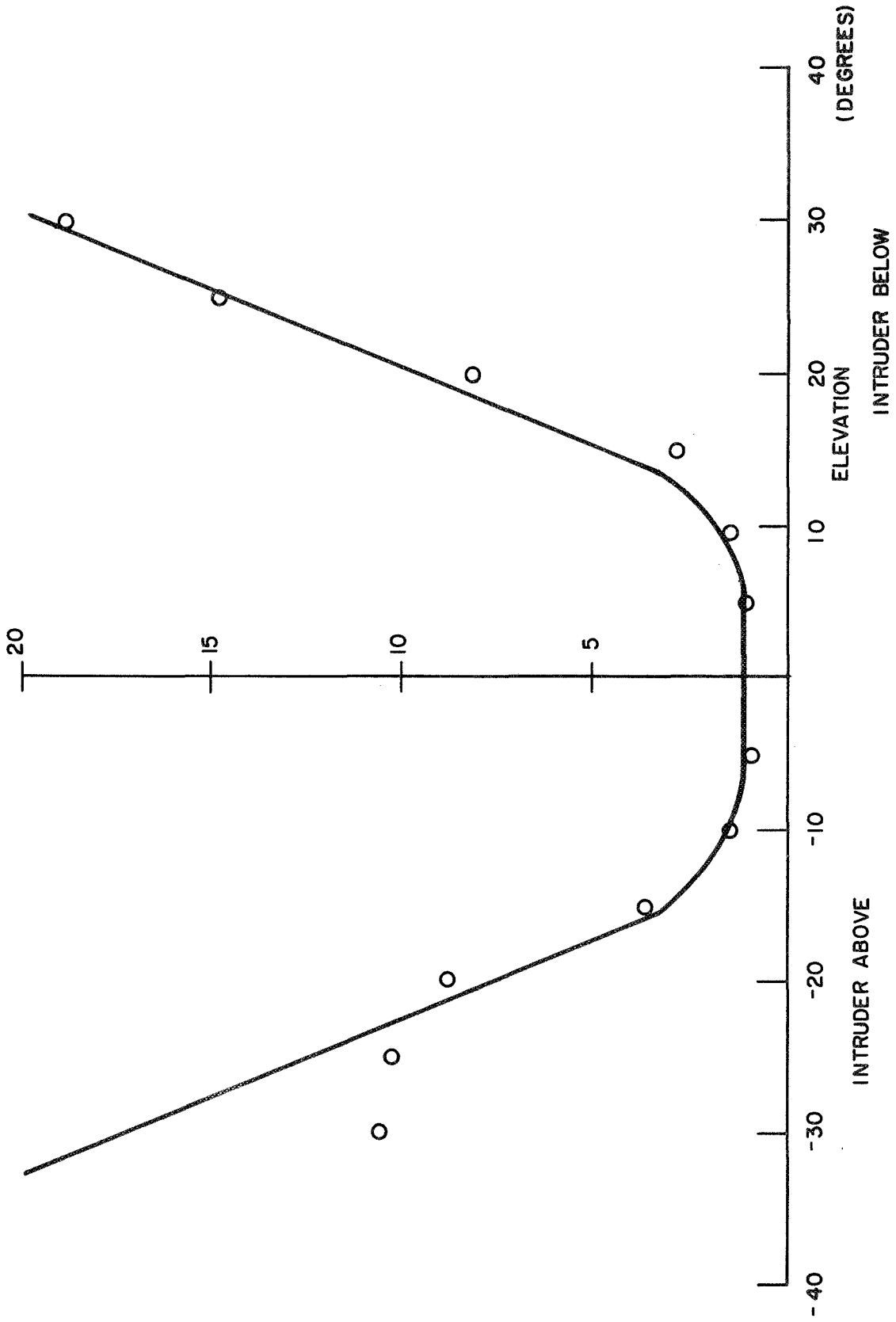


Figure H-1. Measured range/actual range based on $R \sim (Pwr)^{-1/6}$.